Fall 12-2012

Understanding Corrosion Protection and Failure Through Model Polymers in Thin Films

Joshua Smith Hanna
University of Southern Mississippi

The University of Southern Mississippi

UNDERSTANDING CORROSION PROTECTION AND FAILURE THROUGH MODEL POLYMERS IN THIN FILMS

by

Joshua Smith Hanna

Abstract of a Dissertation
Submitted to the Graduate School
of The University of Southern Mississippi
in Partial Fulfillment of the Requirements
for the Degree of Doctor of Philosophy

December 2012

ABSTRACT

UNDERSTANDING CORROSION PROTECTION AND FAILURE

THROUGH MODEL POLYMERS IN THIN FILMS

by Joshua Smith Hanna

December 2012

When developing a model polymeric system to facilitate in the detection of molecular and microscopic events that preface macroscopic corrosive failure; a better understanding of how polymers can indicate corrosion was accomplished. Initially, the thought that molecular chain scission as a necessity for corrosion to occur had to be tested. Through the utilization of high molecular weight thermoplastic (HMWTP) model polymers, it was found that corrosion protection did not correlate to the quantity of weak bonds within an epoxy-amine polymer matrix. Therefore more sensitive methods of detecting corrosion had to be developed since changes within the polymer matrix did not provide thorough data for pre-failure events. Incorporating small molecules that indicate corrosion events into organic polymer coatings, however, did provide sufficient data into when steel substrates were about to fail. It was determined that these molecules, whether colorimetric or fluorescent, were able to capture events at the metal-polymer interface that would directly lead to rust formation. To further the understanding of predicting corrosion, fluorescent molecules were attached to polymer covalently and were able to quantify corrosion events at the highest confidence that no small molecules were moving and providing false results. The development of this corrosion characterization technique

should provide plentiful insight into how polymers and metals fail in a real-time non-destructive manner that is realistic to real-world testing protocols.

The University of Southern Mississippi

UNDERSTANDING CORROSION PROTECTION AND FAILURE THROUGH MODEL POLYMERS IN THIN FILMS

by

Joshua Smith Hanna

A Dissertation
Submitted to the Graduate School
of The University of Southern Mississippi
in Partial Fulfillment of the Requirements
for the Degree of Doctor of Philosophy

Approved:

James W. Rawlins
Director

Shelby F. Thames

Sergei I. Nazarenko

Jeffrey S. Wiggins

Derek L. Patton

Susan A. Siltanen
Dean of the Graduate School

December 2012

ACKNOWLEDGMENTS

The writer would like to thank the advisor to this dissertation, Dr. James Rawlins, and the other committee members, Dr. Sergei Nazarenko, Dr. Shelby Thames, Dr. Derek Patton, and Dr. Jeffrey Wiggins.

The writer would also like to gratefully acknowledge the support from family and friends. Additionally, it is important to thank the financial support of Mandaree Enterprise Corporation (FA8501-06-D-0001), Engineer Research and Development Center (ERDC W9132T-09-2-0019) and The United States Air Force (FA7000-10-2-0014) through funding by the Department of Defense and collaborative efforts for Corrosion Prevention and Understanding via the Technical Corrosion Collaboration working group comprised of The University of Virginia, The University of Hawaii, The Ohio State University, the Air Force Academy, The University of Akron, and The University of Southern Mississippi, and The National Science Foundation GK-12 Program to the University of Southern Mississippi, "Connections in the Classroom: Molecules to Muscles", Award # 0947944.

TABLE OF CONTENTS

LIST OF TABLES

Table

LIST OF ILLUSTRATIONS

Figure

LIST OF EQUATIONS

Equation

LIST OF SCHEMES

Scheme

CHAPTER I

INTRODUCTION

The role of polymers in corrosion prevention has been debated and studied for several decades without obtaining adequate results that identify the timing and mechanics of failure. Despite massive efforts to investigate the root of corrosion problems, the United States loses approximately $276 billion a year [1,2,3] or about 3.1% of the gross domestic product (GDP) in assets due to causes attributed directly to corrosion. Many solutions exist, e.g., statistics verify that if current technology was applied with improved efficiency, up to 30% of wasteful spending could be avoided. [1,2] Several companies/industry specific organizations have published studies quantifying direct corrosion-related losses, e. g., $400,000 a year at sulfuric acid plants, $2 million a year in re-painting steel structures, $1 million a day on petroleum pipelines, $7 per ton of paper produced, and estimated billions spent on the automobile industry. [1] Indirect losses could also be dramatically reduced if the properly designed, selected, and applied coatings were matched with environmental conditions, e.g., shutdowns, damaged product, less-than-desirable application efficiency, product contamination, and over-design. [1] Beyond the monetary losses, the number of lives lost from the result of catastrophic corrosive failure should also be considered. Recent examples included the Silver Bridge collapsing into the Ohio River and the gas pipeline explosion in Mexico. [4,5] Most, if not all, corrosion-related disasters can be avoided if today's coating systems were to be tested thoroughly or if we had accurate service life prediction or remaining service life prediction capabilities.

Many environmental factors affect when and how corrosion occurs; UV radiation, moisture, heat, oxygen, internal stresses, and chemical damage are all considered culprits

towards the eventual degradation of the polymer matrix and degradation of polymer matrix properties.[6,7] Characterization and testing to determine a coating's susceptibility to any of these failure mechanisms needs to be done in a timely manner within a realistic duration.[6] Weeks and months of testing are usually acceptable, however, consistent optimization of formulations has resulted in product evaluations requiring longer periods of time to be completed. Often, years are required to completely test an additive, a new polymer, or new corrosion inhibitors for validation of practical and economic feasibility in advance of new product development and sales. Therefore, those weeks and months must accurately represent longer periods, e.g., several years of exposure through the process of accelerated weathering. Each coating and polymer layer or combinations thereof, often referred to as the coating system, present varying correlation between accelerated versus real atmospheric exposure. It is, therefore, critical to be able to correlate the progress in corrosion to performance properties to allow for advances material research and development.

Typically, UV radiation, water/moisture, temperature, and ions are included within accelerated testing protocols because of their prominent role in disrupting a polymer's ability to protect a substrate and initiate corrosion.[6] The stated goal of accelerated weathering is 'to degrade or corrode a sample by the same mechanism as during natural exposure/weather but at a more rapid pace'.[7] Therefore, the stresses of the tests must not force the system to paths of new failure mechanisms or provide false data. Eventually, there should be an 'accelerated shift factor' that can truly predict a coating's lifetime. A one month/one hour shift would mean that if a sample can survive sixty hours in an accelerated environment, then it will perform to its full ability for at least five years in a specific climate zone.[7] However, variables complicate accelerated weathering

testing of two main participants: newly developed polymer coatings and coating additives for field use.[8] These complications begin when both variables are tested at once. Each set of coatings needs to be tested separately before they are used together as an anti-corrosive coating system.

In any given coating, there is a timeline (*Figure 1*) for the onset of corrosion when a coating is altered or invaded.[7]

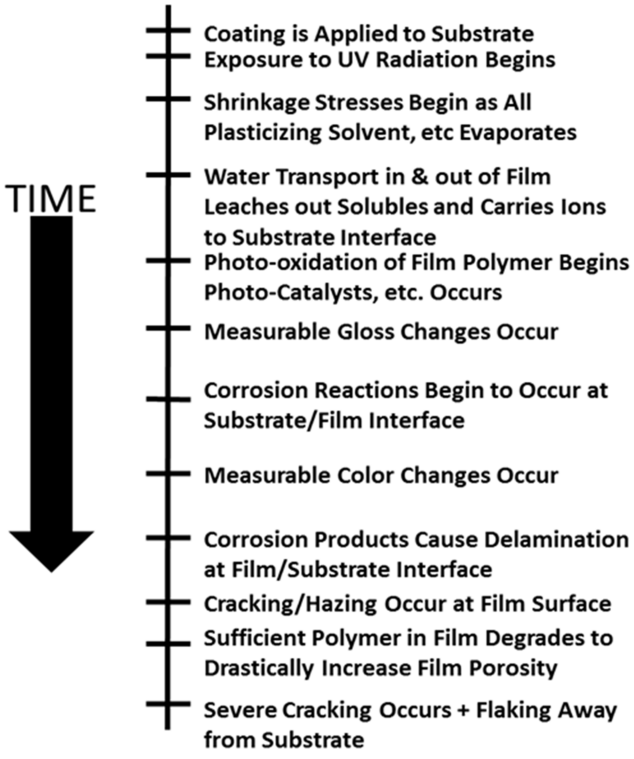

Figure 1. Example of Timeline for Degradation Events in the Lifetime of a Coating.[7]

The first half of the timeline indicates the events before 'corrosion reactions begin to occur at the film/substrate interface'. This leads to the question, when (on this timeline) has coating failure occurred and how is it quantitatively measured?[7] A coating/additive failure has always been a qualitative judgment by a scientist or industry professional. However, to date, there are twenty-three published criteria to detect

changes within a coating during this timeline that could discern the moment before a catastrophic failure.[7] Therefore, there is potential for detecting the slightest of changes within the coating matrix that could lead to the early detection of failure. To begin this transition, it is necessary to develop model polymers that can be analyzed in a number of ways to generate as much useful data as possible.

The use of this model polymer would revolutionize testing standards and begins with the fundamentals of polymer science. Today's industrial standards for anticorrosive coatings is typically a two-component (2K) system comprising of a resin and a crosslinker, which react to form a thermoset polymer.[9] However, using a thermoset polymer during the process of developing new additives limits the ability to measure effects on the polymer matrix. One of the most important and sensitive measurements for determining the onset of polymer failure is the determination of the average molecular weight.

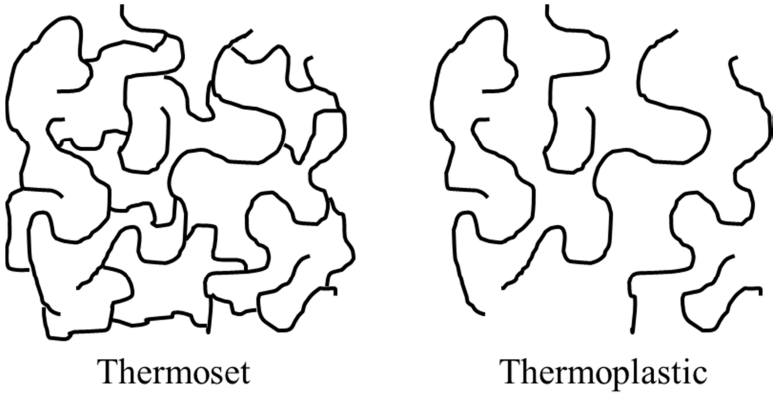

Figure 2. Structural Differences Between Thermoset and Thermoplastic Polymers.

Thermoset systems have permanent crosslinks compared to thermoplastics (*Figure 2*) which cause them to be insoluble in organic solvents. Upon crosslinking, the coating is incapable of being analyzed via gel permeation chromatography (GPC) to

determine molecular weight changes occurring while being subjected to accelerated and natural environments. Thermoplastic models have been suggested by our lab to replace typical 2K systems so that variables like cure times, crosslinker ratio, and heat of cure can be avoided and molecular weight changes are easily monitored. The focus can then be moved to the substrate, additives, or raw materials that have direct impact on the galvanic process of corrosion.

The switch to model polymers may also provide relief from the restrictions imposed by environmental concerns of coating ingredients. The most common and effective anti-corrosion pigment, strontium chromate, is highly toxic and has been banned in several coating applications.[10,11] The coating industry has also been forced to move to systems with little to no volatile organic compounds (VOCs) or hazardous air pollutants (HAPs).[9,12] Under these conditions, there is little time for testing before replacement additives and formulations need to be approved and applied.

Corrosion Process

When two metals with different electronic potentials come into contact through a conductive medium in an electrolyte solution, a very unique chemical reaction occurs that allows chemical energy to be transferred into electrical energy.[9,13] The behavior will eventually cause the physical properties of a metal to change and initiate the macroscopic signs of corrosion.[9] The localized centers where the reactions occur are termed as anode and cathode, of which the anode supplies electrons to the cathode. The loss of electrons at the anode during the electrochemical reaction is the base definition of oxidation. Oxidation is also a thermodynamically driven process because the difference in electronic potential between two metals can act as a driving force of the reaction. The electronic

potentials are recorded through various half-cell reactions that can be added together to find the equilibrium potential of a specific galvanic cell, as seen in Equation 1. [9,13]

$$\boldsymbol{E^o_{Cell} = E^o_{Ox} + E^o_{Red}}$$

Equation 1. Equilibrium potential of a galvanic cell

Values from the Standard Hydrogen Electrode (SHE) can be used to find the overall potential using the Nernst equation where n is the number of electrons, F is Faraday's number, R is the gas constant, T is the temperature, and α is the chemical reactivity for the specific species (*Equation 2*). [9,14]

$$E = E^o + \frac{RT}{nF} ln\left(\frac{\alpha_{Red}}{\alpha_{Ox}}\right)$$

Equation 2. Nernst equation

Since corrosion is a thermodynamically driven process, the electrical equilibrium potential can also be incorporated into the Gibb's free energy equation (Equation 3).

$$\Delta G = -n \times F \times E^o_{Cell}$$

Equation 3. Gibb's free energy

When calculating the Gibb's free energy for the dissolution of iron in the presence of oxygen and water, the $E°_{cell}$ is most often calculated to be about 0.848V using the SHE values. [9,14] This correlates to a free energy of -163.5 kJ/mol, which categorizes the reaction as thermodynamically spontaneous. [9] The drawback to the thermodynamic approach of corrosion is the kinetics of an electrochemical reaction. Some metals may be deemed unstable via these equations, but the actual degradation and metal dissolution can be slowed by formation of oxides on the metal surface as is the case with pure aluminum. [9]

Forms of Corrosion and Corrosion Prevention

Simple equations also have trouble calculating different corrosion morphologies and the means of chemical/electrical attack on a substrate.[4] Traditionally, eight forms of corrosion have been identified: (1) uniform, (2) galvanic, (3) crevice, (4) pitting, (5) intergranular, (6) selective leaching, (7) erosion, and (8) stress.[4] When considering the role of polymeric coatings, uniform corrosion and pitting corrosion are usually targeted as the top priorities for inhibition because filiform corrosion tends to propagate from these two areas to facilitate macroscopic failure.[1] Uniform corrosion is the most common form of corrosion and describes the event in which the electrochemical reaction occurs evenly over the entire surface.[1,4] Pitting corrosion is much more destructive because it is localized in a very small area and digs underneath the substrate surface, thus destroying the substrate's structural integrity.[1,4] Pits are also hard to detect under protective layers and very difficult to predict in a laboratory setting.[4]

There are also many common protection mechanisms for metals other than coatings.[1,4,15] Initially, metal treatment is necessary because metals that are affordable are also more likely to corrode.[15] However, utilizing less expensive metals and treating them to improve their longevity and performance retention is still more cost effective than using noble metals. Metal surface treatments come in a multitude of processes where the metal is mechanically, chemically, thermally diffused, or bombarded into a useful and reliable form.[15] Blasting, hand, electrical, or pneumatic tools are typically used to physically clean the metal surface before any coating can be applied.[4,15] When mechanical cleaning is unable to remove species of an organic nature, solvents, flame, or aqueous phase immersion is employed to cleanse the surface via 'degreasing'.[15] However, if the leftover entities are inorganic, then a common form of treatment called

'pickling' is applied using aggressive acids such as sulfuric and/or chromic acid.[15] After treatment, the metal surface is modified in different stages.[15] Most common is the thermal treatment where the structure is hardened by a strong flame or laser. Ions are also available for thermal treatment but since these processes add cost rapidly and treat only a limited amount of surface area per time, they are used only on a limited basis.[15] The diffusion method is most likely to prolong the life of a metal by allowing a sacrificial or passivating species to be compressed into the metal.[15]

Sacrificial and passivation treatment enables a broader form of corrosion prevention by isolating cathodic, anodic, and passivating powers to prevent the loss of a certain substrate.[1,4] Cathodic protection occurs when there is an electron donor for the corrodible metal.[4] When the electron donor and vulnerable metal come into direct contact, the potential between the anode and cathode essentially becomes equal, which inhibits the flow of corrosion currents.[1] Another method, with the aid of an external power supply, has also been shown to be successful.[4] Typically a direct current (DC) power supply and an inert anode is attached to the substrate to dramatically slow the rate of corrosion. However, for building materials like pipelines, simple galvanic coupling is more useful.[1,4] Galvanic coupling is accomplished by purposefully applying a sacrificial metal that is anodic to the substrate so that the substrate is preserved at the expense of the anode.[4]

Anodic protection supplies anodic currents that promote oxidation instead of inhibiting it.[4] This process of oxidation is not destructive like rust, rather it helps in the development of a thin protective film. This method of protection is rare and needs the help of a potentiostat to find a 'passive' region.[1] Similarly, some pigments make a metal

surface passive without the aid of any external device and is one of the most useful anti-corrosive additives in organic coatings.

Organic Coatings

Metals that have been treated to the satisfaction of customer and user needs, guidelines, and requirements, they are considered ready to be coated. Organic coatings are multifunctional, where they may behave as a barrier to the environment, a carrier of additives to act as inhibitors or sacrificial anodes/cathodes depending upon the substrate (also controlling the inhibitor release rates), and as an aesthetic film that hides, covers, and protects a substrate. The coating system usually starts with as pretreatment, followed by a primer, which is the only layer that is in direct contact with the pretreatment/ substrate.[9] The primer must have good adhesion and provide protective qualities such as the ability to carry sacrificial and inhibitive pigments.[9] Layers applied after the primer may include intermediate coats to build up the coating thickness and increase the barrier properties that inhibit moisture and oxygen.[9,16] Lastly, a top coat is applied, which provides the color and gloss of the coating system while protecting the layers beneath from direct exposure to the environment. Unlike the primer and intermediate coats, the top coat must have superior weathering properties because of its direct exposure to sunlight.[9] The weathering properties are most often controlled by selecting polymeric materials that is stable to ultraviolet (UV) radiation and water to act as a filter/sunscreen or barrier from sunlight.

In demanding environmental conditions, these three layers are most often comprised of epoxies for primers, and acrylics and polyurethanes for topcoats. Less stringent requirements employ alkyds, polyesters, and/or amino resins.[6,12] Substrates in environmental conditions that demand top coat systems usually have topcoats from the

acrylic or polyurethane systems because they are available in an aliphatic base, i.e., these traditionally do not absorb UV light. [12] When a molecule is aliphatic in nature, it lacks unsaturated functional groups that traditionally lead to increased chromophores/UV absorption when exposed to UV light. [17] Most aromatic and unsaturated systems possess chromophores, which tend to turn yellow as the absorption translates to bond scission, oxygen uptake and increase absorption of UV and blue wavelengths in the exposed area(s). [17] Acrylic coating resins are polymerized forms of acrylates, methacrylates, methyl methacrylates, or a more functionalized acrylic that can be reacted with a crosslinker to make a thermoset matrix. [12] Acrylic resins have been used increasingly because they are versatile, i. e., able to be used as high solids, powder coatings, aqueous dispersions, emulsions and thus are environmentally friendly for the application process. [6,12] Polyurethanes may also be waterborne or solventborne, but they generally require additional chemical reactions after application to provide sufficient molecular weight attainment for optimal performance. [12] Typically, a urethane linkage results from the reaction between an isocyanate and an aliphatic hydroxyl, but polyurethane coatings have broadened to include reactions between carboxylic acids, amines, ureas, aspartic esters, and amino resins like urea-formaldehyde resins and melamine resins. [12] Alkyds are also widely used in coatings and are known for slight yellowing. These systems are composed of fatty acids, polyols, and multifunctional acids that produce high gloss coatings. [12] The fatty acid plays an important role in the curing mechanism; as the length and number of unsaturations of the oil segment increases, the 'drying' time decreases through the mechanism of auto-oxidation. [12] Cobalt catalyst may be used to decrease the cure time by accelerating the formation of hydroperoxides/oxyradicals that allow for crosslinking of the oil system. [12] Epoxies have a broad spectrum of reactivity and are

usually cured with a nucleophile strong enough to open a three-membered ring. [12] Polyamides and amines are the standard crosslinker for epoxies but their toxicity requires most coating formulations to be modified so that there is a slight epoxy excess to complete all of the amine reactions. [12] Epoxy systems are popular for their high chemical resistance, thermal stability, good adhesion, great toughness, and are most promising candidates for corrosion prevention. [6,12] However, their downfall is poor weathering since chromophores present in the bisphenol-A based molecule causes the film to yellow in sunlight. [12] Therefore, the use of epoxies is limited to primers that are vital to corrosion protection. [12]

Organic Coating Methods of Protection

For a coating to be considered for anti-corrosive applications, its barrier properties to liquids, gases, and ions are measured to see if these aggressive species are restricted from reaching the substrate in a timely manner. [16,18,19] Superior barrier properties are not limited to a primer, intermediate, or top coat. [9] Instead, all three must work in conjunction to exclude water, oxygen, and ions from penetrating the polymer matrix and corroding the substrate. [9,16] To fortify a coating, inert pigments are introduced into the system to lay perpendicular to the path of the species and decrease permeability. [16,18,19] However, if too much of a pigment is included, the critical pigment volume concentration (CPVC) will be reached and allow gases, liquids, and ions a direct pathway to the metal as shown in *Figure 3*. [16,19]

Aside from the pigmentation, the polymer also has a substantial role in prohibiting or allowing the movement of corrosive species and corrosion inhibitors through the matrix. [16,18] To have a definitive barrier coating, polar constituents and easily hydrolyzable bonds must be minimized and kept in balance as systems like

alkyd/polyester resins often have a high affinity for water and an increasing affinity once hydrolysis is initiated.[9,16] Usually, epoxies and polyurethanes are the best for preventing unwanted species from diffusing because they are hydrophobic in nature, and do not breakdown in the presence of water.[9,16] These systems are also usually crosslinked and it is known that increasing crosslink density will dramatically increase the coating impermeability.[16]

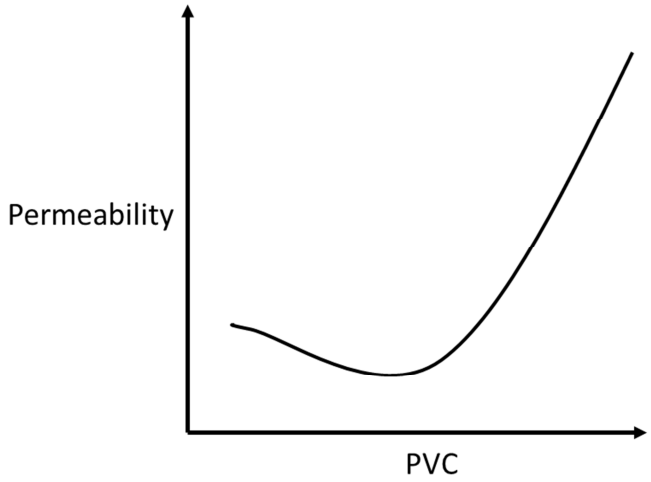

Figure 3. Relationship Between Permeability and Pigment Volume Concentration (PVC).[17]

While barrier pigments are very useful and commonly used, other pigments protect the metals through sacrifice or inhibition.[9] Using the principle of cathodic protection, a sacrificial metal may also be incorporated into a coating. To ensure that the sacrificial metal is in direct contact with the substrate, the primer is formulated at high pigment volume concentrations (PVCs) and a superior barrier top coat is employed to compensate for the voids left in the primer.[9] Inhibitive pigments are often slightly water-soluble and function by the ions migrating to the metal surface to develop a thin oxide barrier via passivation. This method of inhibition often places a limit on the coating PVC because these materials can leach too rapidly in the absence of polymer protection,

thereby depleting the protective nature of the coating system too quickly to be useful for long-term protection.[9] Phosphates, chromates, molybdates, nitrates, borates, and silicates exhibit a passivation mechanism as described generically above and require a coating that facilitates dissolution by providing some limited permeability for water, albeit on a limited basis.[9]

Failure of Organic Coatings

Although pigments have greatly increased the life of many organic coatings specific to environment or corrosion related resistance, failure and degradation of the polymer still occurs. Known environmental influences, such as UV radiation, water, blistering, elevated temperatures, microbial, electrolyte induce property changes, and chemical damage, are widely present in field environments and affect a polymer in several ways: 1) the inhibitor is overwhelmed, i. e., pigments cannot inhibit completely; 2) the polymer properties shift so dramatically that the inhibitors are released either too slowly or too rapidly to continue to maintain corrosion protection; 3) the polymer is delaminated/removed from portions of the substrate whereby environmental contaminants are held/maintained within a pocket/blister or region to accelerate substrate failure; and/or 4) complete removal occurs and the intended protection mechanisms are no longer available.[6]

Additives can be used to elongate and support long-term material survivability, although hindered-amine light stabilizers (HALS) are available, most aromatic coatings are very vulnerable to UV attack.[6] Since UV light has the energy to break carbon-carbon bonds, unlike visible light, it has been suggested to be the cause of yellowing, fading of color, chalking, and loss of gloss in most weathered samples.[6] These side effects are caused from bonds forming and breaking through free radical reactions that cause

increased crosslinking within the polymer matrix and dramatically increase internal stress, hardness, brittleness, crosslink density, and hydrophilicity.[6] Changing the coating hydrophilicity alters the constant movement of water that is being absorbed and desorbed through pores, microcracks, and the inherent film permeability.[20,21] The water can physically find its way into the polymer matrix to plasticize the film, which reduces the T_g by increasing the free volume, and causes other disruptions to the coating.[20,21] Water is a common solvent for many contaminants that cause the onset of corrosion.[6] Water can wash away additives and low molecular weight fractions of the polymer produced via UV degradation.[6] Meanwhile, water also generates a multitude of stresses in the polymer as it compresses and contracts in a constant cycle.[6] This is very damaging to 2K or thermoset systems because the massive contraction during curing is exaggerated by water, stresses the polymer, and causes cracking.[6]

Coupled with corrosion, water also has a prominent role in the phenomena known as blistering.[22] Although it is not known why blisters begin in certain spots, typically hydrophilic solvents, high boiling point solvents, low film thicknesses, low crosslink density, and poor initial adhesion have been shown to increase their occurrence.[22] Progressive loss of adhesion may also predict an upcoming blister and corrosion spot.[22] Through osmosis, a weakened spot will fill with water to form a typically uniform round blister, while the periphery maintains its original adhesion.[22] The process of osmosis will cause that spot to weaken, as water is a hydrogen bond disrupter and diminishes the chemical adhesion between a polymer and metal.[22] While the typical binding energies of metal-polymer interactions are ~ 25 kJ/mol, the metal-water bonds are stronger at 40-65 kJ/mol.[9] Once water has sufficiently replaced the polymer at the interface, corrosive redox reactions begin to produce hydroxyl anions that attract cations, which in turn

increase the osmotic pressure.[22] Meanwhile, the rapidly increasing pH will begin to chemically degrade some of the polymer through saponification.[9] To reduce the number of blisters and defects, conductive pathways must be minimized. A thermoplastic model would prove useful in this situation because of the lack of crosslink density differences.

Crosslinking is a temperature driven process, and temperature is often a mechanism for degradation. As more heat is applied to a thermoset coating, continued crosslinking adds unnecessary stress to the system as the coefficient of thermal expansion (CTE) of metals and polymers differ greatly. High temperatures in accelerated weathering tend to exaggerate the difference in CTE.[6] For example, some epoxy resins have been calculated to have CTEs twice that of aluminum and four times that of steel.[6] More importantly, as the polymer begins to approach its glass transition temperature (T_g), diffusion rates increase and some irreversible absorption of contaminants begin to occur.[20] Those contaminants are usually from the atmosphere and can chemically damage coatings and negate the use of additives within the coating.[6]

The chemical pathway degradation that an organic polymeric coating undergoes is a phenomena that has not been explained with quantitative methods. Many literature reports provide comments and data that suggests polymer-related drivers for failure, e.g., a recent review on corrosion prevention using organic coatings stated that bonds were broken at the 'coating-metal interface' because of alkaline reactions that occur which could ultimately lead to failure.[23] This observation came from a theory that hydrolysis could occur when the pH was high enough to cause chain scission events coupled with other failure modes of cathodic delamination.[24] Both publications were based on the work of the Dickie group who modified epoxy resins to generate a polyester matrix.[25] By correlating increased ester content to a greater loss of adhesion, a hypothesis was

generated that suggested ester bonds were being hydrolyzed and broken.[25] However, when Sorensen *et al.* comment on Dickie's finding, only the importance of adhesion is mentioned because the chemistry of the modified polyester is not analogous to all coatings and cannot be generalized in that way.[26] Very often, these reports are misleading and drive research and development activities to start with a particular hypothesis, e. g., what causes these bonds to break, with little if any definitive proof that bonds are broken or rearranged as a prerequisite for failure. Similarly, Clancy *et al.* cite that 'chemical bonds can break due to hydrolysis and thermo-oxidative aging' per Xiao *et al.*[27] The Xiao group used X-ray photoelectron spectroscopy (XPS) to monitor oxygen/carbon and nitrogen/carbon ratios to see what species could be 'leaching' into water during degradation.[28] Increased amounts of nitrogen were found in the leaching solution, thus chain scission from the attack of water at tertiary amine sites that developed –NH and –OH moieties was hypothesized as the degradation pathway.[28] Numerous research concludes that only a primary testing method followed by a hypothesis will determine if a polymer participates in bond breaking before corrosion. Quantitative methods to track molecular weight and give researchers numerical values for changes in number-average molecular weight, weight-average molecular weight, and polydispersity index would be more beneficial in validating events than uncertain developments when coupled with other primary testing methods.

Testing Protocols

Testing coating and additive systems are very important before they are used in real world applications. Since current coating formulations do not degrade or fail in the field for several years, companies and laboratories must come up with methods of accelerated weathering to screen new coatings and compare the performance of different

anticorrosive technologies. [9] Even with acceleration, testing may take too long without introducing artificial defects to represent typical wear and tear of polymers in field use. [9] The most widely used test is ASTM B117 which tests panels continuously in a salt fog chamber at 35 °C. [6] Regardless of the popularity of this test, it still has no true correlation to natural weathering. [6] Constant contact with water and high temperatures does not happen in the field and neither does nature provide a constant supply of chloride anions that quickly exhaust sacrificial coatings, prevent passivation, and increase osmotic forces. [6] Therefore it has been widely suggested that cyclic testing may be more relevant to compare degradation to real world samples.

Prohesion, Norsok, and QUV are common cyclic tests that are not very complicated and involve UV radiation as one of the irritants. [6] Prohesion, or ASTM D5894, is a 12 week test that exposes samples to UV radiation with intermittent condensation cycles for one week followed by another week of cycling on and off salt spray. [6] Norsok, or ASTM G53, is a 25 week test that involves a continual rotation of 168 hours of salt spray, 16 hours of drying time, and 80 hours of QUV. [6] This test has been proven useful for coatings employed on offshore oil platforms. [6] Finally QUV, or ASTM G154, places panels in a UV chamber where temperature and time of condensation are variables and is useful for samples that will be directly exposed to weathering and sunlight. Although these tests could possibly provide a better field correlation, the variables within the tests can always be changed, and this has allowed for numerous cyclic tests to be developed from the basic principles of Prohesion, Norsok, and QUV. [6]

After samples are removed from either natural or accelerated weathering, numerous evaluations are available to determine how a coating has changed or failed

over time. Although most are subjective, the many macro and microscopic testing methods have given some insight as to how polymers behave during failure. Macroscopical creep, blisters, adhesion, barrier properties, differential scanning calorimetery (DSC), or dynamic mechanical analysis (DMA) give qualitative and quantitative details of a coating. Creep is simply the measurement of how far corrosion has progressed from a scribe line over time.[6] Once corrosion becomes systemic, the anode begins to travel and cause delamination at a specific rate.[6] Apart from artificial scribes, blisters are also monitored by simplicity. By counting blisters per area and measuring their size, blister density and severity can be qualitatively noted.[6] However, this method is too subjective and does not monitor or help predict corrosion or polymer failure.[6] Adhesion tests quantify the interaction between the coating and metal.[6] Since deformation is common when two chemically bonded species are physically pulled apart, it is accepted that polymers deform differently than traditional materials.[6] The direct pull-off and lateral stress methods can both produce quantitative values before and after weathering exposure despite inherent complications.[6]

Other viable parameters to follow throughout a degradation process are the barrier properties like water vapor transmission, T_g, enthalpy of relaxation, coefficient of thermal expansion, tensile strength, and strain. Apart from the barrier properties, the rest are measured via DSC or DMA. The change in T_g will become evident as more or less free volume present in the polymer begins filling with contaminants, developing more crosslinks, or breaking bonds. To find the answer to which process is occurring, gel permeation chromatography (GPC) can be used to monitor molecular weight. Since thermoset systems, which are unable to be put into solution due to a theoretical infinite molecular weight, cannot be used with this method, thermoplastic models could be used

with the same additives to prove if a coating is failing or if additives are not sufficiently effective.

Macroscopic tests are irreplaceable in giving quick insight to the events that might be occurring on a smaller scale. Thankfully, some microscopic methods are able to show images, element analysis, and chemical bond changes that are pivotal to monitoring corrosive degradation in and around a polymer. Scanning electron microscopy (SEM) uses electrons to scan a surface while a receiver detects X-rays, back-scatter electrons, secondary electron emissions, confocal microscopy, and cathode luminescence signals returning to the source to make detailed magnified images.[6] Coupled with the imaging, an electron microscope will use the same bombarding of particles except that the kinetic energy of the returning electrons is measured and correlated to a specific element on the periodic table.[6] This is useful for monitoring the oxidation of metals during corrosion and calculates the percent of oxygen increasing with exposure to weathering.[6] Changes to a surface can be detected over time when a surface is exposed to harsh environments with optical methods but they do not provide details of chemical changes.[6] Infrared (IR) spectroscopy is most useful in corroborating absorbance and transmission of various IR wavelengths to specific chemical bonds.[6] The development and reduction of certain peaks during testing can give valuable information as to what is occurring within the polymer.[6]

Magnesium Fluorescent Probes

Magnesium has been recently employed as an anti-corrosive, sacrificial pigment in primers. However, lifetime prediction of magnesium-rich primers (MgRP) is very difficult. When magnesium is fully oxidized, it is no longer able to cathodically protect a metallic substrate. Using a magnesium ionophore to track the movement of magnesium

during pigment degradation should provide insight into the lifetime of a MgRP. Also, incorporating the fluoro-magnesium probe into various layers away from the substrate will permit monitoring of potential migration pathways.

Coumarin dyes consisting of a nitrogen substituted phenylpropanoid chromophore and a β-dicarbonyl group have been investigated as a fluoro-magnesium probe (*Figure 4*). [29,30,31,32] Crown ethers, amides, carboxylic acids or esters groups from the β-dicarbonyl all show sensitivity although ligation is often credited solely to the two carbonyl oxygen atoms. [29,30,31,32] Although usually not well cited, the heteroatom α to the carbonyl contains electrons fully capable of binding with the electron deficient magnesium. [29,30,31] When the heteroatom is removed, the responsiveness to magnesium dramatically decreases. [33]

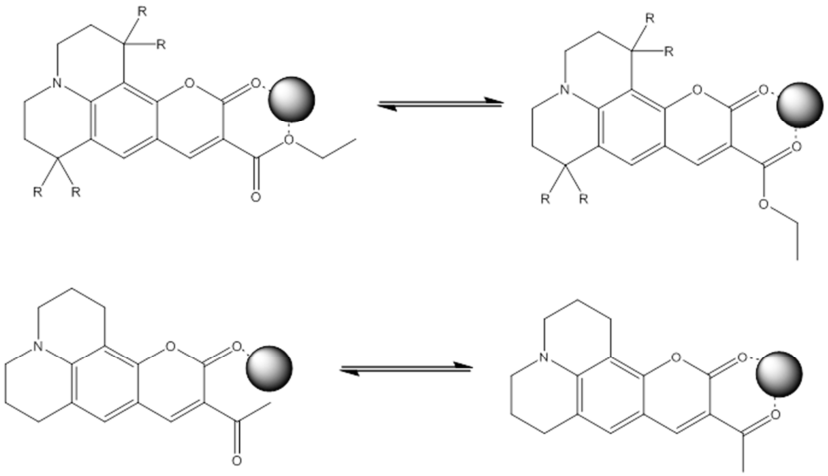

Figure 4. Binding Mechanisms of Fluoro-Magnesium Probes to Magnesium Ion.

Although not necessary, heteroatoms are common at the α position for sufficient magnesium binding. It has been proven that phenyl substituents are also capable of contributing to magnesium binding although that mechanism proposal was not found in literature. [32,34] Rather, Brunet *et al.* suggested that the binding site must remain near the ionic diameter of magnesium (1.32 Å) and possess a β-dicarbonyl substituent. [32]

For coumarin dyes to bind with magnesium, the magnesium must be in its divalent form. When developing a method for detecting magnesium in a solid organic polymer thin film, changes in bulk material polarity immediately hinder confident and facile detection. For example, when magnesium perchlorate is completely dissolved in a polar solvent such as acetonitrile, nearly 70% of magnesium ions are associated with the perchlorate counter anion. [35] Increasing the polarity by adding up to 20% mole fraction of water increases the dissociation of magnesium by a factor of six. [35] This leads to difficulties when trying to determine the amount of magnesium in a solution of magnesium perchlorate and magnesium chloride in a low polarity solvent such as tetrahydrofuran (THF). [36,37] In THF, magnesium perchlorate dissociates into ion pairs more readily than magnesium chloride. [36] Depending on the counter ions present at the coating and metal interface, detection of magnesium ions may be difficult as their dissociation constant may be too low. Therefore, as water moves into an organic coating with low polarity, the solvation of magnesium will drastically decrease in a digylcidyl ether of bisphenol-A (DGEBA) polymer matrix. Magnesium can also complex with the oxygen atoms in the DGEBA backbone in competition with the coumarin dye. [38] The low amount of divalent magnesium may be 'consumed' by the polymer backbone during its slow ionic mobility. [38] Therefore it will be determined how coumarin dyes bind with divalent magnesium in multiple polar environments. After confirmation of the correct mechanism, the dyes will be incorporated into a thermoplastic epoxy coating with known amounts of magnesium salts to determine the efficacy of ionic magnesium detection. The data will provide insight as to whether ions are able to be monitored within apolar polymers or if the focus should remain at their interfaces.

Corrosion Indicating Probes

Non-destructive and real-time monitoring of pH changes within a polymer and at specific interfaces is an important capability of fluorescent probes. [39,40] While they are extensively used in analytical analysis, cell biology, and clinical medical experiments, there is a constant push for innovation to employ stimuli-responsive fluorescent probes in new scientific fields. [41] Organic coatings are frequently used as a protective barrier and/or sacrificial film to prevent corrosive entities and corrosion in general from reaching a metallic substrate. [9] bisphenol-A epoxy polymer-based coating systems are widely used in primer applications since they possess excellent chemical resistance, thermal stability, adhesion, and toughness. [9] Although they provide good substrate protection, the inherent permeability of the polymer allows water, ions, and oxygen transfer through their films, albeit slowly, thus corrosion is delayed but not prevented. [9] The ability to detect the onset of corrosion as early warning information is thought to be critical for the prevention of catastrophic failure. [42,43,44] In particular, researchers have studied ion dissolution during the oxidation reaction of corrosion using fluorescent probes. [43,44,45,46,47,48,49]

The hydroxyl anions produced from the subsequent reduction reaction during corrosion (*Figure 5*) dramatically increases the local pH above 8 which can be indicated with a pH-sensitive dye such as phenolphthalein, fluorescein, or fluorescein isothiocyanate. [42,43,50] However, concerns about chemical interactions such as amine basicity of common crosslinkers influencing the colorimetric response have limited the utility of phenolphthalein in thermosetting epoxy primers. [43] Therefore, a thermoplastic, pH responsive phenoxy resin is proposed to understand the events occurring prior to macroscopic corrosive failure. Also, covalently tethering the fluorescent probe to the

polymer will improve the x-y spatial resolution for pH changes as it will prevent free fluorescein from migrating through a polymer matrix. [41,47,48,51]

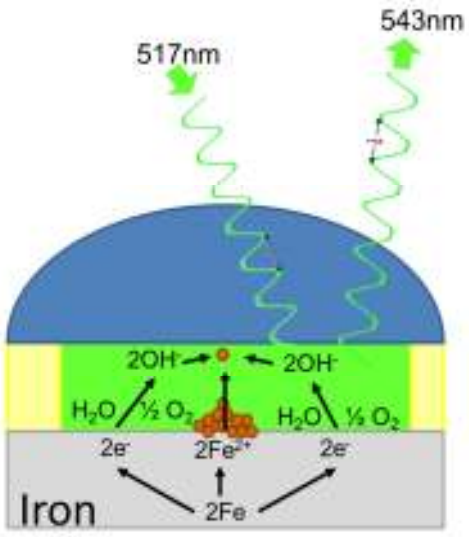

Figure 5. Mechanism of Corrosion Indication with a pH Stimuli Responsive FITC Functional Polymer.

Previous attempts to incorporate fluorescein covalently into a polymer involved using it as monomer for polyester synthesis. [52,53] Terephthalic acid and bisphenol-A are used in polyester synthesis and are able to copolymerize with fluorescein to yield a fluorescent polymer. [52,53] It is unclear whether the pH transformation of fluorescein would cause chain scission during the tautomerization of a phenol into a ketone, even though it was reported that the thermal stability of fluorescein was improved by incorporating the dye in the polymer determined by TGA. [53] To eliminate this variable, it is proposed that fluorescein be incorporated as a pendant group on the polymer backbone via post-polymerization. Specifically, fluorescein isothiocyanate (FITC) will be reacted with a phenoxy resin so that the dye is free to conform to tautomers without being susceptible to leaching. [41] For certain nanoparticles, free fluorescein can be removed from embedding in a polymer matrix by 80% of its original content whereas

bound fluorescein only lost 9%.[41] Improvement upon the 9% loss could have occurred if the particles were washed thoroughly prior to exposure.[41] Current reactions of FITC with functional polymers have yielded high grafting efficiencies of 61%, in which established polymerized chains are able to react with small molecules.[54] Although most chemistry involves using a more reactive amine as the primary nucleophile, this research focuses on reacting FITC with the hydroxyl groups of a phenoxy resin which should reduce grafting efficiency but still possess the high thermal stability associated with phenoxy backbones.[39,54]

Halide Salt Correlation to Corrosion

When steel is exposed to halide salt solutions, corrosion is typically faster than when it is exposed to deionized water or dry air.[55,56,57] Halide ions have been studied for their contribution to the dissolution of iron, i.e., corrosion initiation.[55,58] Chloride, bromide, and iodide solutions behave in a predictable manner, i.e., anionic radii and solution conductivity are very similar (Table 1).

Table 1

Halide Radii and Sodium Halide Solution Conductivities

Anion	Anionic Radii (Å)	0.5 M Conductivity (mS/cm)
Fluoride	1.36	33.6
Chloride	1.81	43.3
Bromide	1.95	44.6
Iodide	2.16	45.7

Fluoride is not well understood regarding its specific role in corrosion.[55] Fluoride-based salt solutions like NaF exhibited little to no effect on the breakdown of oxide layers on iron alloys whereas other halide salts readily remove oxide barriers and participate in iron dissolution. Such halides promote corrosion quickly because they are

able to form the necessary intermediates needed to break down iron. Hypohalites are one of the most important intermediates involved in the mechanism of iron dissolution.[59] Since hypofluorites are very unstable above -20 °C, it is to be expected that fluoride–assisted corrosion of iron will either be inhibited or occur at tremendously reduced rates. When NaF is incorporated into highly acidic environments, only uniform corrosion occurs unlike the pitting and uniform corrosion noted with NaCl, NaBr, and NaI solutions.[57,60] Chloride anions were inherently more active in the corrosion process than bromide or iodide ions.[56] Anion corrosivity ranked as $Cl^- > Br^- > I^-$ and was attributed to increasing ionic radii.[56,57] However, the smallest halide anion did not follow the trend of corrosivity. This was found to be consistent in the literature and attributed to the dissolution of the initial oxide layer on steel. Subsequent catalyzation of iron dissolution prior to catastrophic corrosion was not a productive reaction? in the presence of fluoride.[56,61,62] Thus, the final ranking of halide anions for the corrosion of steel is as follows: $Cl^- > Br^- > I^- > F^-$.[56] This research will illustrate the effectiveness of fluorescence spectroscopy in detecting early trends in corrosion rates of various halide environments using a non-destructive and sensitive characterization technique for organic coatings adhered to metallic substrates. Validation of the process can be accomplished if trends from literature match using a pH stimuli-responsive polymer to detect corrosion times for NaF, NaCl, NaBr, and NaI.

Ionic Diffusion Correlation to Corrosion

The corrosion triangle in *Figure 6* indicates that a certain amount of conductivity is essential to connect the reduction and oxidation reactions. Thus corrosion will not occur if salts are not present in an aqueous solution. Therefore, tracking the movement of

species like NaCl, oxygen, and water is critical for predicting when corrosion reactions are initiated on a coated metal.

Figure 6. Corrosion Triangle

Epoxy resins are known to allow ion diffusion through them without the presence of a physical defect since their free volume is larger than that of a chloride anion. [63,64,65] However, diffusion events are difficult to measure since some electrochemical techniques are destructive and do not measure in real-time. [63] A pH responsive phenoxy resin will aid in detecting ion diffusion prefacing the moments before NaCl reaches a steel substrate to begin the cascade of oxidation and reduction reactions related to corrosion. To meet this objective, dilute sodium hydroxide will be allowed to migrate through the coating as the fluorescence intensity is monitored over time. As the NaOH reaches the metal-polymer interface, a subsequent sample exposed to NaCl solution should be able to detect the initial corrosive response from the reduction reaction. [66] It has been shown that the diffusion of NaOH and NaCl are comparable throughout organic coatings; however NaCl is the more corrosive compound of the two. [66] The amount of time it takes for NaOH to be detected at the metal-polymer interface and to identify NaCl corrosion will provide insight as to how quickly ions diffuse through a coating and the amount of NaCl

necessary to facilitate the iron oxidation. There should be no concern about the NaOH sample producing a large amount of fluorescence from a corrosion event since corrosion of steel is more prominent in neutral and acidic solutions while NaCl corrodes the substrate at a substantially faster rate. [66]

Sodium Chloride Concentration Correlation to Corrosion

The reduction reaction of steel corrosion generates hydroxyl anions. [66] Since chloride anions accelerate the release of iron's electrons to feed this reduction reaction, corrosion is vastly accelerated at higher NaCl concentrations. [66] Interestingly, the hydroxyl anions are thought to cause delamination of organic coatings, but other intermediates with higher oxidative powers may also contribute to this phenomenon. [66] Leng and co-workers exposed a coated metal to NaOH in an oxygen-free environment and found that the naturally produced hydroxyl anions from NaCl in atmospheric conditions were more aggressive towards delamination. [66] Thus, ferrous alloys are very sensitive to NaCl solutions, and changing their concentration levels will alter the amount and magnitude of corrosion and pitting. [67] By changing NaCl concentrations from zero to 5.70M, different behaviors and mechanisms of corrosion can occur leading to various corrosive outcomes. [66,67,68,69] Above 0.5 M of NaCl in water, the amount and severity of corrosion increases with increasing salt concentration. [66,67,68,69] Although some electrochemical methods may have difficulty discerning between 0.71 M and 5.70 M solutions, these samples were orders of magnitude different visibly in the number of corrosion spots on the metals' surface. [69]

At salt concentration below 0.5 M, corrosion behavior changes dramatically as competition with repassivation is very overpowering. [66,67,68,69,70] Chlorides are known to destroy the passive oxide layer on steel and expose virgin material to potential attack. [68]

At low chloride concentrations, the repassivation rate is greater than the oxide destruction rate, resulting in corrosion occurring at a greatly reduced rate. [68] Increasing the chloride content accelerates the dissolution of the oxide layer and the rate of corrosion, and ensures that repassivation occurs at a slower rate. [68] The threshold concentration is speculative and varies depending on the experiment, but generally concentrations below 0.5 M exhibit delayed corrosion reactions while solutions below 0.04 M might not exhibit any corrosion at all. [66,68,69,70] A pH-responsive polymer should be able to distinguish between the low (0.0-0.50M), medium (0.50-1.0M), and high (1.0-5.0M) corrosion environments as a non-destructive corrosion sensing tool.

Natural Weathering

As stated earlier, UV radiation is well-known for degrading aromatic polymers that are typically used as primers in corrosion applications. [6,71] During natural weathering, apart from UV radiation, living organisms, wet/dry cycles, temperature fluctuations, oxidation, and pollution also contribute to coating deterioration. [72,73] Chromophores generated during weathering cause the polymer to shift its absorbance wavelength from UV to violet, thus presenting the typical yellowing associated with outdoor exposure. The groups responsible for such changes are, but not limited to, hydroxyls that form carbonyls, residual epoxide groups converted to unsaturation, and the bridge between aromatic groups that lead to chain scission and carbonyl formation. [71] Therefore, polymers that lack double bonds and aromatic moieties are most useful as topcoats to protect epoxy primers during outdoor exposure since they are resistant to degradation from UV radiation. [72] However, the stability of molecules, like fluorescein, that give the polymer its pH-responsive behavior must also be taken into account since it is known to photobleach even under visible light. [74,75] Photobleaching causes molecules

like FITC to exhibit exponential decay in fluorescence over time, although not reducing completely. [76,77] Even power up to 150W can cause fluorescein to reduce its intensity to 20% of the original value; however the 20% represents a plateauing that stays relatively constant upon further exposure. [77] When used outdoors, despite shrinking emission values the molecule will still retain some ability to detect pH changes even after severe photobleaching. [76] Therefore, tracking the relative standard deviation of naturally weathered samples is important since the reduction in intensity may mask the initial increase in fluorescence from corrosion.

Outdoor weathering also has a temperature component, especially in areas such as Hattiesburg, Mississippi where summer temperatures may exceed 40 ˚C. Fluorescein and its derivatives photobleach faster at elevated temperatures, however below 60-85 ˚C the reduction in emission values is not a concern. [77,78] For the fluorescent polymer tested in this research, the fluorescein is covalently tethered to the polymer backbone. It has been reported that covalently attaching probes like fluorescein and rhodamine to polymers reduces photobleaching, e. g., tethering fluorescein demonstrated a 22% improvement in resisting photobleaching. [41] Likewise, changing to a tethered rhodamine system elicited a 69% improvement compared to free fluorescein, when exposed to artificial light. [41] Overall, the ability of a pH-responsive polymer to detect corrosion events in the real world despite the inherent problems associated with DGEBA based epoxy degradation and fluorescent molecules known to photobleach will be investigated in this research.

Summary

This research will seek to determine how a polymer can facilitate the detection of corrosive events before macroscopic failure can occur. *Figure 7* lists the research

objective and tasks employed to demonstrate epoxy/phenoxy polymer behavior and the detection of pre-macroscopic corrosion events.

Research Objective: Develop a model polymeric system that facilitates the detection of molecular/microscopic changes that preface macroscopic failure

Prerequisite: Determine the ability for thermoplastic model polymers to perform in corrosion testing (Chapter III)

Task 1: Develop model polymers to detect whether chain scission is necessary before corrosion (Chapter III)

Task 2: Determine whether indicating molecules detect ions related to corrosion within epoxies (Chapter IV)

Task 3: Determine if indicating molecules detect ions related to corrosion at interfaces of epoxies (Chapter V)

Task 4: Develop a model polymer that inherently indicates ions related to corrosion at interfaces (Chapter VI)

Task 5: Validate model polymer that inherently indicates corrosion (Chapter VII)
- 5.1: Ability to detect corrosion similar to electrochemistry literature
- 5.2: Ability to detect ionic environment conducive to corrosion
- 5.3: Ability to detect [NaCl] relation to corrosion

Task 6: Determine if model polymer that inherently indicates ions related to corrosion at interfaces in the real world (Chapter VII)

Figure 7. List of Research Tasks.

The succeeding chapters will describe how model epoxy polymers behave before, during, and after a corrosive event and facilitate a quantifiable way of detecting early corrosion. After quantifying and understanding the changes that occur in polymeric materials during varying types of exposure, we shifted focus to developing and proving the utility of more sensitive techniques to detect and quantify *in situ* changes via responsive self-indicating molecules receptive to ions that preface early corrosion. It was determined where and how the molecules can be used within epoxide polymers to optimize the utility of each indicating molecule and polymeric material. Upon optimization, a new model polymer was developed that responded quantifiably to external stimuli correlating to the corrosion process. Subsequent experiments provided a

rigorous validation process for utility and method development. The polymer was then exposed to outdoor weathering to determine whether a broader utility for the polymer was possible and whether the same retained the ability to detect/quantify pre-macroscopic corrosion in real world conditions along with defining what limitations and caveats existed for matching future needs and expectations.

CHAPTER II

MATERIALS, EXPERIMENTAL, CHARACTERIZATION TECHNIQUES, AND PROCEDURES

High Molecular Weight Thermoplastic Model Polymer Materials

Eponol® 53-BH-35, Epon® 828, Epon 1001, and Epon 1007 was purchased from Hexion Specialty Chemicals. Polylink 4200 [4,4'-methylenebis (*N*-sec-butylaniline)] was obtained from The Hanson Group. Purity and equivalence of these materials was confirmed via ^{1}H nuclear magnetic resonance (NMR) spectroscopy operating at 300.13 MHz. Propylene glycol propyl ether (PGPE) and 1-methoxy 2-propanol acetate (Dowanol PMA) were purchased from Aldrich Chemical Company. Methyl ethyl ketone (MEK) and tetrathydrofuran (THF) were purchased from Fisher Scientific. All raw materials were used as received while the linear HMWTPs were synthesized in our laboratory.

Magnesium Fluorescent Probe Materials

Coumarin 314 (99% purity), Coumarin 314T (99% purity), Coumarin 334 (99% purity), magnesium perchlorate and propylene glycol propyl ether (PGPE) were purchased from Sigma-Aldrich®. Acetonitrile and methyl ethyl ketone (MEK) were purchased from Fisher Scientific. Eponol 53-BH-35 was supplied from Hexion®. Magnesium chloride was purchased from Acros Organics.

Incorporating pH-Indicating Microcapsules in Epoxy Primers Materials

A model thermoplastic coating was formulated using the epoxy resin solution, Eponol® 53-BH-35, from Hexion. Reagent grade phenolphthalein was purchased from Sigma Aldrich. A thermoset coating was formulated with Epon® 1001-B-80, Epon 1007-HT-55 and Epikure® 3292-FX-60 from Hexion, and pentaerythritol tetrakis(3-

mercaptopropionate) (PTTT) from Sigma Aldrich as the polymer matrix, pigments (Ti-Pure® 706 from DuPont, Heucorin® RZ from Heucotech, Huberbrite® barium sulfate from J.M. Huber Corporation, Zeeospheres® W-410 from Zeelon Industries Inc., mica 325 mesh from The Tryline Group, and strontium chromate from Alfa Aesar), solvents (toluene from Fisher Scientific, ethyl 3-ethoxypropionate from Sigma Aldrich, propylene glycol propyl ether from Sigma Aldrich, xylenes from Fisher Scientific), and additives (Anti-Terra-U® from BYK-Chemie USA), that were incorporated as received. Phenolphthalein titration reagents included reagent grade phenolphthalein from Sigma Aldrich, *N*-bromosuccinimide from Sigma Aldrich, and sodium hydroxide from Fisher Scientific. The pH-sensitive microcapsules were synthesized at KSC Corrosion Technology Laboratory and supplied to The University of Southern Mississippi for phenolphthalein content evaluation and incorporation into epoxy coatings. Steel (DT and QD) and aluminum (A and Al-2024) panels were obtained from Q-Panel Company and cleaned with acetone before use and their alloy composition is in *Figure 8*.

- DT (ASTM A624)
  - Fe – >99%
  - C – <0.10%
  - Mn – <0.50%
  - P – <0.030%
  - S – <0.035%
  - Tin Plate Finish
- QD (ASTM A1008 D609 Type3)
  - Fe – >99%
  - C – <0.10%
  - Mn – <0.50%
  - P – <0.030%
  - S – <0.035%
  - Smooth Finish
- A (3003 H14)
  - Al – 96.7 – 99.0%
  - Cu – 0.050 – 0.20%
  - Fe – <=0.70%
  - Mn – 1.00 – 1.50%
  - Si – <=0.60%
  - Zn – <=0.10%
- Al-2024
  - Al – 90.7-94.7%
  - Cr – <0.10%
  - Cu – 3.8-4.9%
  - Fe – <0.50%
  - Si – <0.50%
  - Ti – <0.15%
  - Zn – <0.25%

Figure 8. Substrate alloy composition.

pH Stimuli Responsive Polymer Materials

Fluorescein isothiocyanate (FITC) was purchased from Thermo Scientific. Dimethyl formamide, sodium fluoride, sodium chloride, sodium bromide, and sodium iodide were purchased from Acros Organics. Methanol, chloroform, and ethyl 3-ethoxypropionate were purchased from Fisher Scientific. PKHH phenoxy resin was purchased from InChem Corporation. ASTM A1008 D609 Type 3 steel substrate was purchased from Q-Lab Ltd. Titrations were conducted using bromophenol blue and 0.10N HCl purchased from Acros while phenolphthalein, thymol blue, and methyl red were purchased from Sigma Aldrich.

Structures of Important Molecules

Epoxies/Phenoxies

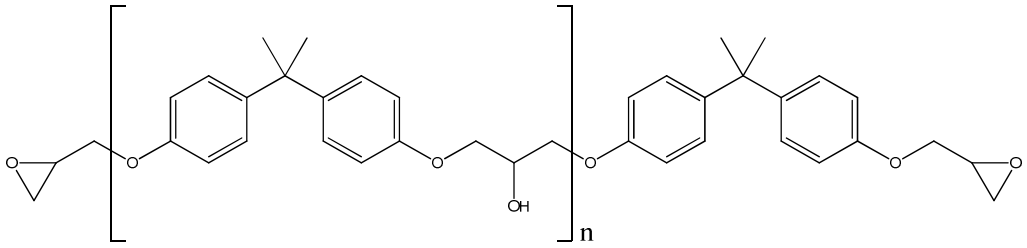

Figure 9. Epoxies - Epon 828 n=0.13, Epon 1001 n=2, Epon 1007 n=11, Eponol n=90

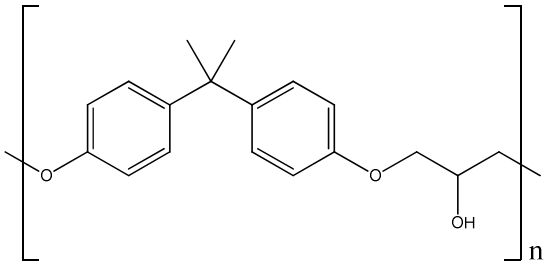

Figure 10. Phenoxy Resin PKHH Mw=19,500g/mol

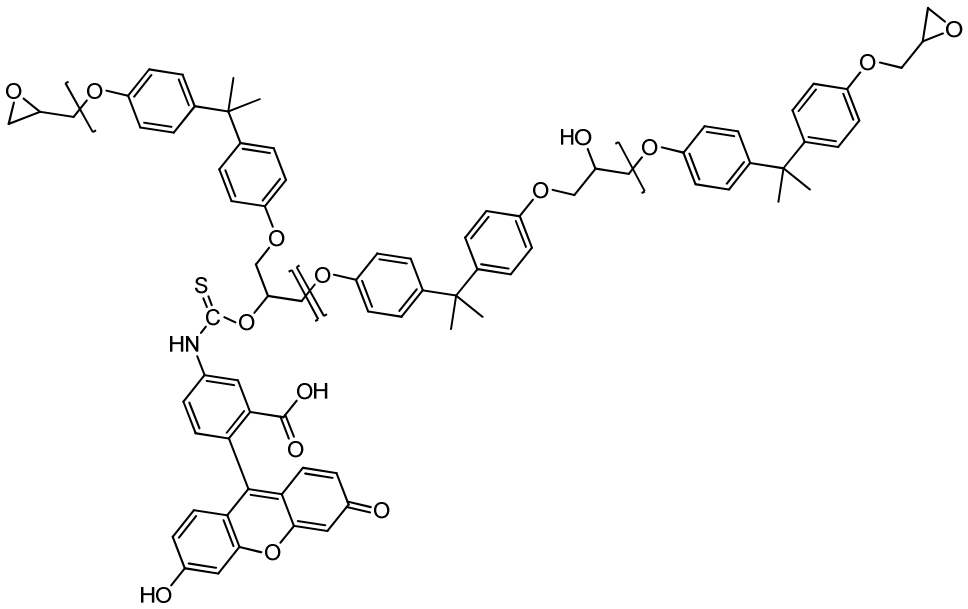

Figure 11. pH Stimuli Responsive Phenoxy Polymer (PKHH-FITC)

Amines/Crosslinkers

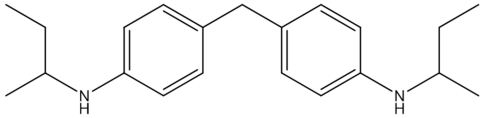

Figure 12. Polylink 4200 [4,4'-methylenebis (N-sec-butylaniline)]

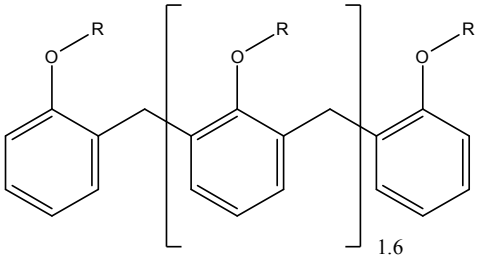

Where the R group is -

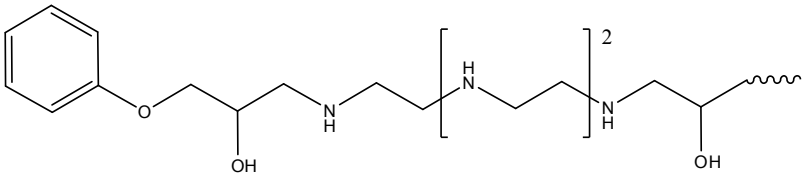

Figure 13. Epikure 3292

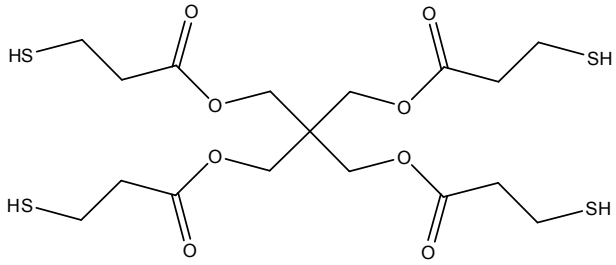

Figure 14. Pentaertyhritol Tetrakis(3-Mercaptopropionate)

Fluorescent Molecules

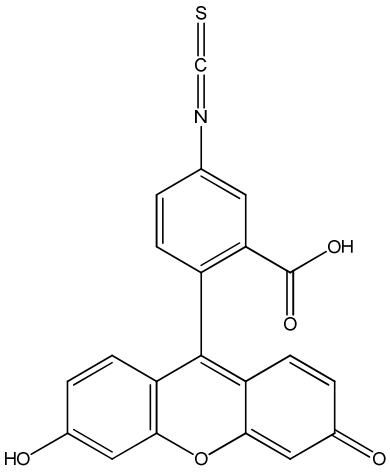

Figure 15. Fluorescein Isothiocyanate (FITC)

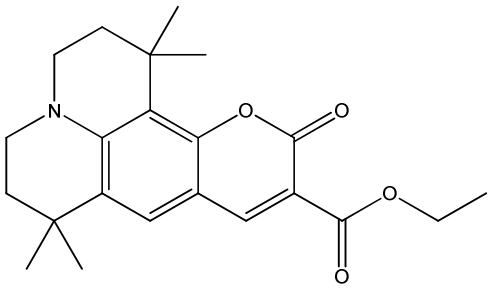

Figure 16. Coumarin 314T

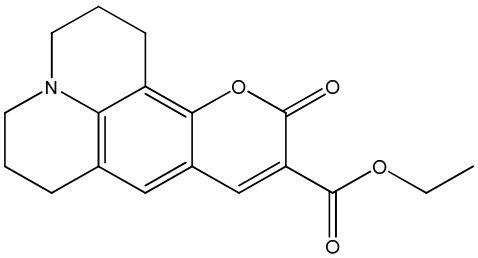

Figure 17. Coumarin 314

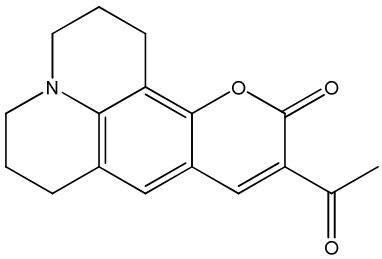

Figure 18. Coumarin 334

Experimental Procedures

Validation of Thermoplastic Anti-Corrosion Performance

For the comparison of thermoset to thermoplastic coatings, a comparison study was conducted using the formulations found in Table 2 and Table 3. Both pigmented and non-pigmented samples were tested, where the non-pigmented had the same levels of epoxy and amine without any other additives listed in either table.

Table 2

Pigmented Thermoset Epoxy-Amine Formulation

Material	Grams
Part A	
EPON 1007-HT-55	163.94
EPON 1001 80	97.58
Anti-Terra U	1.03
Xylenes	32.63
Ektasolve EEP	39.62
Ti Pure R706	26.10
ZP-10 Zinc Phosphate	36.00
Sparmite Barium Sulfate	90.00
Zeeosphere 400	81.00
Strontium Chromate	180.00
Water Ground Mica 325 Mesh Ball Mill to Hegman 7	24.12
Total Part A	772.02
Part B	
Epi-Cure 3292-FX-60	61.08
Total	833.10

Table 3

Pigmented Thermoplastic Epoxy Formulation

Material	Grams
Part A	
Eponol 53-BH-35	204.88

Table 3 (continued).

Material	Grams
Solvent	189.97
Anti-Terra U	1.03
Ti Pure R706	26.10
ZP-10 Zinc Phosphate	36.00
Sparmite Barium Sulfate	90.00
Zeeosphere 400	81.00
Strontium Chromate	180.00
Water Ground Mica 325 Mesh Ball Mill to Hegman 7	24.12
Total Part A	833.10

Once fully blended and mixed, the formulated samples were stored for 24 hours and then cast on untreated, acetone degreased Al-2024 substrates via a 6 mil draw down to produce films with an approximate 1 mil dry film thickness (consistent draw rate and solids to normalize thickness) and allowed 7 days ambient STP residence time before we performed additional testing. For a direct comparison, these two cure/dried formulations were exposed in ASTM B 117 testing for a qualitative analysis and validation of the thermoplastic polymers are able to perform similarly with as a well-developed thermosets coating formulation.

Synthesis of High Molecular Weight Thermoplastic (HMWTP) Epoxy/Amine

The different Epon resins were solubilized in a 4.89:1 wt. mixture of PGPE and PMA and allowed to mix for one week to ensure complete dissolution (56% solids). Polylink 4200 was then added at a stoichiometric balanced (1:1) ratio of epoxides to replaceable amine hydrogens. The targeted molecular weight was one of several aspects towards the studies objectives. It was also thought to be important to utilize the varying the epoxy block lengths, i.e., distinct epoxy block starting molecular weights, to enable a varied final resulting nitrogen content. For instance, Epon 828 blended with Polylink

4200, theoretically results in 4% final nitrogen content while, the higher molecular weight Epon 1007 singularly, and a 50:50 blend of Epon 1001/1007 resulted in nitrogen contents of 0.65% and 1%, respectively. The HMWTP copolymers were compared to the control and commercial epoxy resin, Eponol measured in our labs as 16,800 g/mole (Mn) and a polydispersity of 2.48 while being composed in the main from DGEBA and Epichlorohydrin and containing no detectable nitrogen (0% nitrogen). Each of these polymers were of sufficient molecular weight to provide excellent coatings properties as shown in Table 9 in Chapter III.

After several hours of mixing, approximately 300g of the homogeneous blend of Epon and Polylink 4200 was added to the reaction set-up that consisted of a 500 mL three-neck round-bottom flask equipped with a condenser, a mechanical stirrer, and a nitrogen purge. The mixture was heated under controlled conditions to 120°C within 30 min and held for 48 hours. The reaction was cooled to 20°C over 30 min while diluting with MEK to facilitate easy discharge. The polymer was purified via an acetone wash and dissolved in THF for storage. [79,80]

Film preparation and experimental procedure for degradation studies

Prior to exposure, polymers were cast on untreated, acetone degreased Al-2024 substrates via a 6 mil draw down to produce films with an approximate 1 mil dry film thickness (consistent draw rate and solids to normalize thickness). Coatings were then exposed to ASTM B 117 (with and without a scribe), QUV, and thermal weathering while monitoring the IR spectra, T_g, and molecular weight.

Methods of exposure for degradation studies

Salt fog accelerated weathering was performed as guided by ASTM B 117 and panels were evaluated using both virgin and scribe panels to delineate between any

potential subtle but important substrate corrosion driven rate and mechanism differences for bond scission or rearrangement.

The QUV weatherometer was operated in cycles of 340 nm UVA (4 hours at 60°C) and condensation (4 hours at 40 °C) according to ASTM D 4587. Thermal degradation was accomplished in an forced fan electric oven at 105 °C equipped with desiccant to ensure zero percent humidity.

Coumarin Dye Loading Levels

Into a glass vessel, 2.5 mL of 3.21 x 10^{-5} M of Coumarin 314T, 314 or 334 was added with acetonitrile or a solvent mixture of methyl ethyl ketone and propylene glycol propyl ether (MEK/PGPE). Then each solution was injected with a preparation consisting of the same solvent combination of 0.01 M magnesium salt (magnesium perchlorate or magnesium chloride) with a volume of 2.5 µL repeating from zero to nineteen injections. The solutions were incubated for 24 hours and characterized by absorbance and fluorescence measurements.

Phenolphthalein Loading Levels in Epoxy

Pure phenolphthalein was incorporated into a HMWTP epoxy coating at approximately 0.25%, 1.00%, and 10.00% by weight on the resin. A coating without any phenolphthalein was employed as the control. The resins were applied to QD-36 panels via a 6 mil draw down applicator. After drying for a week at ambient conditions, the panels were annealed for 24 hours at 75°C to remove any residual solvents and improve adhesion. The panels were scribed and immersed in salt water (5% NaCl solution) for 46 hours.

Synthesis pH Stimuli Responsive Polymer

Approximately 7.39g of a standard phenoxy resin PKHH (MW≈18000g/mol, FEW=286.32g/mol) was dissolved in 120mL of N,N-dimethylformamide (DMF) at 50^{o}C while stirring under nitrogen atmosphere. Once PKHH was dissolved, the mixture was then allowed to heat to 120^{o}C. Subsequently, FITC (389.38g/mol) was added in a 10:1 molar ratio of PKHH's hydroxyl to FITC's isothiocyanate group. Approximately 50mL of additional DMF was added to ensure complete addition of FITC. The reaction was monitored for 72 hours with thin layer chromatography (mobile phase - 9:3:1 Chloroform:Ethanol:Hexanes by wt.). After completion, the yellow-orange polymer was purified with repeated methanol/chloroform precipitation cycles until all unreacted FITC was removed. [51] Polymers PF.1, PF.2, PF.3, PF.4, PF.5, and PF.6 were prepared in this manner.

The last batch synthesized followed a procedure that attached FITC to dextran polymers. [81] Approximately 53.33g of a standard phenoxy resin PKHH (MW≈18000g/mol, FEW=286.32g/mol) was dissolved in 490mL of dimethyl sulfoxide (DMSO) at 50^{o}C while stirring under nitrogen atmosphere with 60 drops of pyridine. Once the PKHH dissolved, 187.6μL of dibutyl tin dilaurate was added to the solution and it was allowed to heat to 95^{o}C. Subsequently, FITC (389.38g/mol) was added in a 72.1:1 molar ratio of PKHH's hydroxyl to FITC's isothiocyanate group. Approximately 10mL of additional DMF was added to ensure complete addition of FITC. After 2 hours, the yellow-orange polymer was purified with repeated methanol/chloroform precipitation cycles until all unreacted FITC was removed. [51] Polymer PF.7 was prepared in this manner.

Grafting Efficiency of FITC to PKHH

To measure the grafting efficiency of FITC to the polymer, UV-VIS spectroscopy was used. The sample preparation included 7.8 micrograms of the PKHH-FITC polymer in 1mL of potassium hydroxide saturated DMF. This was measured against a FITC standard that was 0.78 micrograms of FITC in 1mL of potassium hydroxide saturated DMF. Four samples of each kind were measured by UV-VIS spectroscopy. An average absorbance at 517nm was then calculated for the FITC and the polymer sample in order to determine the concentration of FITC in the polymer with Beer's Law.

Diffusion versus corrosion studies

Following synthesis, the polymer was dissolved into ethyl 3-ethoxypropionate (EEP). The PKHH-FITC polymer was present at 20% solids. Another coating was made by dissolving PKHH polymer in EEP at the same concentration. Steel panels (QD-36) were used as the substrate that measured 4 inches long by 2.5 inches wide. All panels were equipped with a three-layer coating. An 8 path thin film applicator was used to apply all three layers. Each layer was applied 2 mils thick. Each panel was coated with two layers of PKHH polymer and one layer of PKHH polymer containing FITC. Coatings were named according to which layer contained FITC. If the layer closest to the QD-36 surface contained FITC, the panel was a "bottom coat" panel, if the layer furthest from the surface contained FITC, it was a "top coat" panel, and if the layer containing FITC was one layer away from the surface, it was a "mid coat" panel, as shown in *Figure 19*.

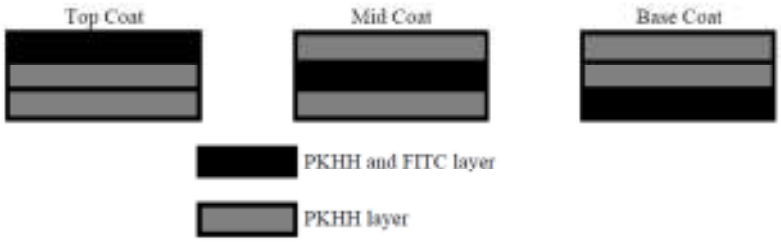

Figure 19. Schematic of Film Naming System

Table 4

Solutions Schematic

Solvent Composition Deionized H_2O:DMF	Solute in 1M Concentration
100% Deionized H_2O	None
100% Deionized H_2O	None
100% Deionized H_2O	NaOH
100% Deionized H_2O	NaCl
9:1	NaOH
9:1	NaCl
8:2	NaOH
8:2	NaCl
7:3	NaOH
7:3	NaCl
6:4	NaOH
6:4	NaCl
5:5	NaOH
5:5	NaCl

After each layer was applied, the panels were allowed to dry in a sequestered lint-free environment. This prevented dust and other contaminants from introducing variables to the film during the one week of ambient drying. Once all layers had been applied and dried, the panels were annealed in an oven at 75^{o}C for 24 hours. After they had been annealed, the thicknesses of the films on all panels were measured with a film thickness gauge and recorded (0.55-1.00 mil). All panels were masked with Shercon PC21

polyester film with a silicone adhesive. Once all panels were coated, measured, and sealed, they were subjected to the conditions seen in Table 4.

A new condition was introduced each week, and monitored rigorously during that week. Subsequent testing reduced to once a week until a satisfactory amount of time was given for diffusion and corrosion. Stock solutions were made for each of the conditions in Table 1. To subject the panels to the solutions, the panels were adhered into a uni-well plate, and then 35mL of stock solution was poured into the uni-well plate. The top of the plate was sealed with a Mylar film followed by the lid of the uni-well plate securely on top.

Titrations of 1M Water:DMF solutions

Using 1M NaOH solutions with 100% water to 91% water by volume containing dimethylformamide, 1.000 mL was titrated with 0.10M HCl. Using a few drop of either phenolphthalein, methyl red, bromophenol blue, or thymol blue, the endpoint was found and recorded. The results were compared to each indicator to see if DMF has changed the amount of base in the system.

Diffusion comparison with control substrate

The pH stimuli responsive polymer was dissolved into ethyl 3-ethoxypropionate (EEP). The PKHH-FITC polymer was present at 20% solids. Another coating was made by dissolving PKHH polymer in EEP at the same concentration. Steel panels (QD-36) and Shercon PC21 polyester masking tape were used as the substrate that measured 4 inches long by 2.5 inches wide. All panels were equipped with a three-layer coating. An 8 path thin film applicator was used to apply all three layers. Each layer was applied 2 mils thick. Each panel was coated with two layers of PKHH polymer and one layer of PKHH polymer containing FITC. Coatings were named according to which layer

contained FITC. If the layer closest to the QD-36 surface contained FITC, the panel was a "bottom coat" panel, if the layer furthest from the surface contained FITC, it was a "top coat" panel, and if the layer containing FITC was one layer away from the surface, it was a "mid coat" panel, as shown in *Figure 19*. After each layer was applied, the panels were allowed to dry in a sequestered lint-free environment. This prevented dust and other contaminants from introducing variables to the film during the one week of ambient drying. Once all layers had been applied and dried, the panels were annealed in an oven at 75^{o}C for 24 hours. After they had been annealed, the thicknesses of the films on all panels were measured with a film thickness gauge and recorded (0.75-1.20 mil). All panels were masked with Shercon PC21 polyester film with a silicone adhesive. Once all panels were coated, measured and sealed, they were subjected to 99:1 water to DMF solutions containing either 1M NaOH and 1M NaCl.

Sodium chloride concentration versus corrosion

The PKHH and PKHH-FITC polymer was dissolved into Ethyl 3-Ethoxypropionate (EEP) at 20% solids. The PKHH-FITC polymer was cast with an 8-path thin film applicator at 2 mils wet film thickness onto ASTM A1008 D609-Type3 steel substrate followed by an intermediate and top coat of PKHH applied by the same method. After film formation, the dry film thickness was measured at approximately 1 mil. The panel was masked with a polyester film with a silicone adhesive and secured into an OmniTray 1536 single-well plate. Next, 35 mL of either 0.00, 0.01, 0.10, 0.50, 1.00, 3.00, or 5.00M NaCl aqueous solution was poured onto the coated steel, and the well plate was sealed with a Mylar® film and lid. The fluorescence intensity (excitation 517 nm and emission 543 nm) was measured periodically over the entire panel at every square millimeter.

Halide salt versus corrosion

The PKHH and PKHH-FITC polymer was dissolved into Ethyl 3-Ethoxypropionate (EEP) at 20% solids. The PKHH-FITC polymer was cast with an 8-path thin film applicator at 2 mils wet film thickness onto ASTM A1008 D609-Type3 steel substrate followed by an intermediate and top coat of PKHH applied by the same method. After film formation, the dry film thickness was measured at approximately 1 mil. The panel was masked with a polyester film with a silicone adhesive and secured into an OmniTray 1536 single-well plate. Next, 35 mL of either 0.50 M NaF, NaCl, NaBr, NaI or deionized aqueous solution was poured onto the coated steel, and the well plate was sealed with a Mylar® film and lid. The fluorescence intensity (excitation 517 nm and emission 543 nm) was measured periodically over the entire panel at every square millimeter.

Substrate Comparison

The PKHH and PKHH-FITC polymer was dissolved into Ethyl 3-Ethoxypropionate (EEP) at 20% solids. The PKHH-FITC polymer was cast with an 8-path thin film applicator at 6 mils wet film thickness onto ASTM A1008 D609-Type3 steel, ASTM A 624 stainless steel, 3003 H14 aluminum, and Al-2024 aluminum substrates. After film formation, the dry film thickness was measured at approximately 1 mil. The panel was masked with a polyester film with a silicone adhesive and secured into an OmniTray 1536 single-well plate. Next, 35 mL of 1.00M NaCl aqueous solution was poured onto the coated samples, and the well plate was sealed with a Mylar® film and lid. The fluorescence intensity (excitation 517 nm and emission 543 nm) was measured periodically over the entire panel at every square millimeter.

Natural Weathering

The PKHH and PKHH-FITC polymer was dissolved into Ethyl 3-Ethoxypropionate (EEP) at 20% solids. The PKHH-FITC polymer was cast with an 8-path thin film applicator at 2 mils wet film thickness onto ASTM A1008 D609-Type3 steel substrate followed by an intermediate and top coat of PKHH applied by the same method. Two more sets of panels also had an additional topcoat to determine whether aliphatic or pigmented systems are able to deter photobleaching. Therefore a clear and pigmented acrylic (Joncryl 74A and DTM acrylic Primer/Finish respectively) were applied on top of the three layer system at 2 mil wet film thickness. After film formation, the dry film thickness was measured at approximately 1 mil for the non-acrylic top coated and 1.2 mil for the acrylic top coated. The panel was masked with a polyester film with a silicone adhesive and secured into an OmniTray 1536 single-well plate. Next, the sample was secured on a natural weathering stand on the roof of the Shelby F. Thames Polymer Science Research Center in Hattiesburg, MS angled at 45˚ facing due south. The fluorescence intensity (excitation 517 nm and emission 543 nm) was measured periodically over the entire panel at every square millimeter.

Characterization Techniques

Gel Permeation Chromatography (GPC)

Gel permeation chromatography was performed on a Varian PL GPC-50 equipped with dual angle light scattering, differential pressure, refractive index detectors, a series of four Polymer Laboratory columns (three Polypore and one 50 Å PLGel column), and the eluent (THF) at a flow rate of 0.8 mL/min at 40°C. An internal standard was used with fixed volume quantities of toluene and GPC data was collected from polystyrene

standards using corrected Mark-Houwink constants from literature, i.e., K and a values of 2.28 and 0.97, respectively. [82]

Differential Scanning Calorimetry (DSC)

Differential Scanning Calorimetry was used to obtain the T_g of the synthesized polymers using a DSC Q2000 (TA Instruments, Inc.) operated with a three cycle heat/cool/heat temperature profile (temperature range 0 - 150°C) with heating and cooling rates of 10°C/min. The T_g was calculated from the inflection point on the third DSC cycle.

Fourier Transform Mid and Near-Infrared Spectroscopy (NIR)

Fourier Transform Near-Infrared spectra (NIR) were obtained with an Antaris II FT-NIR Analyzer over a frequency range of 4,000 -10,000 cm^{-1}. The polymerization conversion was monitored following the disappearance of an epoxy peak (4527 cm^{-1}) and secondary amine peak (6678 cm^{-1}) while referencing the unchanging aromatic peak (4622 cm^{-1}). Meanwhile mid-IR spectra were obtained with a Thermo Scientific diamond ATR operating at 32 scans with a resolution of 2 cm^{-1} while following the peaks associated with degradation. [83]

Nuclear Magnetic Resonance Spectroscopy (NMR)

Nuclear magnetic resonance spectroscopy was obtained on a Varian Gemini 300 spectrometer operating at 300.13 MHz spectral frequency for proton. The spectra were acquired while sample were in solution ($CDCl_3$ or d-DMSO) at ambient conditions with tetramethyl silane (TMS) as an internal reference. Spectra were used to test the purity of monomer and the ability for secondary hydroxyls to react with FITC.

Ultraviolet-Visible Spectroscopy (UV-VIS)

Magnesium absorbance and fluorescence measurements were conducted using a TECAN Sapphire I spectrometer. Excitation wavelengths were chosen based on absorption maximum from UV-Vis analysis with a 2.5 nm width excitation using 10 flashes with a 10 μs delay before emission measurements.

Fluorescence Spectroscopy

Fluorescence spectroscopy was performed using an Infinite M1000 TECAN fluorescence spectrometer equipped with an auto stacker. Tests were performed for single intervals, and for kinetic intervals, that tested every hour for 16 hours at a time. The parameters used are in Table 5.

Table 5

Parameters for TECAN Cycles

Single Interval Mode		
Excitation Wavelength	517	nm
Emission Wavelength	543	nm
Excitation Bandwidth	5	nm
Emission Bandwidth	5	nm
Gain	75-131	Manual
Number of Flashes	10	
Flash Frequency	400	Hz
Integration Time	20	μs
Lag Time	0	μs
Settle Time	0-100	ms
Z-Position (Manual)	18050	μm
Kinetic Interval Mode		
Interval Time		1:00:00
Excitation Wavelength	517	nm
Emission Wavelength	543	Nm

Table 5 (continued).

Kinetic Interval Mode		
Excitation Bandwidth	5	nm
Gain	75-131	Manual
Number of Flashes	10	
Flash Frequency	400	Hz
Integration Time	20	µs
Lag Time		µs
Settle Time	0-100	ms
Z-Position (Manual)	18050	µm

Confocal Microscopy

Three-dimensional images that confirm the non-migratory behavior of tether FITC was captured using the Zeiss LSM 710 with an excitation of 488nm used to allow the fluorescent polymer to emit light and white light used to image the substrate surface. Images will provide the z-position the fluorescent polymer is away from the substrate depending whether it was cast in the top, middle, or base coat.

Colorimeter

Coating color was quantified with a BYK colorimeter using the color space L*, a*, and b*. Component L* represents the white and blackness of the coating with a high value representing more white. The next value, a*, represents the red and greenness of a coating where positive values are reddish and the negative values are greenish. Finally b* describes the blue or yellow color shown where positive values are more yellow and negative values are more blue. If this technique is used to detect premature triggering of phenolphthalein in a thermoset coating, a purple hue will be detected with a negative shift in b* and a positive shift in a*. If this behavior is noticed, the curing agent used for that

particular formulation will not be suitable for detecting corrosion, and another chemistry will have to be selected.

CHAPTER III

HIGH MOLECULAR WEIGHT THERMOPLASTIC MODEL POLYMERS

Introduction

Chapter I explores the most widely used anticorrosive coatings, which consist of two-component (2K) thermoset, epoxy-amine systems. Although they exhibit excellent application and performance characteristics, thermoset systems are not amenable to a broader and full set of characterization methods that can precisely quantify molecular level changes during environmental exposure. To purposefully define a starting point in quantifying and understanding the process of polymer/coating degradation, changes in molecular weight as a function of varying exposure including weatherability were monitored. The baseline of polymer performance was established by comparing the synthesized model high molecular weight thermoplastic polymers (HMWTP) and validating consistently these polymers in fully formulated coatings perform similarly with the traditional two component epoxy-amine coating systems via coating failure. The intended advantages were to (i) validate baseline performance and then evaluate the HMWTP while retaining the *in-situ* potential to re-introduced solvent to the exposed materials, and (ii) use any technique necessary for characterization. Dissociation energy of some common chemical bonds/linkages which are normally present in HMWTP model polymers are shown in Table 6. Similar to Musto and co-workers, FTIR was utilized as it tracks the change in functional group development of polymer properties to evaluate the degradation mechanisms.[83] Musto could have eliminated variables such as cure times, crosslinker ratio, side reactions with other formulation raw materials, and degree/heat of cure versus performance if he had used a thermoplastic system. Delineating between thermoset formation and polymer material failure mode was critical to move our

understanding forward and quantify exactly why and how certain polymers fail during utilization. The key was thus to understand which polymeric properties are involved in corrosion failure mechanisms. The use of a high molecular weight thermoplastic model polymer may reduce variables such as extent of reaction, kinetics, and characterization and simultaneously allow the influence of substrates, additives, and raw materials specifically required for corrosion mechanism. Basically, the application of high molecular weight model thermoplastic polymers eliminates the characterization required for *in-situ* polymer formation so that corrosion can be detected in the earliest possible stages. The first steps towards these goals were focused on detecting and quantifying the degradation effects of 1) ASTM B 117, 2) QUV, 3) thermal exposure using FTIR, DSC, and measuring the molecular weight and molecular weight distribution changes occurring during exposure on a variety of synthesized epoxy thin films.

Table 6

Dissociation Energy Values at 25 °C of Bonds Commonly Found in an Epoxy-Amine Coating [84]

Bond	kcal mol^{-1}	kJ mol^{-1}
O-H	110-111	460-464
C-H	96-99	400-415
C-O	85-91	355-380
C-C	83-85	345-355
C-N [85]	69-75	290-315

Validation of Thermoplastic Anti-Corrosion Performance

Before the synthesis of thermoplastic model polymers in the laboratory, it was determined whether commercially available thermoplastic epoxy resins could macroscopically supplement a thermoset epoxy-amine formulation. Eponol 53-BH-35 was used in comparison with a thermoset coating formulation, detailed in Chapter II, to prove that thermoplastics could provide the same qualitative corrosion performance as

traditional materials. Both polymer compositions were exposed to ASTM B 117 as a bare polymer and fully formulated with strontium chromate adhered to the Al-2024 aluminum metal. Non-pigmented coatings were used to determine whether each polymer was resistant to developing corrosion because the substrate was easy to monitor visually, through a clear film. Then the same set of experimental and commercial polymers were fully formulated with various pigments, including strontium chromate, to improve the barrier, inhibition, and the corrosion passivation ability of the coating. The use of pigment was monitored to establish whether thermoplastics are able to carry and facilitate dissolution of inhibitor pigments similarly with the traditional thermoset matrix materials and in turn deliver corrosion protection to aluminum substrates.

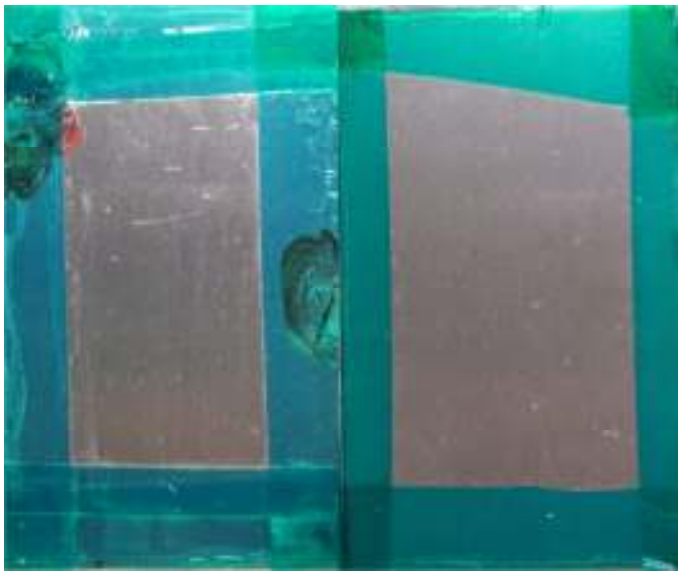

Figure 20. Non Pigmented Thermoset (left) and Thermoplastic (right) After 3000 Hours of ASTM B 117

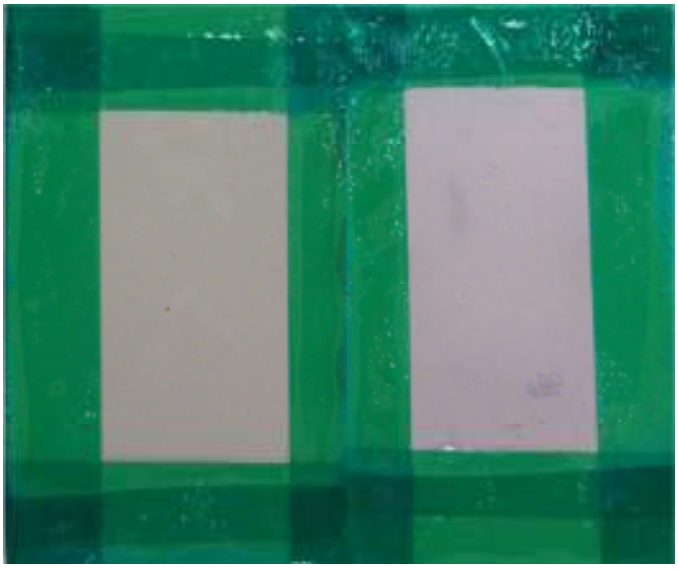

Figure 21. Pigmented Thermoset (left) and Thermoplastic (right) After 3000 Hours of ASTM B 117

Summarizing visually *Figure 20* and *Figure 21*, it appeared that thermoset and thermoplastic based coatings were visually identical after salt fog exposure for 3000 hours with or without pigmentation. Since the thermoplastic coatings were able to qualitatively pass the same corrosion testing standard as the thermoset, a series of thermoplastic models were synthesized to better represent the chemical basis/composition of a common epoxy-amine thermoset matrix and each of these was controllably degraded under several sets of conditions.

Synthesis of HMWTP Model Polymers

A high molecular weight thermoplastic epoxy-amine model polymer was synthesized by reacting an oligomeric epoxy with a secondary diamine at high solids content as shown in Scheme 1. [86,79,80] Epoxy-amine reaction, molecular weight, and glass transition temperature of synthesized thermoplastic polymers were characterized by near-IR, GPC, and DSC successfully.

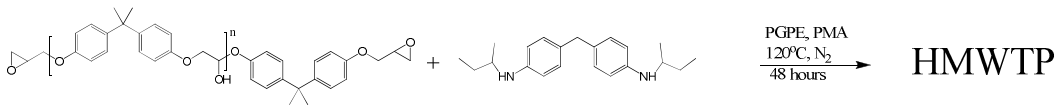

Scheme 1. HMWTP synthesis.

Table 7

Nitrogen Percentage for Varying Epoxy Lengths with Polylink 4200

Epon	828	1001	1002	1004	1001/1007	1007	1009
Repeat units (n)	0.13	2	2.5	5	-	11	14
%Nitrogen	4.00	2.00	1.75	1.35	1.00	0.65	0.45

Shown in Table 7, the epoxy-amine reaction specific to the copolymer(s) used will result in a specific % of nitrogen. Therefore, once the reactants were chosen for their potential variety in nitrogen content, FT-NIR was utilized to monitor characteristic bands of epoxy-amine system were observed at 6678, 4622, and 4530 cm^{-1} due to the presence of secondary amines, aromatics (phenyl), and epoxides respectively. [87,88] As shown in *Figure 22*, *Figure 23*, and *Figure 24*, the disappearance of peaks at 6678 cm^{-1} and 4530 cm^{-1} verified the reaction between the amine and epoxy groups, resulting in a polymer of 1% nitrogen, while the constant peak at 4622cm^{-1} indicated full retention of an the same concentration of the aromatic species, which were used as a spectroscopic internal standard for measuring/plotting conversion.

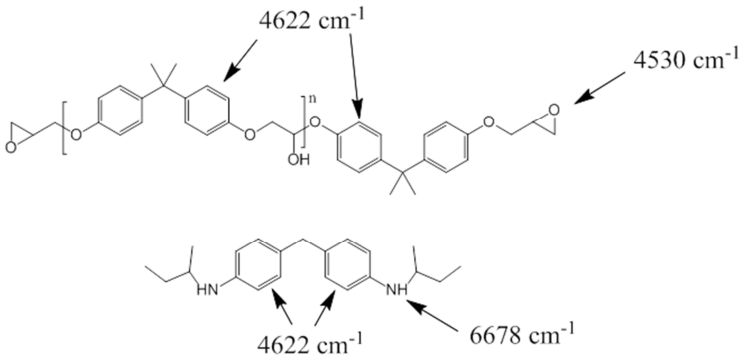

Figure 22. NIR Functionalities for Epoxy/Amine Reactions

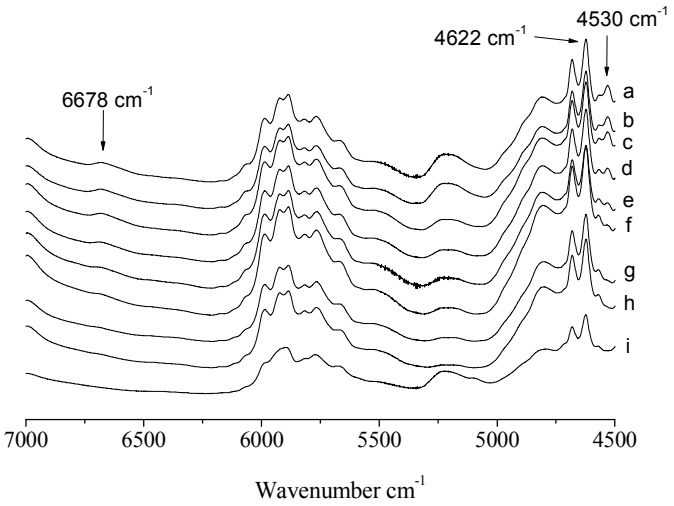

Figure 23. FT-NIR Spectra of an Epoxy/Amine Reaction. (a) t = 0 hour,(b) t = 0 hour (temp ramp), (c) t = 1 hour, (d) t = 3 hours, (e) t = 7 hours, (f) t = 12 hours, (g) t = 24 hours, (h) t = 36 hours, and (i) t = 48 hours (after cool down and MEK dilution).

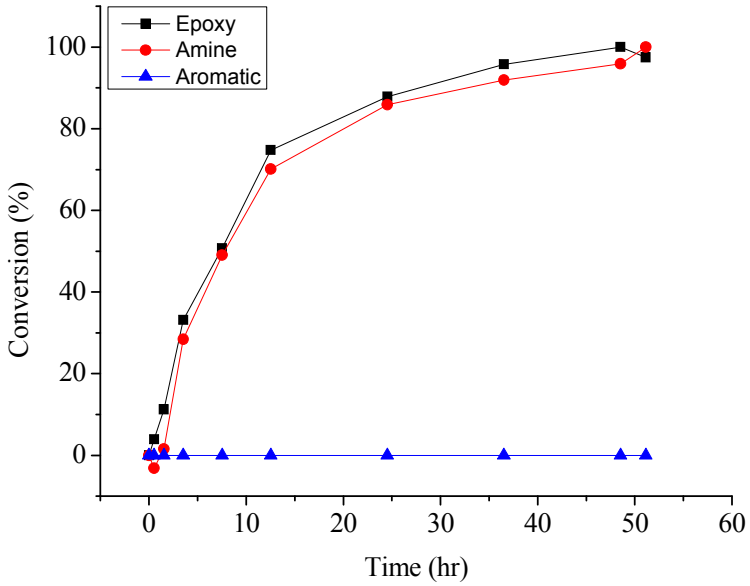

Figure 24. Conversion of Epoxy/Amine Reaction (1% Nitrogen).

The 4% and 0.65% nitrogen containing polymers used in this chapter were also synthesized while monitoring near-IR spectroscopy. The 4% nitrogen sample's conversion was easily monitored between the epoxy and amine (*Figure 25*) since well-defined epoxy and amine peaks were available using a low equivalent weight epoxy (Epon 828) which allowed the weight percentage of functional groups to be high for near-IR absorbance.

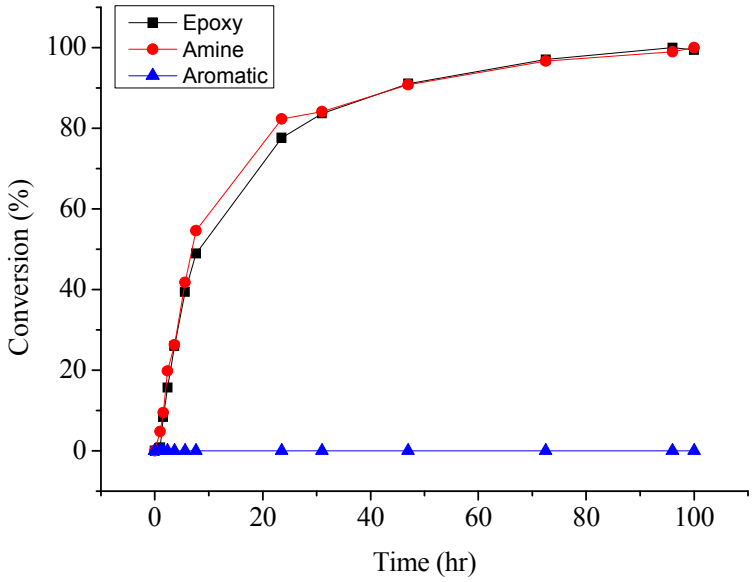

Figure 25. Conversion of Epoxy/Amine Reaction (4% Nitrogen).

The 0.65% nitrogen containing polymer proved more difficult to monitor conversion because the epoxy monomer, Epon 1007, has approximately eleven repeat units. Therefore *Figure 26* did not provide conclusive data on the epoxide conversion since the absorbance band at 4530 cm^{-1} starts at very low levels. The amine conversion followed previous trends seen in the 1% and 4% nitrogen polymers. Fortunately, further characterization through differential scanning calorimetry (DSC) and gel permeation chromatography (GPC) confirmed the synthesized polymers were advanced in molecular weight and attained the desired glass transition temperature and molecular weight respectively, as summarized in Table 8 and Table 9.

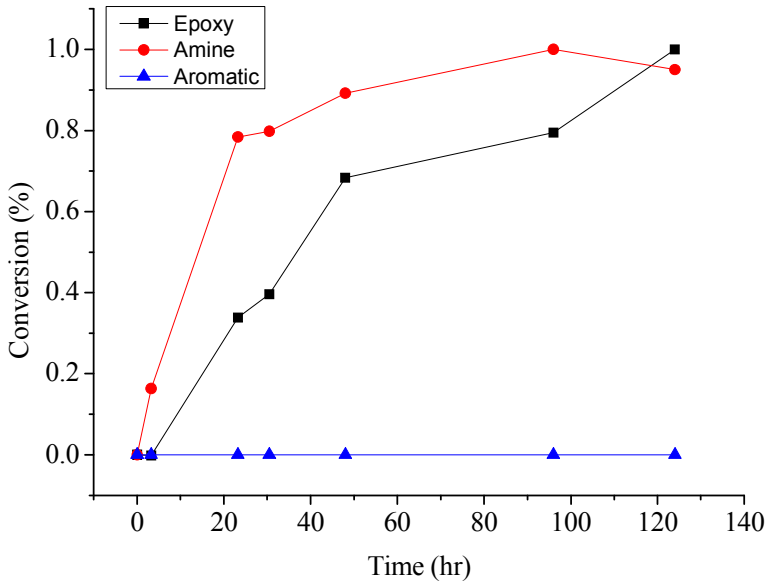

Figure 26. Conversion of Epoxy/Amine Reaction (0.65% Nitrogen).

Returning to the 1% nitrogen system as an example, the following molecular weight data describes the manner in which molecular weight was advanced and how the final materials were purified to capture a defined range of resulting model polymers. Characterizing the purified polymer via GPC consistently measured molecular weight increases in combination with low molecular weight oligomer consumption during the reaction between epoxide and amine (*Figure 27* and *Figure 28*). During the early oligomerization stages of the reaction, the higher molecular weight products eluted at 36.52 min correlated to a M_n of 2,200 g/mol and M_w of 6,690 g/mol (*Figure 27*c) for samples heated for only an hour. Meanwhile, as time progressed, elution times constantly shortened which is indicative of higher molecular weight (*Figure 27*d-h). After 48 hours of reacting, the high molecular weight peak shifted to shorter elution time, 34.55 min, with a M_n of 11,550 g/mol and M_w of 28,070 g/mol and the reaction was halted (*Figure 27*i).

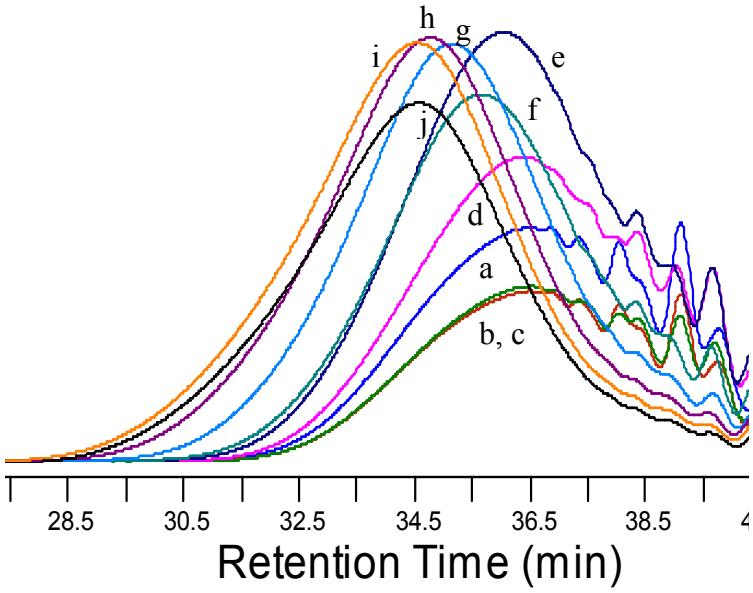

Figure 27. High MW GPC Profiles of an Epoxy-Amine Reaction. (a) t = 0 hour, (b) t = 0 hour (temp ramp), (c) t = 1 hour, (d) t = 3 hours, (e) t = 7 hours, (f) t = 12 hours, (g) t = 24 hours, (h) t = 36 hours, and(i) t = 48 hours (after cool down and MEK dilution).

While the high molecular weight was developing, oligomeric low molecular weight peaks at retention times of 46.2, 44.3, and 40.9 min (*Figure 28*) decreased in intensity in sequential order as each of these "mers" were consumed during polymerization. After approximately 36 hours, these three peak retention times of the starting materials (*Figure 28*a-g) supported a conversion attained of over 90%. Therefore, high molecular weight oligomers and polymer were the only detectable solution peaks. *Figure 29* represents a GPC trace for the washed final materials and confirms that acetone washing is a viable way to remove low molecular weight species and side products to yield a pure product that elutes at 33.77 min with a M_n of 25,700 g/mol and a M_w of 59,400 g/mol. [79,80]

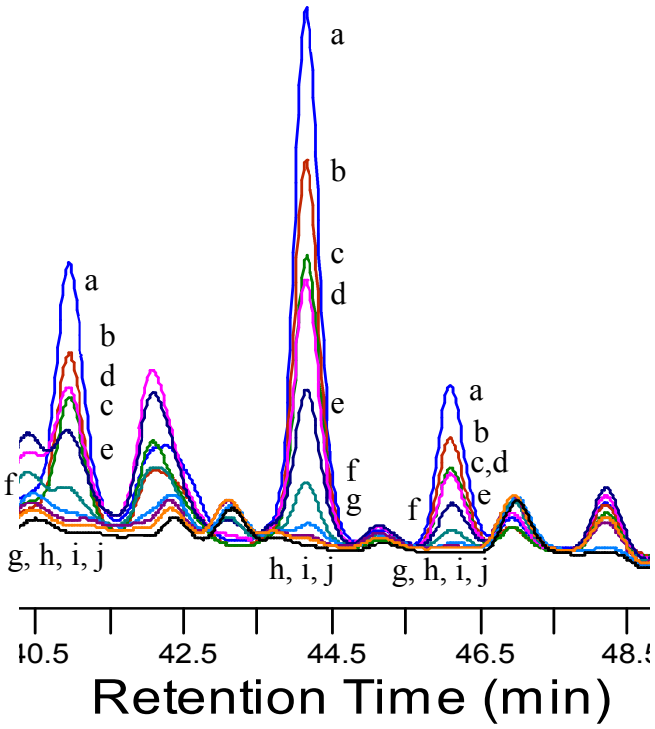

Figure 28. Low MW GPC profiles of an Epoxy-Amine reaction. (a) t = 0 hour, (b) t = 0 hour (temp ramp), (c) t = 1 hour, (d) t = 3 hours, (e) t = 7 hours, (f) t = 12 hours, (g) t = 24 hours, (h) t = 36 hours, and (i) t = 48 hours (after cool down and MEK dilution).

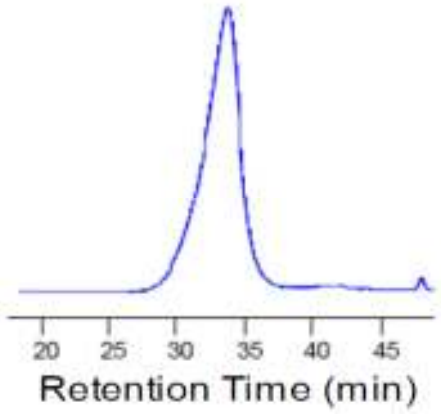

Figure 29. GPC Profile of HMWTP. After acetone wash to remove any low molecular weight impurities or insoluble products (prior to environmental exposure).

The T_g of the polymer containing 1% nitrogen varied drastically before and after purification via acetone wash (*Figure 30*). Prior to the wash, the T_g was recorded at

81.41 °C. Once the cyclic oligomers and other low molecular weight side-products were removed, the narrowed molecular weight thermoplastic result exhibited a higher T_g of 93.56 °C. [79,80] Each of the synthesized polymers was purified in this manner prior to final characterization. Table 8 and Table 9 display the final T_g and molecular weights for the three HMWTPs that were synthesized compared to the commercial HMWTP epoxy Eponol 53-BH-35 (absent nitrogen content).

Table 8

Initial T_gs of the Model Polymers used for Degradation Study

Percent Nitrogen Polymer	Initial T_g (°C)
4.0	80.85 ± 0.58
1.0	93.22 ± 0.36
0.65	95.09 ± 0.24
0.00	86.50 ± 0.69

Table 9

Initial Molecular Weights of the Model Polymers used for Degradation Study

Percent Nitrogen Polymer	Initial M_p (g/mol)	Initial M_n (g/mol)	Initial M_w (g/mol)	Initial PDI of High MW Peak
4.0	24,800	16,400	32,300	1.97
1.0	22,600	25,700	59,400	2.31
0.65	16,500	13,100	94,700	7.23
0.00	19,300	16,800	41,700	2.48

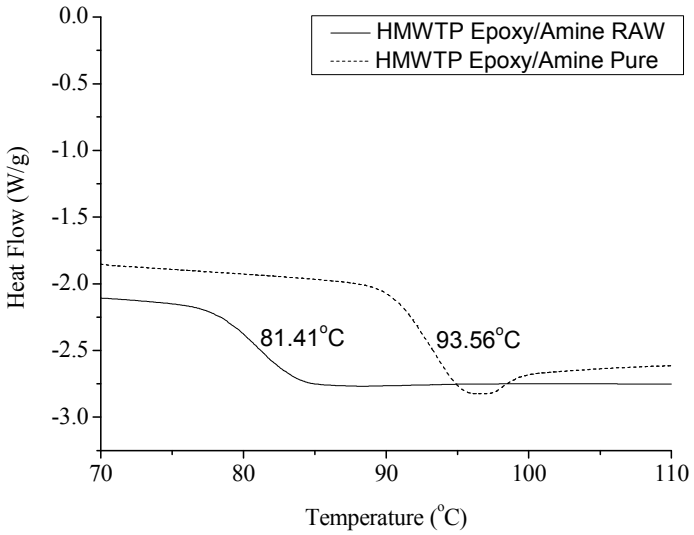

Figure 30. DSC of Raw and Purified HMWTP.

Post Exposure Characterization of HMWTPs

ASTM B 117

To mimic the most corrosive environment, samples were exposed to ASTM B 117 which applies a constant salt spray at 35˚C for 24 hours. Although there is not an environment in the real world that behaves in this manner, the testing protocol was designed to accelerate the corrosion process and reduce the necessary testing times compared with natural exposure/weathering. Many of the corrosion related literature available claim, even supplying cursory proof without definitive data that polymers chains and bonds are breaking over time as a means to provide explanation of the common coating system performance characteristics.[27,25,24,23,26,28] Polymeric materials often provide resistance to corrosion early and then at some maturation point the performance of the same materials diminishes rapidly and catastrophically. The same literature papers indicated that polymers have to degrade or these characteristic changes would not occur, i.e., often it is stated that bonds must break, in order for corrosion to

occur as previously described. [27,25,24,23,26,28] However, polymers perform many functions towards protecting a given substrate in order to reduce the water and oxygen permeation. Although the same polymers are susceptible to absorption of water, oxygen and electrolytes thereby facilitating greater and greater environmental drivers to shift a given materials starting point characteristics and performance. [20,21]

A set of questions we sought to answer include 1) whether polymers could resist corrosion initially and then begin to fail without chain scission? 2) whether any polymeric properties had detectable changes that prefaced corrosion while in environmental exposure? and 3) which characterization methods are the most sensitive to detect any material rearrangement or scission events?

The four HMWTP polymers were monitored via mid-IR versus exposure to determine if chain scission could be detected before, during, or after environmental exposure and accelerated weathering. Specific functional groups are more detectable and indicative of chain degradation and readily monitored by mid-infrared spectroscopy. The most definitive peak in mid-FTIR for early detection was thought to be the carbonyl and initially absent from the starting point polymers, both model and commercial. However, literature reports have defined the degradation related linkages common to DGEBA polymers are ketone, aldehyde, and amide bond formation that result from chain scission. The specific literature examples are summarized in *Figure 31* in combination with each respective mid-IR peak wavenumber. [83,90]

After exposing scribed and unscribed coated Al-2024 panels for 2000 hours, the mid-IR spectra (*Figure 32*) were consistently absent of any of these specific chain scission results (*Figure 31*). [83,90] These results support that within detectable limits,

bond rearrangement, degradation and chain scission are not requirements either before, during, and after corrosion in order to allow substrate corrosion.

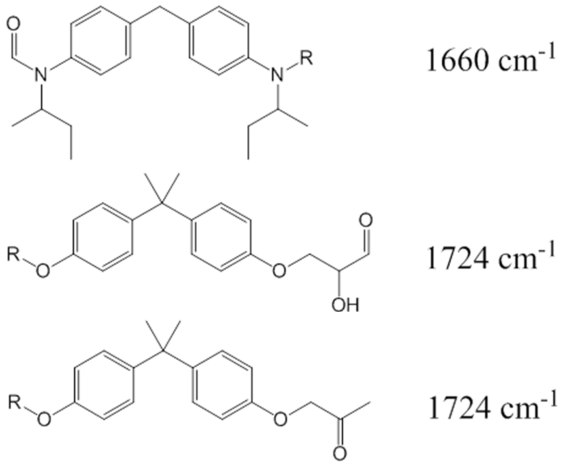

Figure 31. Functionalities Present During Epoxy/Amine Degradation and their Respective FTIR Absorbance.

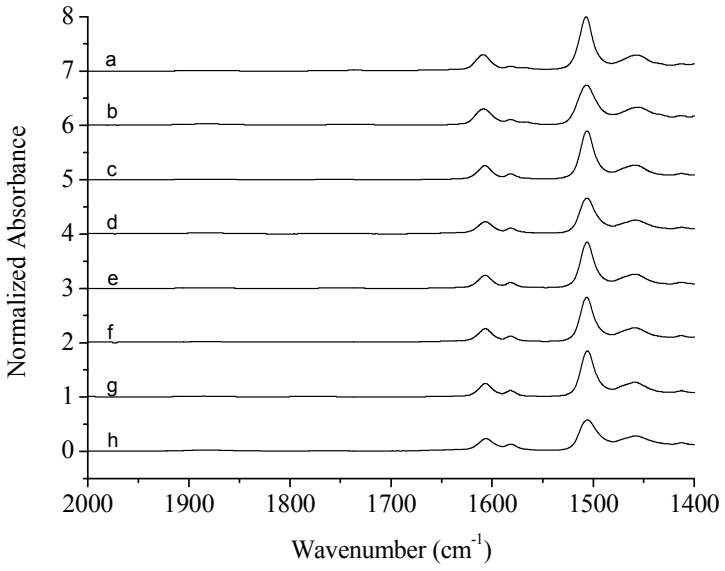

Figure 32 . ASTM B 117 exposure mid-IR spectra. (a) 4% N t = 0 hours, (b) 4% N t = 2000 hours, (c) 1% N t = 0 hours, (d) 1% N t = 2000 hours, (e) 0.65% N t = 0 hours, (f) 0.65% N t = 2000 hours, (g) 0% N t = 0 hours, (h) 0% N t = 2000 hours.

Figure 33 and *Figure 34* are the result of monitoring the glass transition temperature by DSC for the each of the salt water exposed polymer samples versus time

and directly compared with the starting material results. The decreased glass transition temperature was attributed to plasticization of polymer chains through increased water content (greater free volume, hydroplasticization, and slight swelling). These polymers absorb water and have inherent permeabilities to contaminants that cause corrosion.[21] Interestingly, samples which were scribed and unscribed resulted in depressed T_g's as follows based upon nitrogen content; 0.65% > 0% > 1% > 4% which mirrors the trend noted in the initial PDIs (Table 9). The influx of water enhances the unordered state of polymers that possess higher PDI and were less efficient in packing. Although the polymers continue to resist water penetration to the substrate, the data support that improved control over the polymerization results are important with specificity to water ingress rates and total water content after environmental exposure .

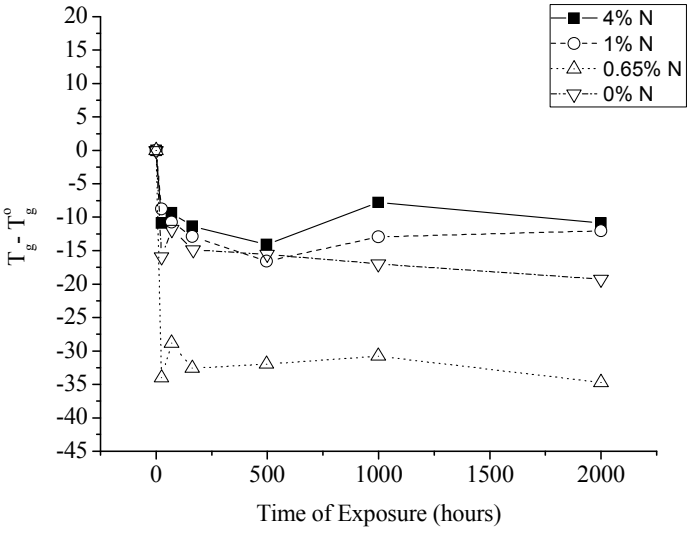

Figure 33. ASTM B 117 Exposure Change in the T_g for Unscribed Samples.

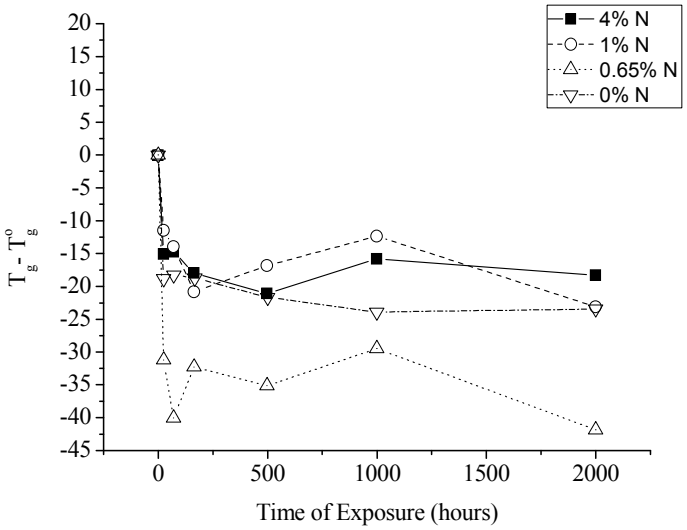

Figure 34. ASTM B 117 Exposure Change in the T_g for Scribed Samples.

Although water had sufficiently permeated the polymer, the molecular weight characterization by GPC confirmed that the molecular weight of the exposed samples were the same before and after exposure and therefore did not result in relevant chain scission events. The data further supports the previously reviewed mid-IR spectroscopy as the polymeric materials remain unchanged, indicating the absence of chain scission during exposure. The entire analogous series were measured periodically throughout the 2,000 hour environmental exposure span, *Figure 35*, *Figure 36*, *Figure 37*, *Figure 39*, *Figure 40*, and *Figure 41* inconclusively show a scattering of the molecular weight distribution while the PDIs in *Figure 38* and *Figure 42* are less scattered. A more in-depth look at the data suggests that the chromatogram peak shapes of each polymer are remaining constant and yet the average elution times are shifting slightly back and forth over the 85 days of exposure and characterization. The results support that water uptake and varying degrees of hydroplasticization and swelling were the driving force for the GPC variability. It can be rationalized that water plasticization and varying ratios of

swelling alter the polymer solubility in a given mobile phase, THF in this case, i.e., the polymer's radius of gyration during analysis. The radius of gyration influences the elution time and the average RI difference of a polymer through a GPC column to give varying values. [91] Meanwhile, PDI values remain almost identically constant (besides the 2,000 hour scribed polymer containing 0.65% N) as the chromatogram peak sizes remain the same despite the change in elution times.

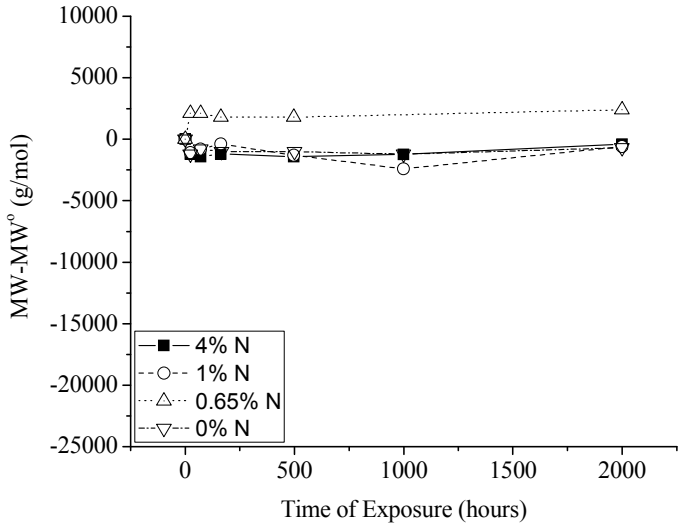

Figure 35. ASTM B 117 Exposure Change in Molecular Weight Peak-Average (Unscribed Samples).

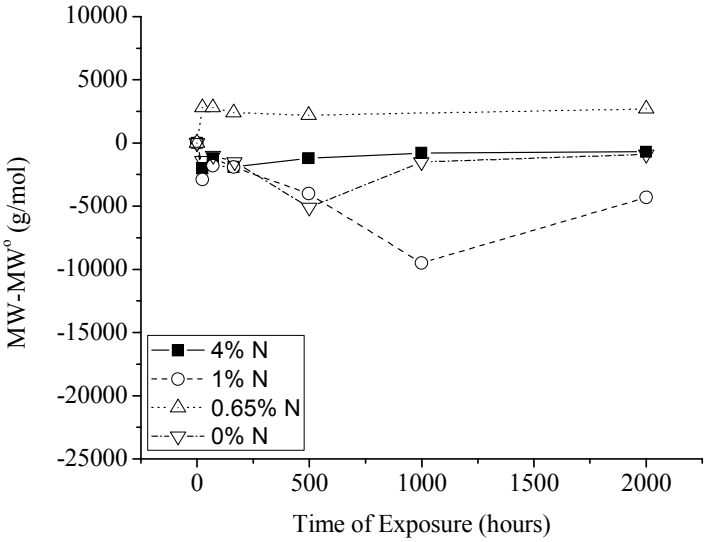

Figure 36. ASTM B 117 Exposure Change in Number-Average (Unscribed Samples).

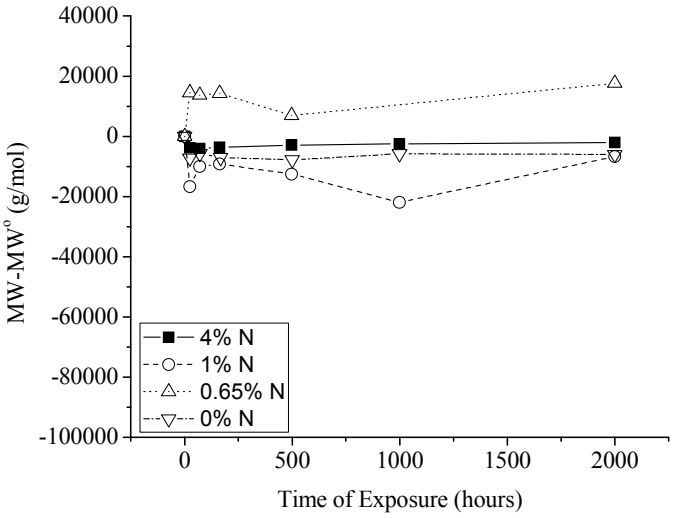

Figure 37. ASTM B 117 Exposure Change in Molecular Weight Weight-Average (Unscribed Samples).

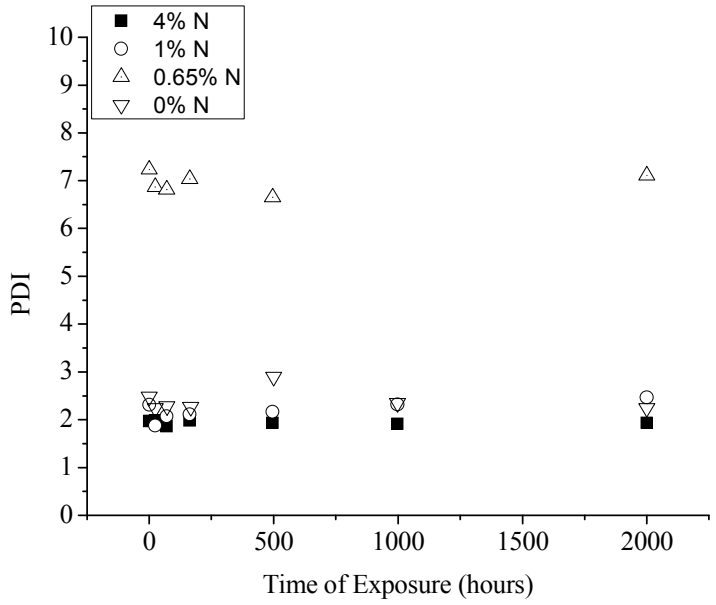

Figure 38. ASTM B 117 Exposure Change in PDI (Unscribed Samples).

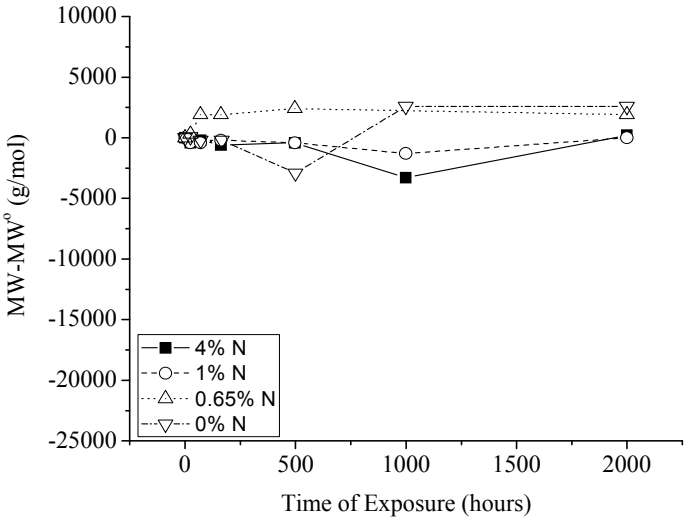

Figure 39. ASTM B 117 Exposure Change in Molecular Weight Peak-Average (Scribed Samples).

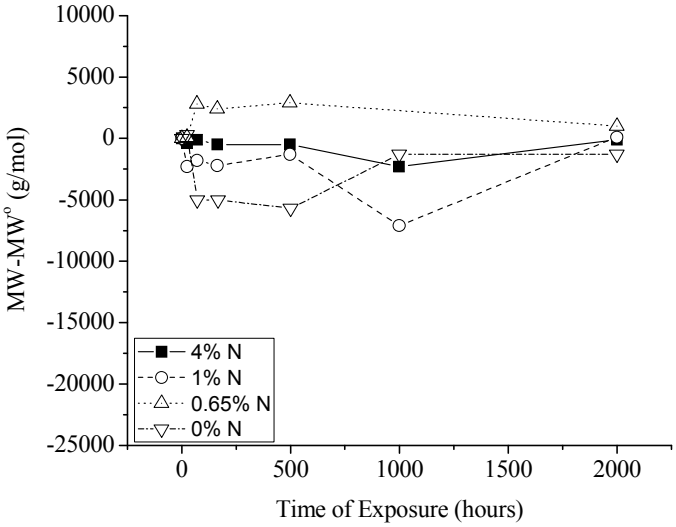

Figure 40. ASTM B 117 Exposure Change in Molecular Weight Number-Average (Scribed Samples).

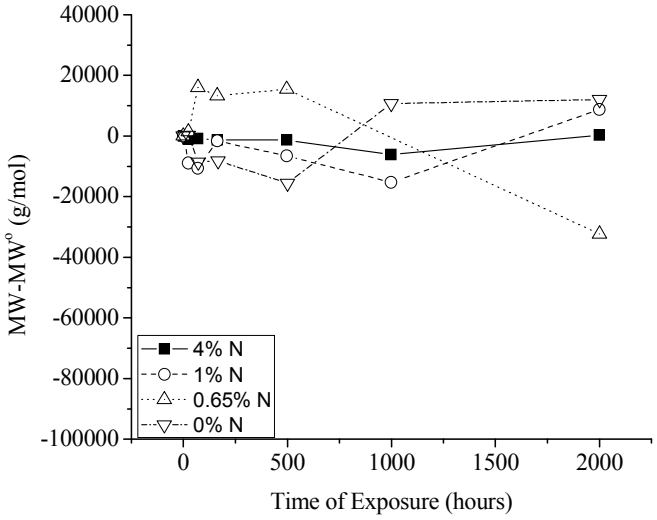

Figure 41. ASTM B 117 Exposure Change in Molecular Weight Weight-Average (Scribed Samples).

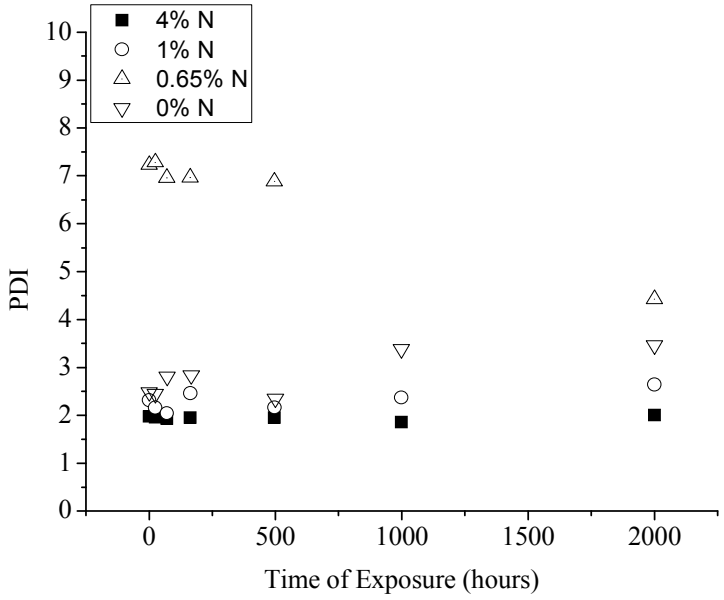

Figure 42. ASTM B 117 Exposure Change in PDI (Scribed Samples).

QUV

While ASTM B 117 represents exposure to salt water environments, QUV is used to demonstrate the power of solar radiation that is known to degrade DGEBA based polymers. Although aromatic polymers, like the ones used in this study, are typically used as primers and are commonly hidden from exposure to direct sunlight, the weathering method was still important in order to understand which bonds are susceptible to breaking that were expected to be seen in ASTM B 117. Upon exposure to UV radiation, rampant chain scission was observed regardless of nitrogen content, and mid-IR was able to distinguish between polymers with high and low nitrogen percentages. In *Figure 43*, the specimen containing 4% nitrogen exhibits a large increase in absorbance ratio of 1660cm^{-1} to 1724cm^{-1} relating to the formation of amide and ketone/aldehyde functionality as shown in several photodegradation studies, respectively. [83,90] With decreasing nitrogen content, the absorbance ratio of 1660cm^{-1} to 1724cm^{-1} also decreases as there is more availability for ketone and aldehyde

functionality to form during oxidation. Meanwhile, decreases in T_g due to the effects of chain scission seen in *Figure 44* are confirmed by molecular weight analysis in *Figure 45, Figure 46, and Figure 47.*

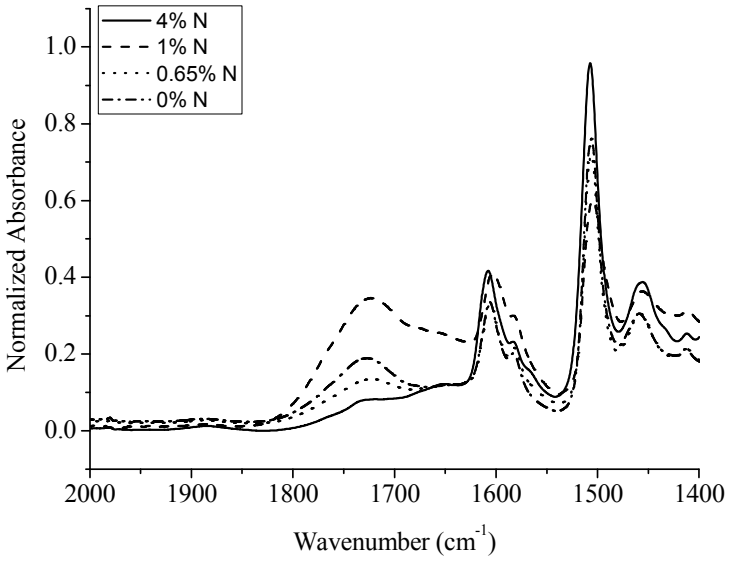

Figure 43. QUV Exposure Mid-IR spectra @ 1000 hours of Nitrogen Containing Polymers During QUV Exposure

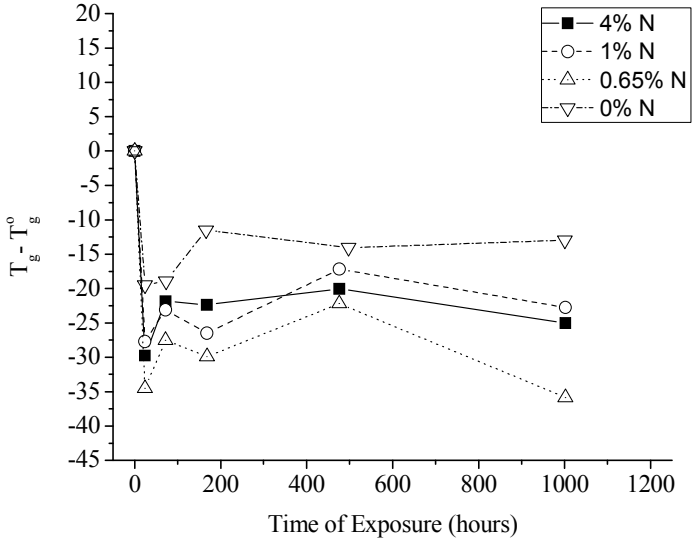

Figure 44. QUV Exposure Change in the Glass Transition Temperature Versus QUV Exposure

The comparison between the peak-average, number-average, and weight-average molecular weights in *Figure 45*, *Figure 46, and Figure 47* (respectively) exhibited that the nitrogen content, the initial molecular weight, and the PDI each need to be considered. The data support a selective QUV degradation whereby the UV exposure either statistically cleaves bonds that are in a higher quantity, or specifically cleaves the weaker bonds. Confirmation of either pathway can be determined by the order in which the polymers lost molar mass in relation to nitrogen content, initial molecular weight, or PDI (*Figure 48*).

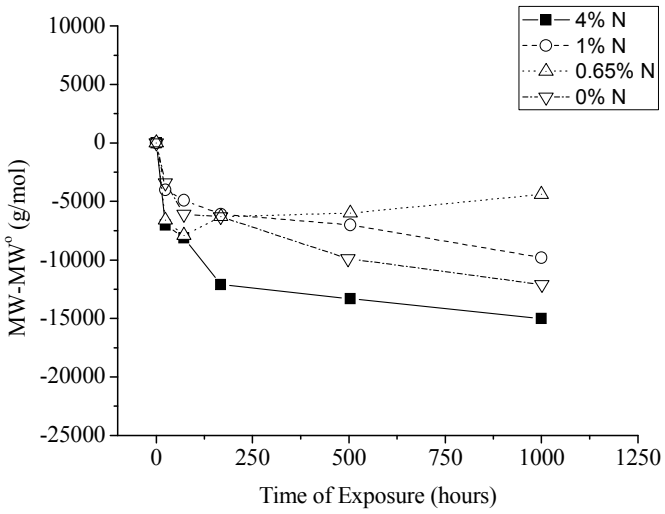

Figure 45. QUV Exposure Change in Molecular Weight Peak-Average.

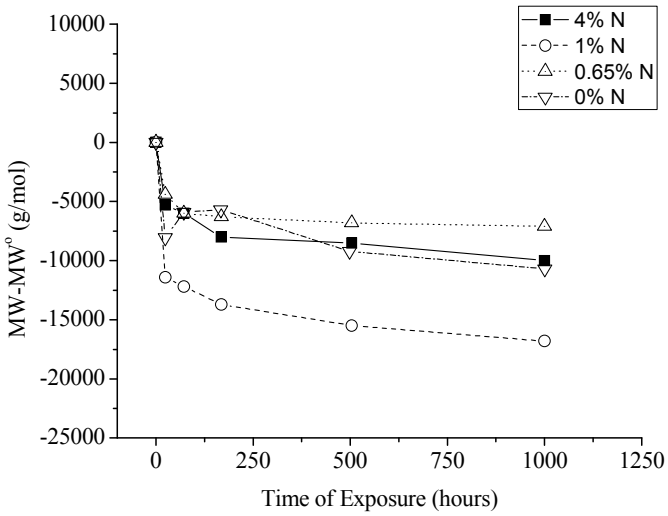

Figure 46. QUV Exposure Change in Molecular Weight Number-Average.

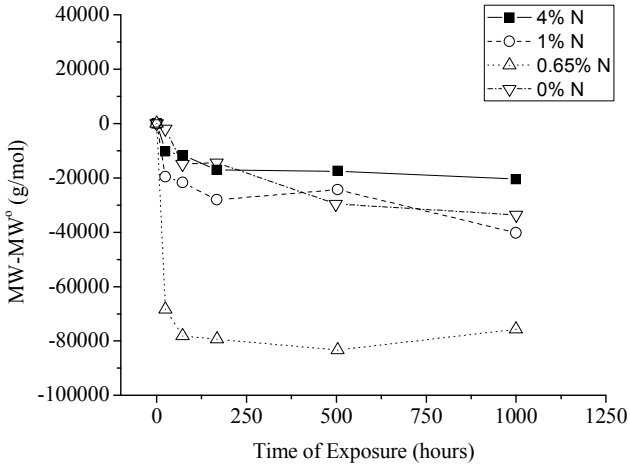

Figure 47. QUV Exposure Change in Molecular Weight-Average.

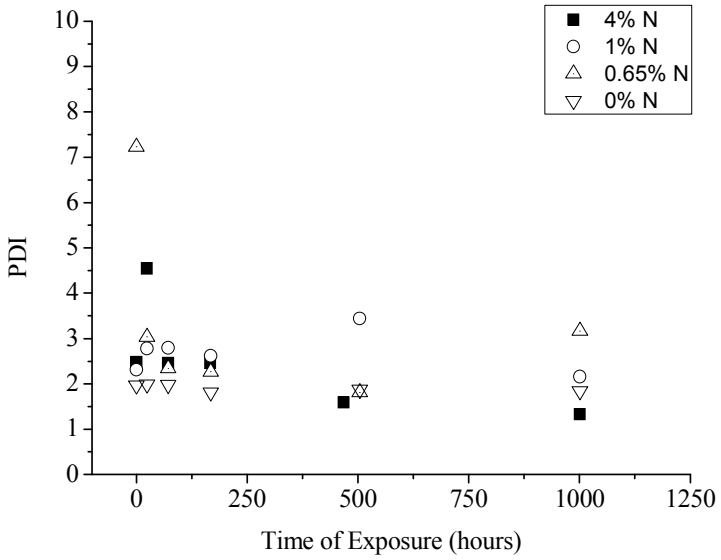

Figure 48. QUV Exposure Change in PDI.

The peak average molecular weight decreased most dramatically in the order 0.65%N < 1%N < 0%N < 4%N, i.e., polymers containing higher nitrogen content exhibited greater loss in molecular weight except for the control 0% nitrogen polymer. The control polymer system seemed to be an outlier from the consistent trend, however, Table 9 shows that the initial number-average molecular weight trended in the order of 0.65%N < 4%N < 0%N < 1%N and the degradation in number-average molecular weight followed the same order in *Figure 46*. Therefore the control sample of 0% nitrogen was determined to be a result driven by the larger quantity of bonds available for chain scission. Thus, particular bonds were broken more by quantity rather than by order of their strength. This suggests that degradation in the QUV was not bond selective and yet resulted in a greater quantity of scission events from longer polymer chains.

Scission events also exhibited a pattern with the weight-average molecular weight in the order of 4%N < 0%N < 1%N < 0.65%N, following the same order as that

of the initial PDI of each polymer (Table 3). Larger PDIs represented an increased fraction of high molecular weight chains. Increasing the quantity of these chains in the QUV allows for more chain scission (thought to be driven by the branching potential and specific linkages at these molecular weight ranges), thus they lose the most molecular weight during QUV exposure. However, after 24 hours of QUV exposure, the PDIs are approximately the same (Figure 48) and a plateau was noted in molecular weight losses.

Thermal Degradation (105°C)

Since ASTM B 117 did not show decreases in molecular weight and QUV showed seemingly rapid and dramatic decrease in molecular weight, thermal energy was applied singularly to the same set of polymers to evaluate material failure by another common energy input. Since each bond has specified bond strengths as summarized in Table 6, when thermal energy is used to degrade the model polymer, the samples with the most carbon-nitrogen bonds should exhibit the greatest amount of chain scission and thereby exhibit consistent trends in losses of molecular weight. If so, thermal degradation will confirm that molecular weight loss and chain scission occur differentially when a varying bond strengths of synthesized polymers. The results from extended time thermal exposure resulted in a consistent trend as was first detected via mid-IR spectra for the polymers containing 4%N, 1%N, and 0.65%N maintained a similar ratio of 1660 cm^{-1} to 1724 cm^{-1} while the 0% nitrogen polymer did not exhibit a peak at 1660 cm^{-1} (amide formation is not possible in the absence of nitrogen based bonds). Whereas QUV did not show preference for specific bonds during chain scission, thermal degradation at 105°C resulted in a direct correlation between the highest rate/quantity of chain scission and the highest polymer backbone containing nitrogen

content (*Figure 49*). T_g measurements also revealed another trend, where by the polymer containing 4% nitrogen were observed to exhibit higher T_g versus time and we attributed these material property changes to post excitation crosslinking via recombination of the products from scission events. The amount of T_g loss from chain scission (as seen in QUV) is less severe than expected as the excited stated/rearranged bonds were shown capable of undergoing crosslinking. The hypothesis was supported from observations revealed when preparing the samples for GPC characterization, as all each of the nitrogen containing polymers possessed THF insoluble portions after thermal exposure (THF is the mobile phase for all of the GPC data within this dissertation). Therefore, molecular weight losses measured in *Figure 51*, *Figure 52*, and *Figure 53* relate only to the linear polymer chains that were not further crosslinked after exposure and recombination/rearrangement.

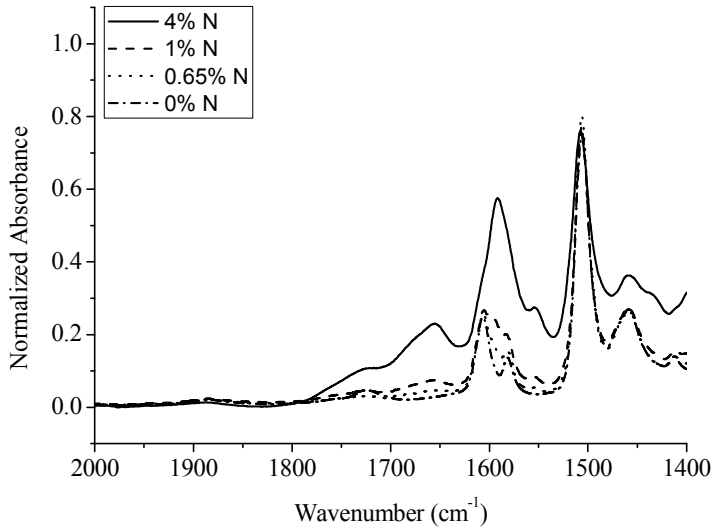

Figure 49. Thermal (105°C) Exposure Mid-IR Spectra @ 2000 Hours.

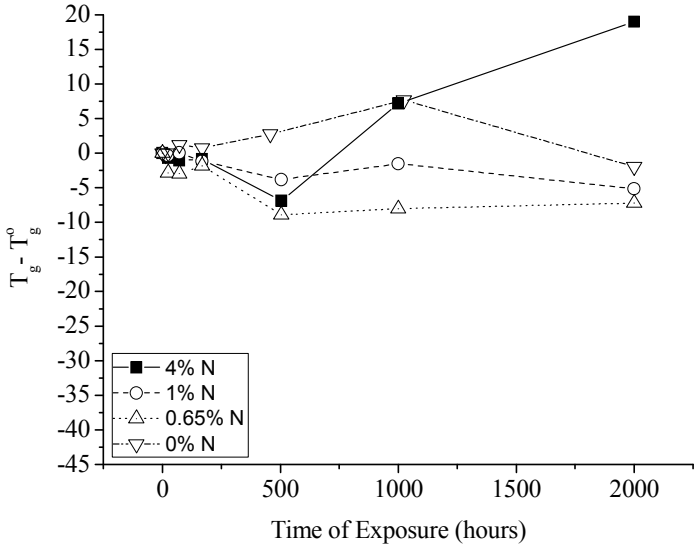

Figure 50. Thermal (105°C) Exposure Change in the Glass Transition Temperature

Peak-average molecular weight losses (*Figure 51*) occurred in the order of 0% < 0.65% < 1% < 4% since the increase in amine content increased the number of thermally weaker carbon-nitrogen bonds. However, the trend did not continue for the number-average molecular weight since the initial number-average molecular weight still contributed to molecular weight losses. When considering the weight-average molecular

weight and PDI (Figure 53 and *Figure 54*), the initial PDI still had a contributing factor in the loss of molecular weight. The change in PDI confirmed that polymer chain branching occurred. Thermal degradation, at the 500 hour time point, reconfirmed the 4% N polymer developed branches as recombination of cleaving chains occurred during exposure, while the 0.65% N polymer lost branch points during chain scission events that were developed during synthesis. The two systems increase to a PDI range of 5-6 then each decreased in PDI to approximately 2.5-3.5. Critical to remember, was that as these materials were similarly increasing PDI versus exposure, the total linear polymer portion able to be solubilized was consistently less and less of the actual exposed material as further degradation forced less and less linear non thermally degraded material e.g., gelled products out the practical accessibility for characterization since they were rendered insoluble in THF.

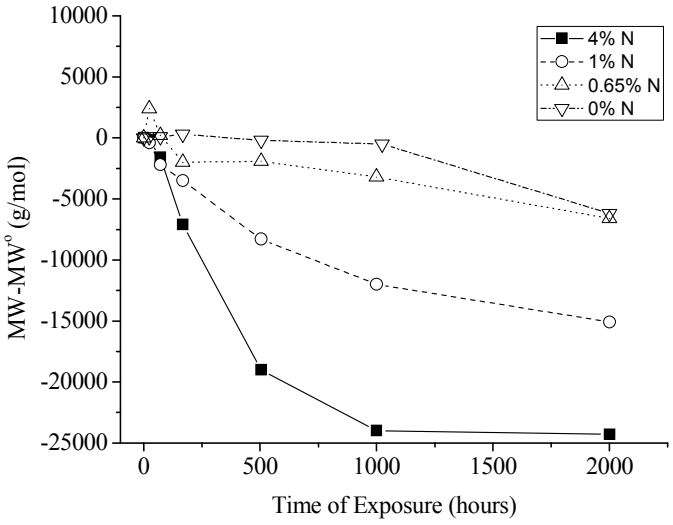

Figure 51. Thermal (105°C) Exposure Change in Molecular Weight Peak-Average.

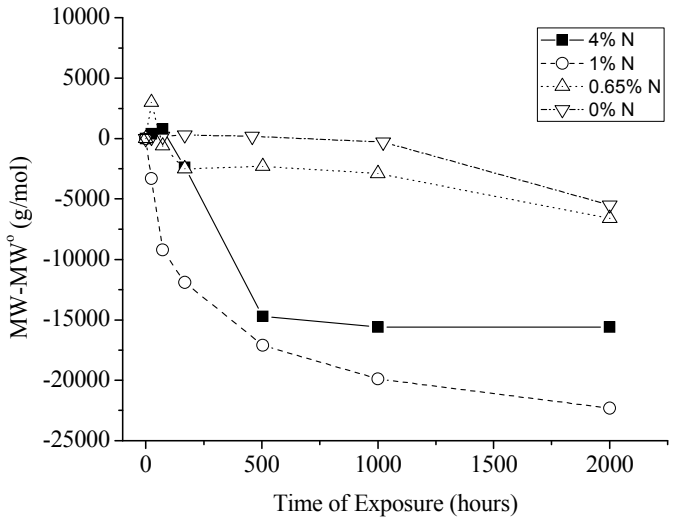

Figure 52. Thermal (105°C) Exposure Change in Molecular Weight Number-Average.

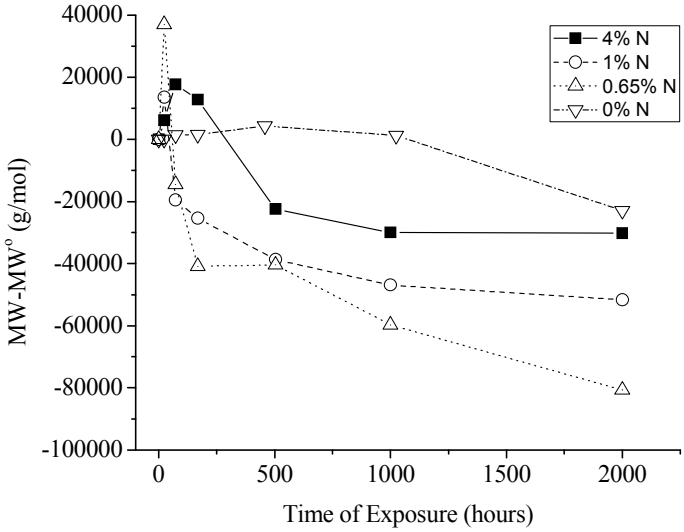

Figure 53. Thermal (105°C) Exposure Change in Molecular Weight Weight-Average.

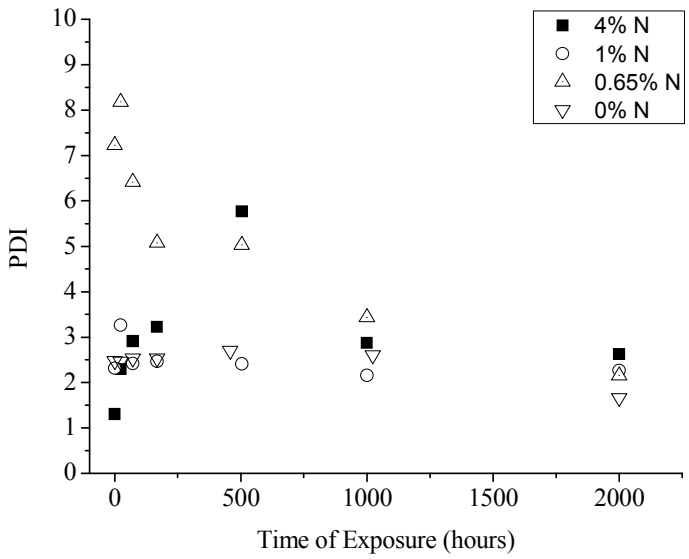

Figure 54. Thermal (105°C) Exposure Change in PDI.

Conclusions

The synthesis and characterization results provided a series of polymers with varying nitrogen content. Weaker bonds were incorporated into the polymer backbone, for several goals, to mimic the common range of nitrogen contents within normal thermosetting epoxy amine primers while allowing a broader range of more sensitive techniques for characterization before, during, and after environmental exposure.

Monitoring polymer degradation via mid-IR spectroscopy, DSC, and GPC, versus time of exposure from two of three environments, 1) QUV and 2) thermal environments provided consistent and conclusive results. QUV radiation induced chain scission events in DGEBA-based epoxy coatings and polymers with drastic reduction in the initial molecular weight. Although increasing the amount of what we considered to be the weaker bonds did not correlate directly with a quantifiable chain scission points. A caveat of concern is relevant since each resulting polymeric material was not initially the same molecular weight (very difficult to control) and therefore the starting length of

the polymer correlates with the total molecular weight loses. UV radiation was simply validated to degrade a polymer by the quantity of UV absorbing bonds available rather than the quality of bonds available. DGEBA based polymers are generally overwhelmed or saturated with chromophores and were not capable of remaining unchanged in the presence of such a dramatic input of UV energy. Primers are not generally exposed to UV light as the common practice is to apply additional coatings, however the testing was considered necessary to reveal and quantify what occurs when corrosion protecting primers were exposed to UV energy. It was also noted that initial PDI of a starting material affects the loss in the weight-average molecular weight, while branching during polymerization could affect the lifetime of a coating.

Meanwhile, the thermal degradation resulted in polymers consistently cleaving at what we determined to be the thermally weaker bonds more frequently as the starting point nitrogen content trended with greater molecular weight losses versus time of exposure. Fortunately and unfortunately, ASTM B117 exposure did not result in detectable chain scission events as observed from our thermal and QUV exposure and yet as an often made claim in literature, we have validated that polymer failure is not a prerequisite in order for corrosive failure to occur. The experiments were successful in providing support to ask new and important questions regarding what are the prerequisite mechanisms, processes, equilibrium concentrations of water, electrolytes, oxygen, or other environmental species in order for the dissolution of metal and macroscopic corrosion to initiate and propagate towards substrate loss/failure.

CHAPTER IV

MAGNESIUM FLUORESCENT PROBES

Introduction

To protect substrates like steel and aluminum, it is useful to incorporate the appropriate sacrificial metals into layers above the substrate in the form of coatings containing sacrificial/inhibiting pigments. [92,93] For example, magnesium is commonly used as an anti-corrosive pigment because it demonstrates sacrificial/inhibiting protection properties when applied over aluminum substrates. However, the combination of materials lacks the ability to notify when its sacrificial capacity is exhausted, e.g., no indication of remaining service life. The goal of the experiments described directly below were (1) to quantify and understand how the lifetime of magnesium related to concentration and form, and (2) to show that the mode of protection is rooted in the mechanisms for the electrochemical breakdown of pure magnesium to other magnesium compounds. It was well established before our research and development initiated that the cathodic mechanism for corrosion protection required physical magnesium to magnesium contact, i.e. pigment loading above CPVC was a requirement for optimized corrosion protection. [92]

Initially magnesium will dissociate into an ionic form as an intermediate shown in *Figure 55*, commonly known as oxidation. The reaction of magnesium is abundant when it is in direct contact with another metal that has a higher reduction potential. [92] The magnesium's electrons from the oxidation reaction are donated to the more noble metal, and the excess amount of electrons for the substrate allow for its oxidation reaction to be shifted toward the reactants. Therefore, the substrate remains in its pure

form while magnesium will continue to oxidize until all of it has converted into new inorganic compounds. [92,93]

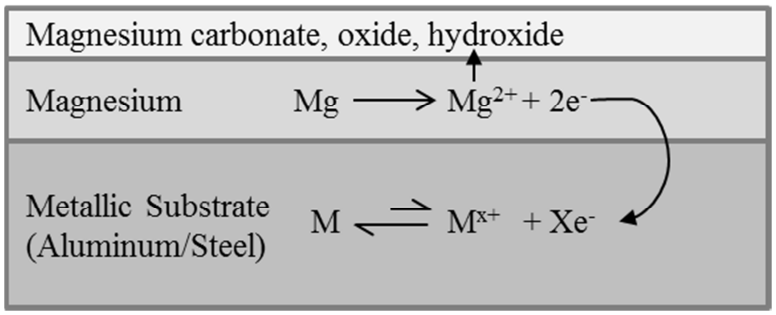

Figure 55. Magnesium Sacrificial Mechanism.

It was investigated whether a fluorescent dye was selective towards cationic magnesium, as if it were, then the dye incorporation in a coating could directly quantify the remaining service life of a magnesium rich primer (MgRP). The goal would be accomplished by monitoring the dye versus time and severity of environmental exposure. After the corrosion inhibition activity ends, the quantified dye responses can be correlated with active magnesium depletion. Success would facilitate the quantification of an end of life moment and then the coating could be removed from service and replaced before any destructive harm occurred at or within the previously protected metallic structure. Prior to the in situ use of a magnesium selective fluorescent dye, a particular set of dyes needed to be selected and studied to determine whether dye activity was possible within an organic coating and if an optimal environment for quantifiable detection was possible. Therefore, experiments were conducted to determine how certain dyes bind with divalent magnesium and whether polarity will influence the effectiveness of the dye within an organic polymer, as most primers are apolar. [29,30,31,32]

Coumarin binding mechanism with magnesium perchlorate in acetonitrile

When comparing Coumarin 314T, 314 and 334 (*Figure 56*), it was concluded that they all possessed a β-dicarbonyl functionality, however, each of these did not respond to divalent magnesium in the same manner.[29,30,31,32] The absorbance curves for Coumarin 314 T and 314 in *Figure 57* and *Figure 58* exhibit an approximately 0.60 increase in absorbance between 460-480 nm as the magnesium perchlorate concentration increased to 88.73 μM. The new absorbance peak was shown to be directly related to the dye binding with magnesium specifically dissolved in acetonitrile.[35] The same system excited at the new absorbance band provides an increase in fluorescence intensity at approximately 500 nm also seen in *Figure 59* and *Figure 60*. Increasing the magnesium perchlorate concentration from 0.00 to 88.73 μM resulted in a doubling of fluorescence intensity and provided a solid response to the experimental changes. The presence of divalent magnesium with Coumarin 314T and 314 allowed for sufficient detection at low concentrations.

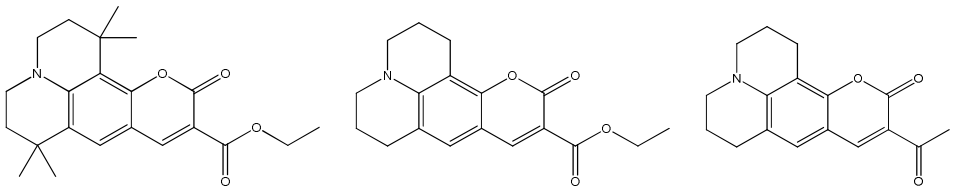

Figure 56. Coumarin 314T (left), Coumarin 314 (middle), and Coumarin 334 (right).

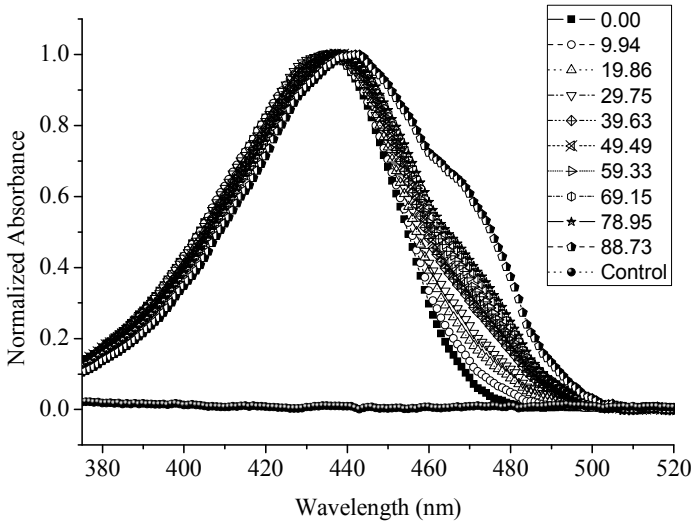

Figure 57. Absorbance Spectra of Coumarin 314T in Solvent with Various μM Concentrations of $Mg(ClO_4)_2$.

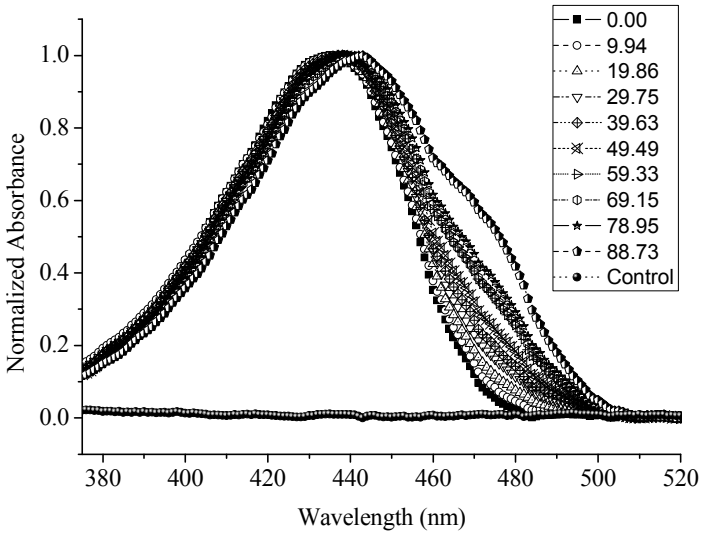

Figure 58. Absorbance Spectra of Coumarin 314 in Solvent with Various μM Concentrations of $Mg(ClO_4)_2$

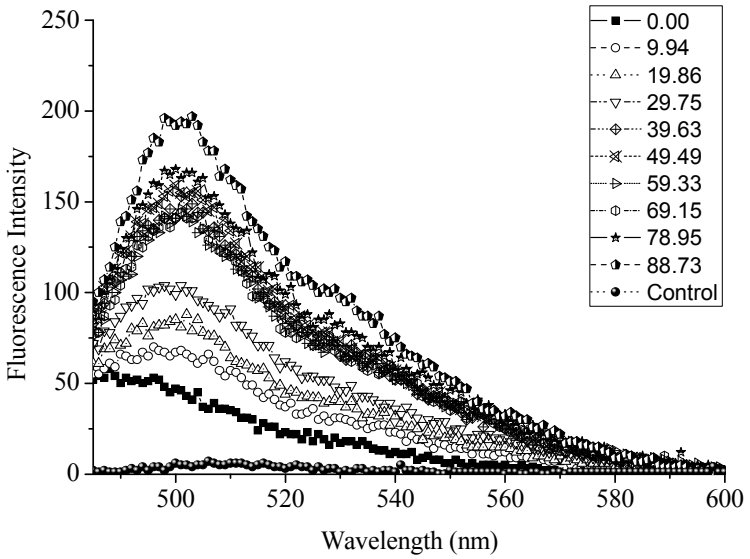

Figure 59. Coumarin 314T 475 nm Excitation Fluorescence Spectra in Solvent (μM of $Mg(ClO_4)_2$).

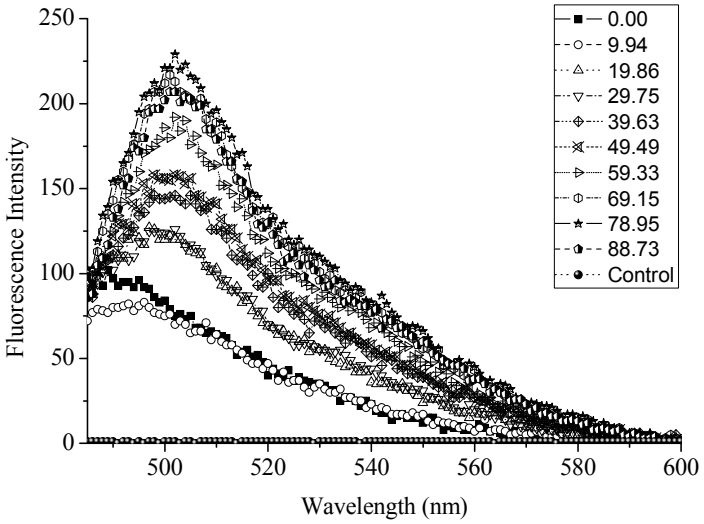

Figure 60. Coumarin 314 475 nm Excitation Fluorescence Spectra in Solvent (μM of $Mg(ClO_4)_2$).

Although Coumarin 334 is similar to Courmarin 314T and 314 structurally, the new absorbance band at 460-480 nm, that was initially attributed to divalent magnesium association, is absent in *Figure 61*. Increasing the magnesium perchlorate concentration to 88.73 μM resulted in no new absorbance wavelengths for Coumarin 334 unlike the responses from Coumarin 314T and 314, thus their ability to bind must be related to the

slight chemical differences in their molecular structure. Furthermore, fluorescence intensities at 500 nm from a 475 nm excitation revealed no increase as noted in *Figure 62* since binding was not available. The combination of divalent magnesium and Coumarin 334 was not detectable at the low concentrations as seen with Coumarin 314T and Coumarin 314 since heteroatoms near the binding site are absent for Coumarin 334.

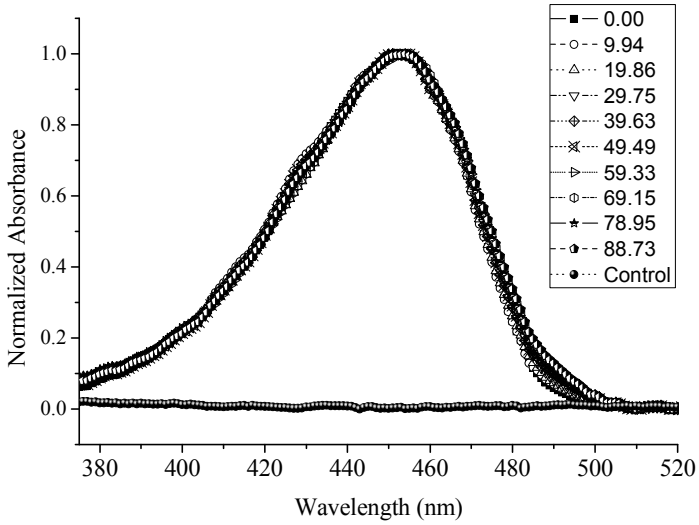

Figure 61. Absorbance Spectra of Coumarin 334 in Solvent with Various μM Concentrations of $Mg(ClO_4)_2$.

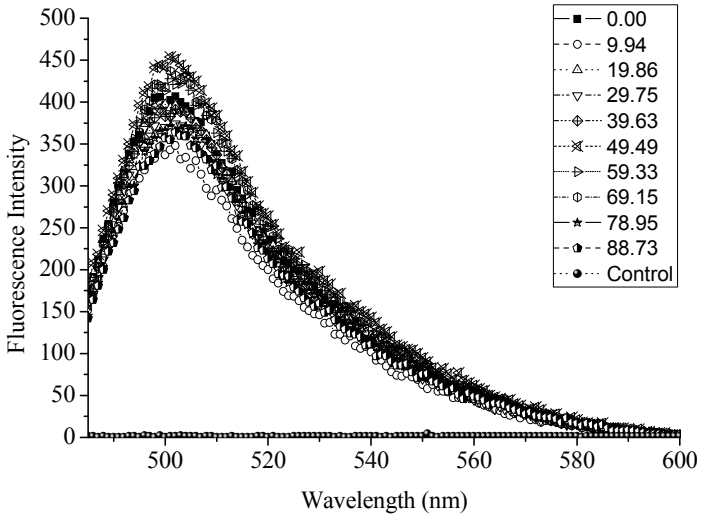

Figure 62. Coumarin 334 475 nm Excitation Fluorescence Spectra in Solvent (μM of $Mg(ClO_4)_2$).

When plotting the new absorbance band at 475 nm for Coumarin 314T and 314, the response of magnesium perchlorate in acetonitrile was confirmed in *Figure 63*. The detected absorbance changes for Coumarin 314T and 314 were linear versus magnesium perchlorate concentration whereas, the 475 nm band in Coumarin 334 has a peak intensity that remains unchanged across other magnesium perchlorate concentrations. The Benesi-Hildebrand plot (*Figure 64*) for Coumarin 314T and 314 also show a linear increase in absorbance differences at 475 nm with correlation coefficient values of 0.991 and 0.996, respectively.

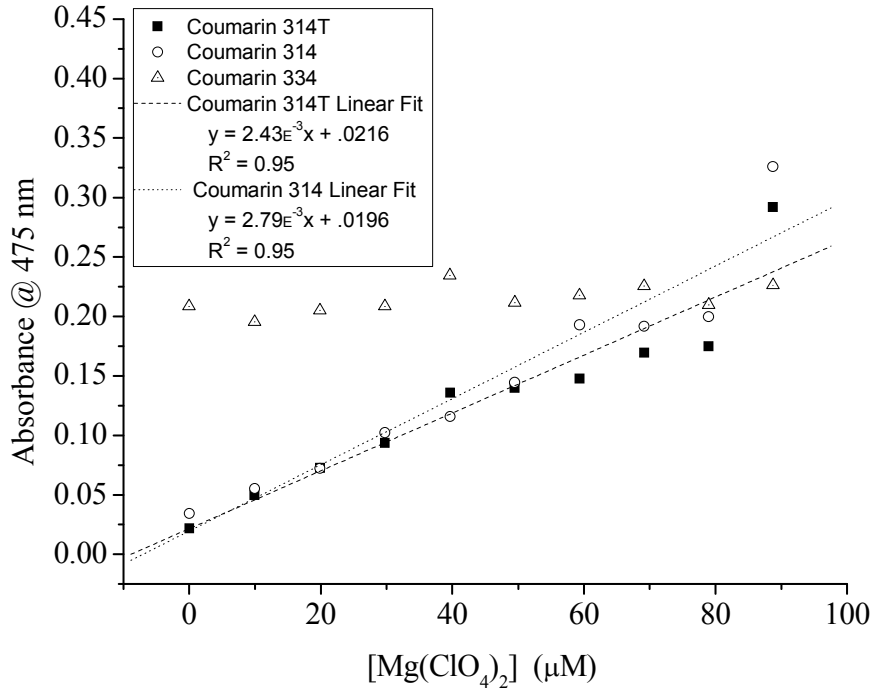

Figure 63. Coumarin 314T, 314, and 334 Absorbance Trends with $Mg(ClO_4)_2$.

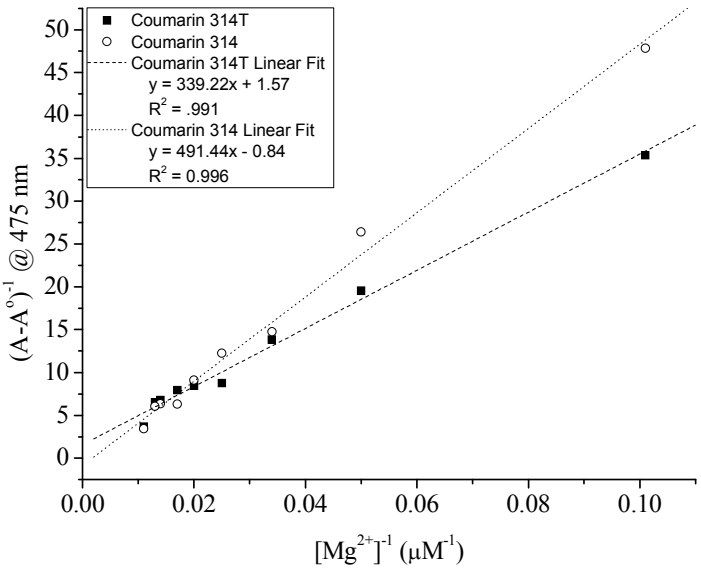

Figure 64. Coumarin 314T and 314 Benesi-Hildebrand Plot with $Mg(ClO_4)_2$.

The ratio of fluorescence intensities from an observation at 500 nm with 470 nm and 425 nm excitations provide the measurement of fluorescence changes with respect to Coumarin dyes with and without association to divalent magnesium respectively shown in *Figure 65* and *Figure 66*. Both characterization curves demonstrate a linear increase for Coumarin 314T and 314 with respect to magnesium perchlorate concentration and support an increasing concentration of associated dye with divalent magnesium. Coumarin 314T showed a higher correlation of 0.988 when plotting linearly versus and correlation of 0.967 when plotting logarithmically while Coumarin 314 had the opposite trend where the linear plot correlated with 0.963 versus 0.983 when plotted by logarithm shown in *Figure 65* and *Figure 66* respectively. Both methods of plotting are acceptable and both were included in this chapter to show similar correlation to magnesium bind. However, Coumarin 334 regardless of magnesium concentration maintains the same slope (both graphs) and near zero intensity change.

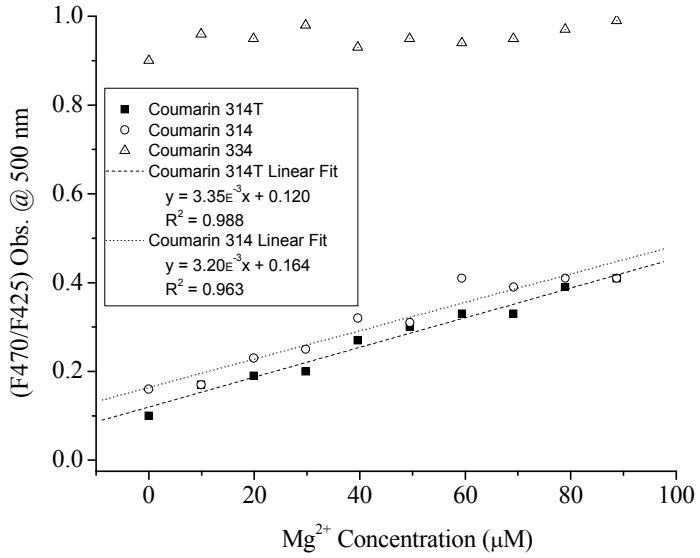

Figure 65. Coumarin 314T, 314, and 334 Fluorescence Linear Trend with $Mg(ClO_4)_2$.

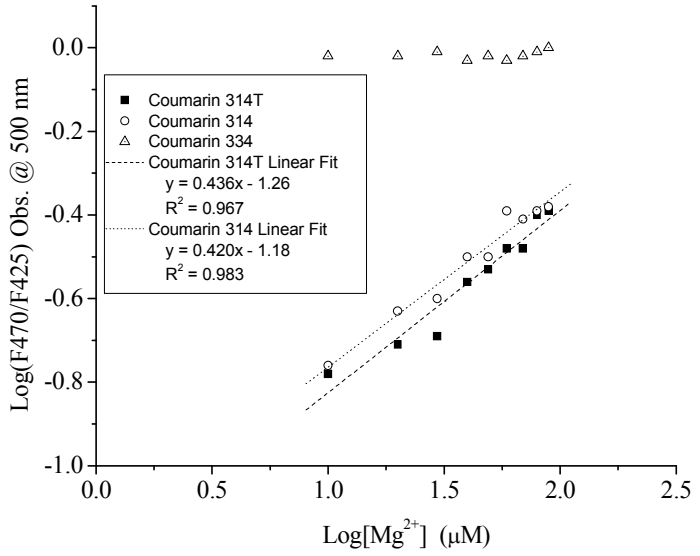

Figure 66. Coumarin 314T, 314, and 334 Fluorescence Logarithmic Trends with $Mg(ClO_4)_2$.

Since Coumarin 314T and 314 respond with similar slopes in both absorbance and fluorescence spectroscopy measurements, the conclusion is that each has a near identical association mechanism with divalent magnesium. Meanwhile Coumarin 334 shows no intensity trends while divalent magnesium is present, therefore the data

supports the absence of a magnesium binding mechanism for Coumarin 334. *Figure 67* demonstrates, the availability of an electron donor α to the β-dicarbonyl is essential to gaining high sensitivity to divalent magnesium.

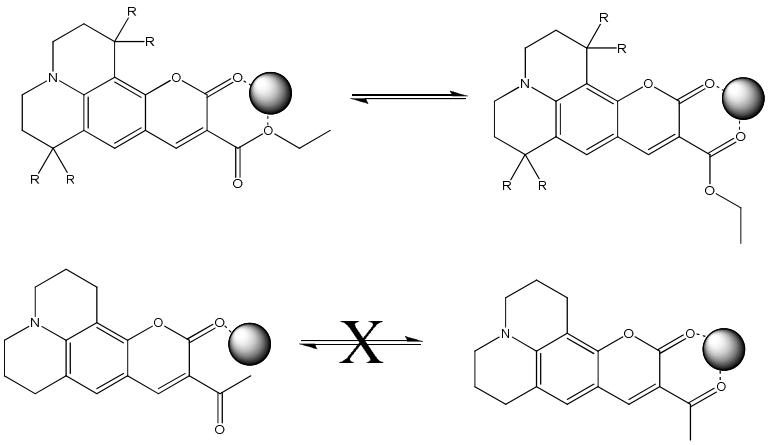

Figure 67. Coumarin 314T/314 (top) and Coumarin 334 (bottom) Binding with Divalent Magnesium.

Dissociation and Polarity Differences

When considering a Mg-rich primer, the magnesium is incorporated into a thin polymer film at above critical pigment volume concentration. Thus, during environmental exposure, the dissolution and loss of magnesium are capable of binding to multiple counter ions available. Each counter ion also has varying dissociation constants that determine the amount of freely associated magnesium cations available. The multi-ion experiments were designed to determine the sensitivity of each probe and the resulting excitation and emission intensities starting with the combination of magnesium chloride and magnesium perchlorate.[36] Coumarin 314T's change in absorbance and fluorescence intensity varied drastically compared between magnesium chloride and magnesium perchlorate. It also exhibited changes when the two salts were introduced to a lower polarity solvent mixture of MEK/PGPE, similar to what is found in the coating resin Eponol 53-BH-35. Magnesium chloride has a lower dissociation constant than

magnesium perchlorate although they were each soluble in acetonitrile and MEK/PGPE at low concentrations.[36] The acetonitrile absorbance spectra shown in *Figure 69* confirms Coumarin 314T is binding with the divalent magnesium. However, the new absorption maximum developing at 466 nm and is higher in intensity for magnesium perchlorate (*Figure 69*) than for magnesium chloride (*Figure 68*). The Benesi-Hildebrand plot in *Figure 70* confirms that there is a higher availability of divalent magnesium from magnesium perchlorate than from magnesium chloride.

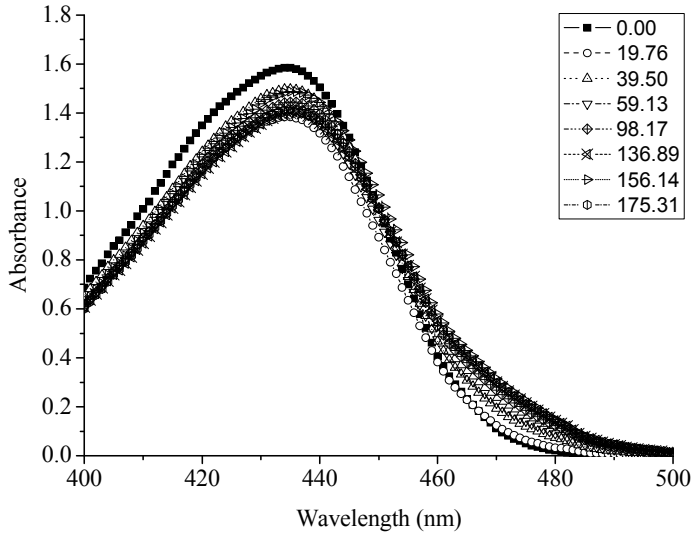

Figure 68. Absorbance of Coumarin 314T in Acetonitrile with Magnesium Chloride in μM.

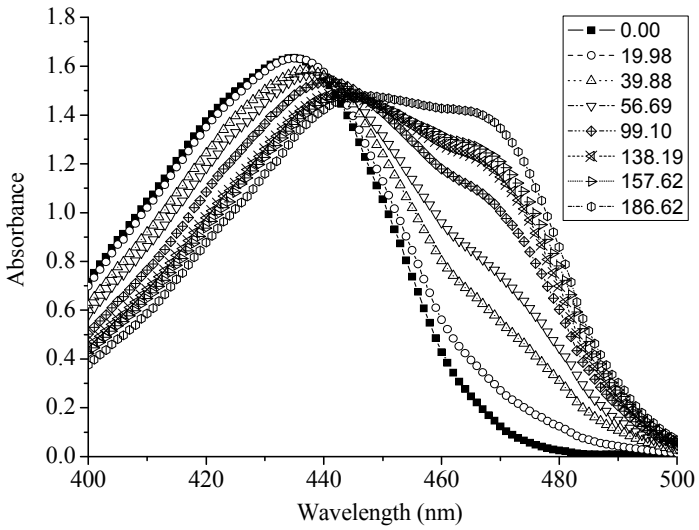

Figure 69. Absorbance of Coumarin 314T in Acetonitrile with Magnesium Perchlorate in μM.

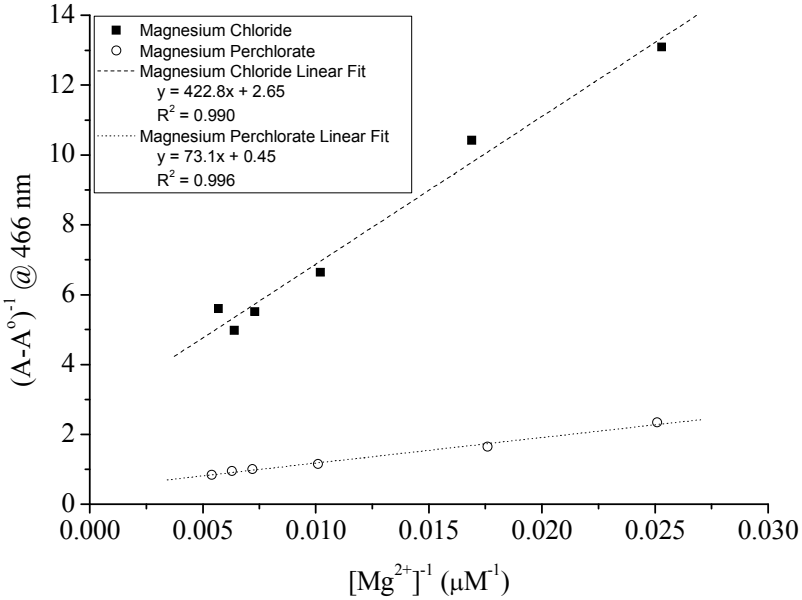

Figure 70. Magnesium Chloride and Magnesium Perchlorate Absorbance Trends with Coumarin 314T in Acetonitrile.

Comparing the fluorescence intensities from *Figure 71* and *Figure 72* confirms that a greater percent dissociation of the magnesium ion occurs from magnesium perchlorate when dissolved completely in acetonitrile. The ratio of 466 and 425 nm excitations while observing the intensity at 500 nm, shown in *Figure 73* in relation to the

magnesium salt concentration, also confirms that magnesium perchlorate is providing Coumarin 314T with greater binding and concentrations of divalent magnesium.

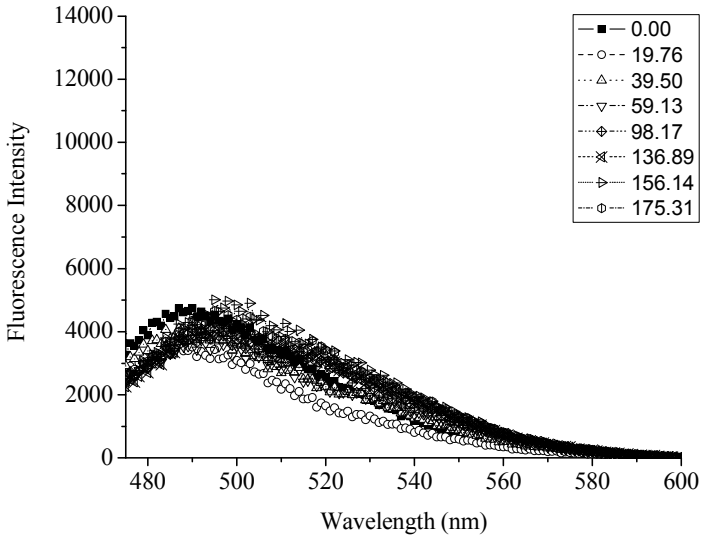

Figure 71. Fluorescence (466 nm Excitation) of Coumarin 314T in Acetonitrile with Magnesium Chloride in μM.

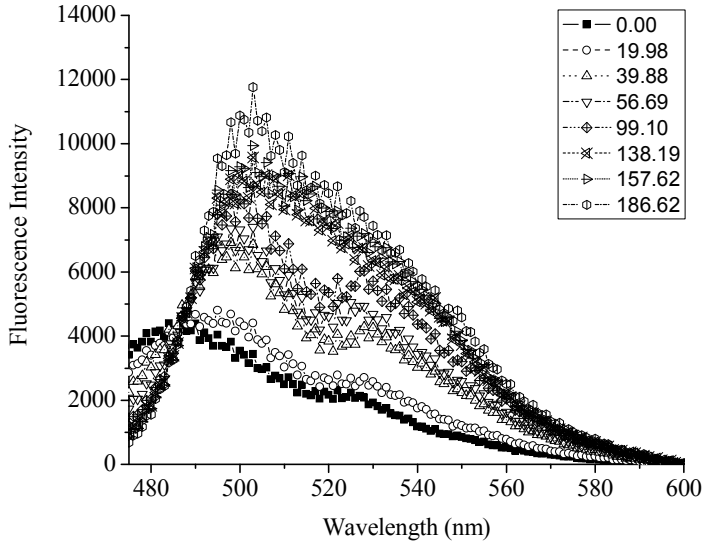

Figure 72. Fluorescence (466 nm Excitation) of Coumarin 314T in Acetonitrile with Magnesium Perchlorate in μM.

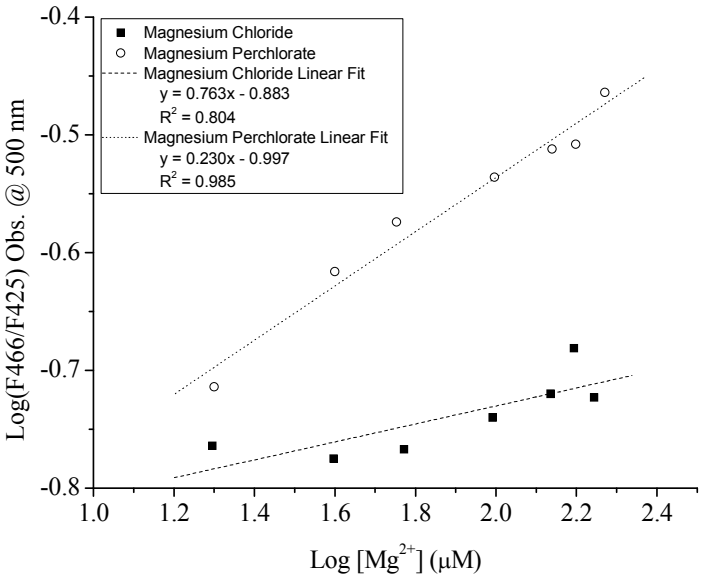

Figure 73. Magnesium Chloride and Magnesium Perchlorate Fluorescence Trends with Coumarin 314T in Acetonitrile.

This dissociation has been shown to proliferate with increasing solvent polarity.[35] Typical MgRP consist of low polarity polymers such as DGEBA. Therefore, when using a solution media similar to Eponol-53-BH-35 (MEK/PGPE), the equilibrium of dissociation should shift towards a decrease of divalent magnesium available for binding with Coumarin 314T. *Figure 74* validates that analogous concentrations from the acetonitrile experiment, dissolving magnesium chloride and magnesium perchlorate in a blend of MEK/PGPE, do result in lower absorbance values at 466 nm. The data revealed in *Figure 75*, confirms that fluorescence intensities decrease as the systems decrease in polarity.

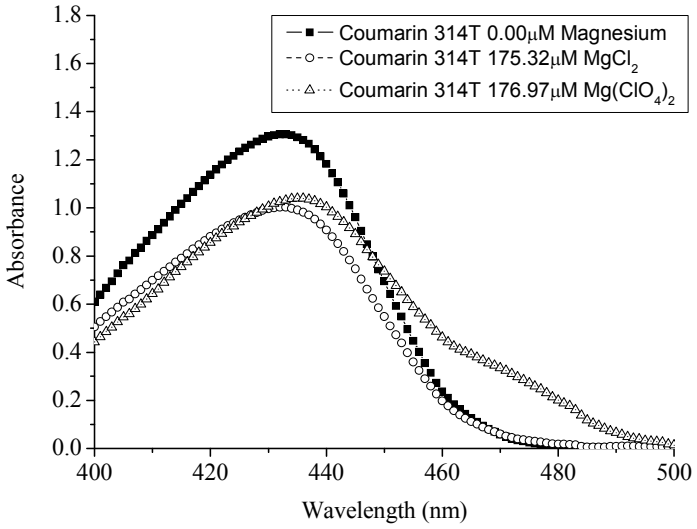

Figure 74. Magnesium Chloride and Magnesium Perchlorate Absorbance with Coumarin 314T in MEK/PGPE.

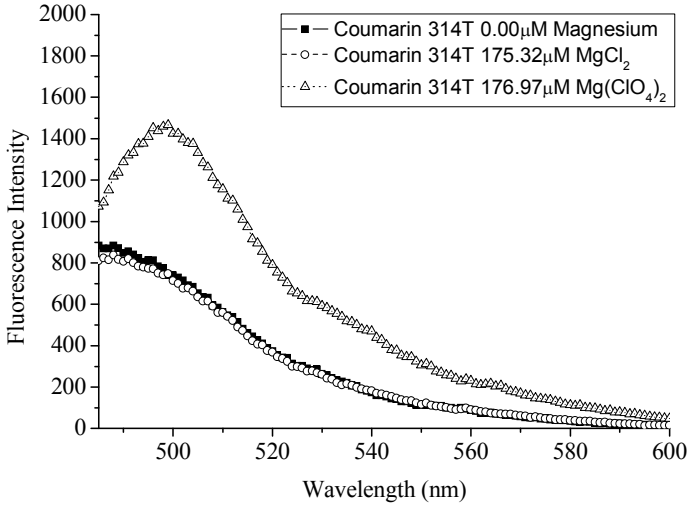

Figure 75. Magnesium Chloride and Magnesium Perchlorate 466 nm Excitation Fluorescence with Coumarin 314T in MEK/PGPE.

DGEBA Based Polyepoxide Results

When Coumarin 314T was incorporated into a coating solution mixture (Eponol 35-BH-35), magnesium perchlorate was added to the solution since it had better dissociation compared to magnesium chloride. However, upon addition, Coumarin 314T

exhibited no increase in absorbance and no new shifts with or without the presence of magnesium perchlorate. The polarity of the DGEBA based polyepoxide (*Figure 77*) polymer is apparently very low compared to a polar solvent like acetonitrile and thereby the divalent magnesium dissociation is drastically reduced.

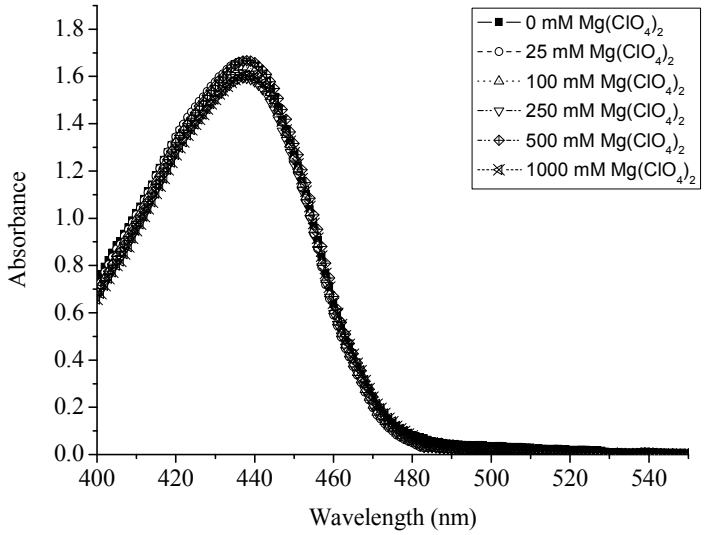

Figure 76. Magnesium Perchlorate Absorbance Spectra with Coumarin 314T in Eponol 53-BH-35.

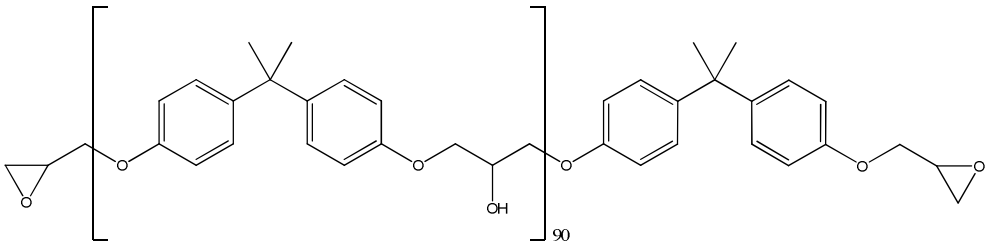

Figure 77. Eponol 53-BH-35 Resin DGEBA Structure.

Conclusions

The experiments were planned and implemented to confirm absorption and fluorescence emission results while varying the Coumarin dye type, concentration, solvent polarity, and in the presence and absence of a common polyepxoide backbone. The incentive for the research was to establish limits of detection, limits of

differentiation, and the presence or absence of soluble magnesium during the environmental exposure of magnesium rich primers. The results distinguished differences in binding mechanisms and dissociation-polarity. Data revealed that the dye molecular structure must contain an electron donor α to the β-dicarbonyl for efficient binding with divalent magnesium species. Without the α electron donor, the β-dicarbonyl functional group on Coumarins is not sufficient enough to detect magnesium ions as previously reported in literature.[29,30,31,32] Therefore, when utilizing the correct magnesium detecting molecule, absorbance and fluorescence measurements of Coumarin 314T confirmed that the dissociation constants of magnesium salts in varying-polarity environments decrease with polarity and are dependent on the counter anion. Unfortunately, extremely low polarity conditions resulted in drastically diminished intensity from Coumarin dyes and thus hindered the ability to track the MgRP lifetimes as originally desired. Therefore the ability of fluorescent indicating molecules to detect pre-corrosion events within an epoxide polymer was proven to be very limited and the use of dyes was shifted in focus towards monitoring metal-polymer interfacial changes for the detection of corrosion.

CHAPTER V

pH-INDICATING MICROCAPSULES INCORPORATION IN EPOXY PRIMERS

Introduction

Important to note are the massive amounts of corrosion detection methods that singularly rely upon visual macroscopic corrosion detection, whether in the form of rust spots, blisters, or creep from the scribe. However, these events are clearly not the initial moments of corrosion or even the precursor events that occur in advance of any detectable corrosive initiation. From the prior chapter, the data validated that detecting ions in an apolar medium was ineffective in that specific case. Shifting towards potential methods to detect and determine if other technologies allow for direct interpretation of changes at a metal-polymer interface was the research goal of this chapter. Traditionally, organic coatings are used as a corrosion protective barrier to prevent corrosive entities from reaching a metallic substrate. In particular, epoxy polymer-based coating systems are widely used in primer applications due to their excellent chemical resistance, thermal stability, adhesion, and toughness. In spite of their outstanding substrate protection, water, ions, and oxygen can still transfer slowly through their films and corrosion can occur at any point. Therefore, early detection, prior to the macroscopic appearance of corrosion, is highly desired. Early detection information would be invaluable in preempting catastrophic failures and also lead to greater understanding of the pre-macroscopic events and chemical changes occurring that provide dependency and order in the overall corrosion protection process. [94,95,96]

Attempts to detect any mechanistic or kinetic events that serve as precursors to macroscopic corrosion are the central theme of many research groups around the world. Specifically, researchers have studied the dissolution of metal ions during corrosion

using fluorescent probes.[95,96] The hydroxide ions (OH^-) produced during corrosion dramatically increases the local pH. This increase in pH can be monitored with a pH indicator such as phenolphthalein.[94,95,97] However, concerns about chemical interactions between the indicator and the paint components, such as, amine basicity influencing the pH colorimetric response, have limited the utility of phenolphthalein in thermosetting epoxy primers.[95] Therefore, the research presented here focuses on harnessing synthesized microcapsules by NASA that encapsulate phenolphthalein to detect corrosion events in modified coating formulations.

NASA/KSC Corrosion Technology Laboratory developed a pH-triggered controlled-release microcapsule system that combines the advantages of corrosion detection and corrosion protection.[98,99,100] A key component of this technology is a pH sensitive-microcapsule that releases the encapsulated contents under basic pH at the cathodic site of localized corrosion (*Figure 78*). Microencapsulation is a versatile approach to encapsulate various materials, including corrosion indicators, inhibitors, self-healing agents, and dyes. Microcapsules have been incorporated into coating formulations to enable early corrosion detection, protection, and self-repair of mechanical damage initiated by an electrochemical reaction associated with corrosion (*Figure 79*).

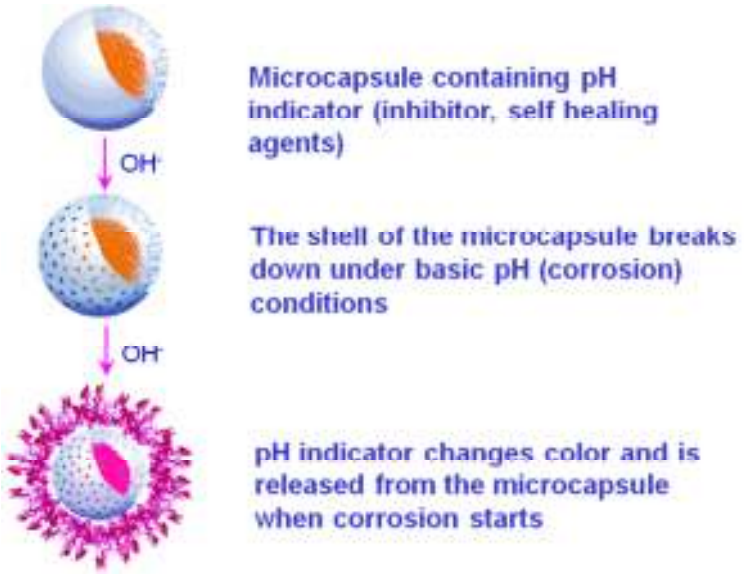

Figure 78. The Mechanism of Decomposition of a pH-Sensitive Microcapsule that is the Key Component of the Smart Coating System. (Used with permission of NASA.)

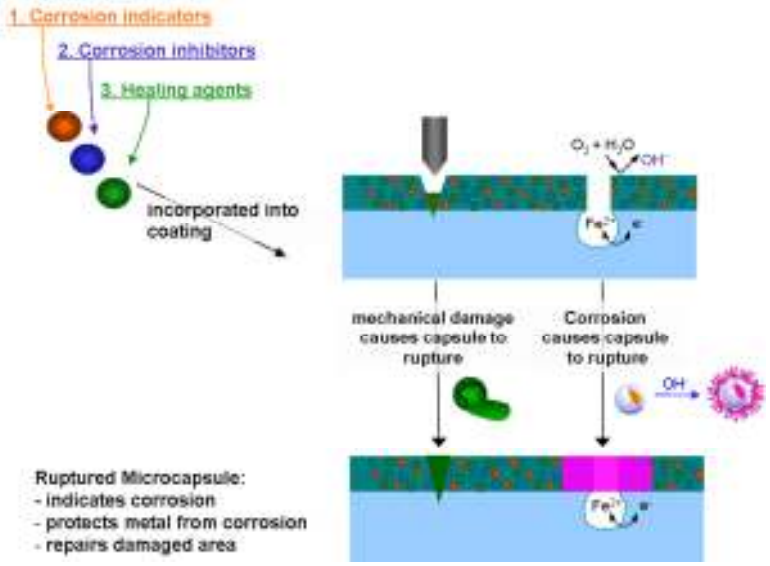

Figure 79. Schematic Showing the Smart Coating with pH-Sensitive Microcapsules for Corrosion Detection and Protection Applications. (Used with permission of NASA.)

In the research reported here, high molecular weight thermoplastic (HMWTP) epoxies and modified epoxy thermoset formulations with crosslinkers, that are less

nucleophilic, were used to evaluate free and microencapsulated phenolphthalein as a corrosion indicator in clear and pigmented coatings, respectively.

Free phenolphthalein in HMWTP epoxy clear

To determine the compatibility of phenolphthalein within a HMWTP polymer, it was mixed into a clear epoxy formulation (Eponol 53-BH-35) at concentrations of 0.00%, 0.27%, 1.13% and 10.97%, based on resin solids. With loading levels up to 10.97% phenolphthalein, adhesion remained unchanged compared to controls (5B), after drying for a week and subsequent annealing at 75˚C for 24 hours (*Figure 80*).

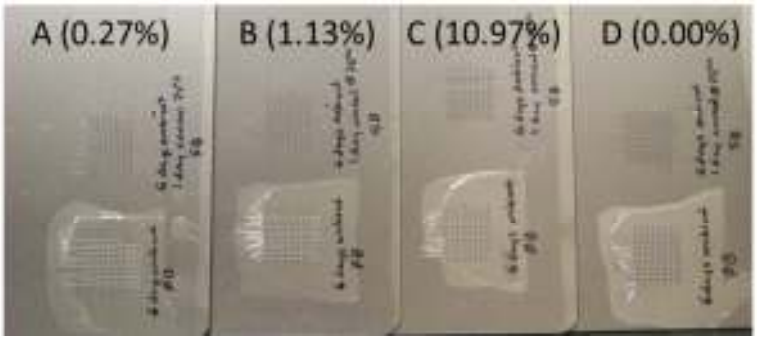

Figure 80. Cross Hatch Adhesion of Epoxy Coatings with Phenolphthalein Before and After Annealing.

Flexibility after the previously mentioned drying procedures also showed no change in coating performance since complete elongation was achieved (*Figure 81*). Although the loading level of phenolphthalein did not change the coating properties that were measured, each system did not perform equally when indicating corrosion.

Figure 81. Flexibility of Epoxy Coatings with Phenolphthalein After Annealing.

As the concentration of free phenolphthalein increased from zero to 10.97%, the color indication intensity increased (*Figure 82*) appearing only with the systems containing 10.97% phenolphthalein. Since this concentration gave the earliest and most pronounced color change, future formulations were designed to contain approximately the same concentration of phenolphthalein. Theoretically, a fully pigmented coating containing NASA's microcapsules would detect the earliest and most measurable changes in pH associated with corrosion indication.

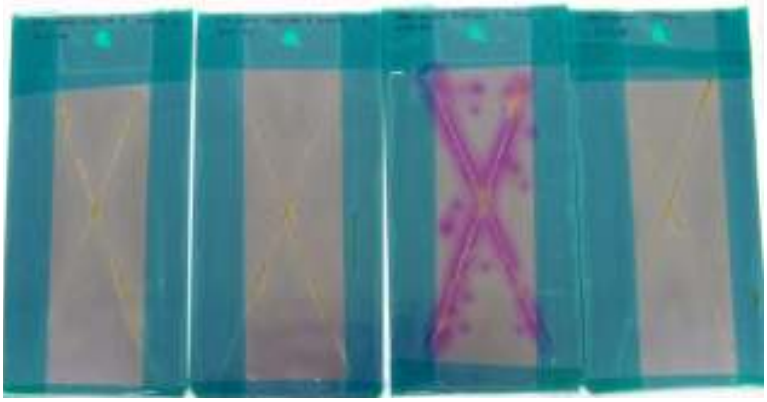

Figure 82. From left to right: Panels Coated with 0.27%, 1.13%, 10.97%, and 0.00% Phenolphthalein in HMWTP Epoxy after 46 hours of Salt Water Submersion.

ATR-IR of phenolphthalein Conversion

The conversion of the 5-membered ring ester to a carbonate substituent (*Figure 83*) in high pH environments of phenolphthalein was initially examined and monitored via mid-IR spectroscopy since it is accompanied by a color change to fuchsia and a characteristic peak at 1556 cm^{-1}. Phenolphthalein carbonate formation from the 5-membered ring ester did not overlap with any peaks from the epoxy resin (*Figure 84*). [101]

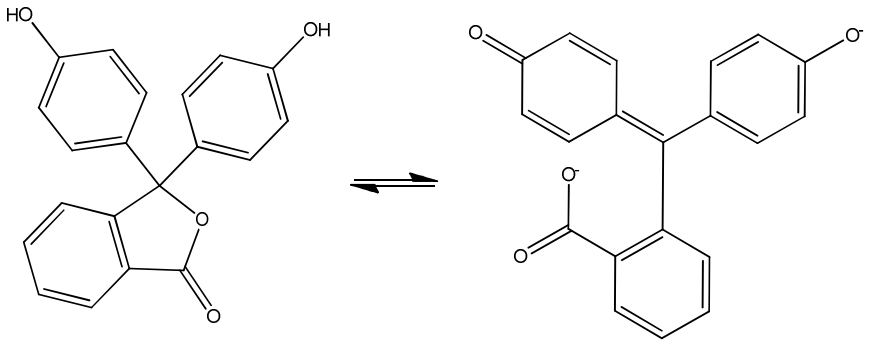

Figure 83. pH Induced Conformations of Phenolphthalein.

Submersion in salt water resulted in a fuchsia color from pre-corrosion (high pH), ATR-IR spectroscopy at the air-coating interface did not show the peak at 1556 cm^{-1} (*Figure 84b*). However, when the coating was removed from the substrate and reanalyzed with the substrate interface in contact with the ATR diamond, a shoulder was noted at 1556 cm^{-1} (Figure 10a). The mobility of hydroxide ions through an epoxy coating is very limited and the peak at 1556 cm^{-1} may not be identifiable via ATR-IR through a pigmented coating. To capture the color changing events, the visual observations were complemented by digital photography and ImageJ® software.

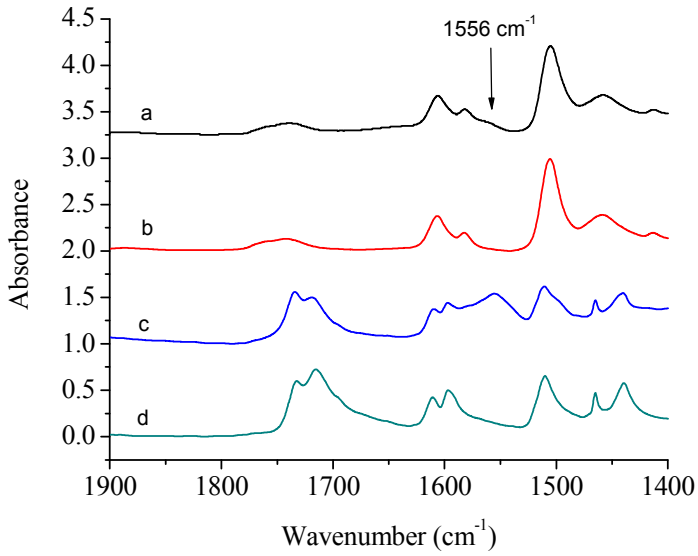

Figure 84. ATR-IR Spectra. (a) Eponol with 10% phenolphthalein @ 138 hours ASTM B 117 substrate-coating interface, (b) Eponol with 10% phenolphthalein @ 138 hours ASTM B 117 at air-substrate interface, (c) pink phenolphthalein, and (d) white phenolphthalein.

Quantification of Phenolphthalein in Microcapsules

Six samples of phenolphthalein microcapsules synthesized at NASA/KSC Corrosion Technology Laboratory were tested for phenolphthalein content using a pharmaceutical technique. [102] This procedure used two stock solutions consisting of KOH (0.042M) and N-bromosuccinimide (0.004M). Then the samples were prepared by adding approximately 0.0318g of phenolphthalein (control) or microcapsules into a 100mL volumetric flask and filled with 0.042M KOH to extract and/or release phenolphthalein from the microcapsules (*Figure 85*).

Figure 85. Solutions of Phenolphthalein (left) and Microcapsules (right) in 0.0042M KOH.

Next the 0.004M N-bromosuccinimide solution was added to 15mL aliquots of the phenolphthalein or microcapsules solutions via a burette and the amount of the solution recorded during the transition from purple to bluish-green ended the titration (*Figure 86*).

Figure 86. Titration Endpoint for Phenolphthalein Concentration Determination.

Weight percentages of phenolphthalein were determined to range from 10.4 to 29.3% (Table 10). Samples 1, 2, 5, and 6 contained greater than 20% measurable

phenolphthalein, therefore they qualified for use in future thermoset formulations similar to Table 11. Meanwhile, microcapsules 3 and 4 possessed phenolphthalein concentrations too low to be detected in coatings without compromising the control primer formulation properties significantly and thus were not used.

Table 10

Percent Phenolphthalein Determination

Microcapsule	Phenolphthalein (%)
1	20.1
2	20.0
3	10.6
4	10.4
5	29.3
6	24.7

Crosslinker-dependent False Corrosion Indication

When microcapsules were incorporated into a chromate-based commercial coating (DEFT Type I Class C2), a false positive color indication quickly developed as a result of the alkaline contribution from the amine crosslinker (*Figure 87*). Therefore, the Deft Part B component was titrated to determine its amine value and was replaced by Epikure 3292-FX-60 in the coating formulation at the same amine content. Epikure 3292-FX-60 was chosen since it has only secondary amines that are less nucleophilic than the traditional primary amines. Although the color, imparted via chrome pigments and other unknown pigments/colorants, remained yellow with the Epikure 3292-FX-60 system, the coating had a slight purplish hue to it. When measured by colorimeter, the control coating exhibited L*, a*, and b* values of 78.21, -13.62, and 56.25, respectively,

while the coating with microcapsules had values of 75.74, -11.13, and 47.22, respectively. The increase in the a* value indicates a red shift while the decrease in the b* value indicates a blue shift, which results in the coating having a detectable purple hue.

Figure 87. Top Row from left to right are Panels with Microcapsules Labeled DEFT Type I Class C2 (diluted), DEFT Type I Class C2 Cured with Epikure 3292-FX-60, Chrome-Free Coating Cured with Epikure 3292-FX-60, and Chrome-Free Coating Cured with Tetra(3-Mercaptopropionate). Bottom Row are without Microcapsules.

To confirm the source of the color shift, an epoxy coating was formulated without the yellow pigment (strontium chromate), and the resulting white coating turned a distinct fuchsia upon microcapsule incorporation indicating alkalinity. Therefore a new crosslinker was chosen devoid of amines. Upon crosslinking the new formulation with pentaerythritol tetrakis(3-mercaptopropionate), the cured film did not exhibit any color change, indicating that the cure pH in the films were not sufficiently alkaline to facilitate the release of the microcapsule contents. Color measurements confirmed the absence of any pink/purple transition as the control coating exhibited L*, a*, and b* values of 82.66, -1.18, and -0.52, respectively, while the coating with microcapsules had corresponding values of 76.36, -0.88, and 0.10, respectively. The change in L* and b*

values were attributed to the 45% reduction in white pigments to accommodate the grey toned microcapsules (Table 11).

Table 11

Coating Formulations

Material	Grams	Material	Grams
Part A		Part A	
Epon® 1007-HT-55	30.42	Epon® 1007-HT-55	30.38
Epon® 1001-B-80	18.00	Epon® 1001-B-80	17.97
Anti-Terra® U	0.18	Anti-Terra® U	0.19
Xylene	6.04	Xylene	6.22
Ektasolve® EEP	7.31	Ektasolve® EEP	7.33
Ti-Pure® R706	8.20	Ti Pure® R706	4.38
Heucorin® RZ	11.46	Heucorin® RZ	6.08
Huberbrite® Barium Sulfate	28.36	Huberite® Barium Sulfate	15.42
Zeeospheres® 400	25.57	Zeeospheres® 400	13.77
Water Ground Mica 325 Mesh	7.54	Water Ground Mica 325 Mesh	4.31
Solvents (mixture)	38.70	Solvents (mixture)	38.70
		Microcapsules*	37.49
Part B		Part B	
Tetra(3-mercaptopropionate)	8.20	Tetra(3-mercaptopropionate)	8.20

Curing of Chrome-free Formulation with Pentaerythritol Tetrakis (3-mercaptopropionate)

A chrome-free thermosetting coating cure profile was characterized via DSC. As this thermoset formulation was a crosslinked system, the glass transition temperature (T_g) increased as chain mobility and free volume reductions transitioned. The practical degree of crosslinking, e.g., the cure reaction, can be concluded as complete when the T_g plateaus. In this formulation, the epoxides and thiols were stoichiometrically balanced and, as *Figure 88* reveals, they were cured at a temperature of 75 °C for 192 hours. At this point the coating yielded a T_g of 75 °C, suggesting that vitrification had occurred resulting in a drastic decrease in the polymer chain mobility in the glassy state. Post-

curing at 135 °C raised the T_g slightly to 78°C after 8 hours, indicating that conversion was temperature limited and only minimal additional conversion was achievable at elevated temperatures. Crudely, the high coating crosslink density was validated via passing over 100 methyl ethyl ketone (MEK) double rubs.

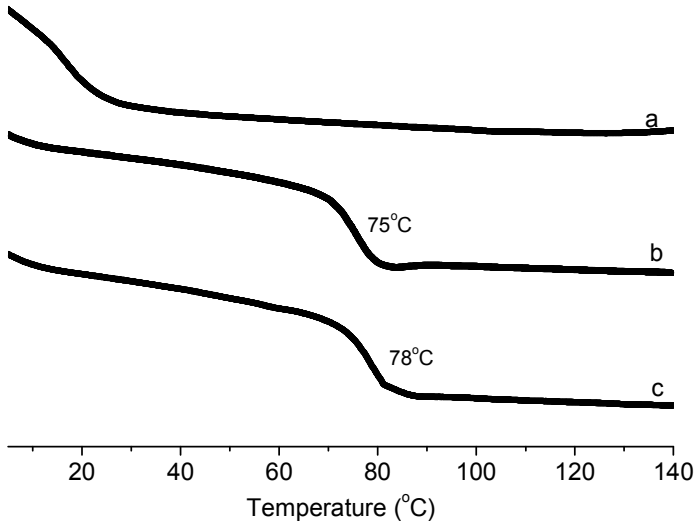

Figure 88. DSC Thermograms. (W/g) – (a) before cure, (b) 192 hours @ 75°C, and (c) 8 hour post-cure @ 135°C.

Salt Water Submersion Testing

Coatings from Table 3 were applied to steel (QD) panels using a 6 mil film applicator that resulted in 1 mil dry film thicknesses. The coatings were cured to the same cure schedule mentioned previously to high conversion without any change in color. Two glass immersion tanks were set up with salt water (5% NaCl solution) and the coated panels were immersed for accelerated corrosion testing. The panel exposure results were periodically captured digitally and the images were enhanced for optimal contrast using ImageJ®. The results accentuate detection of pink coloration during corrosion testing. After 51 hours of submersion (*Figure 89*), the coatings containing

microcapsules exhibited a visually distinct fuchsia color indicating the onset of corrosion before any other corrosion-induced change or failure could be observed. Furthermore, in the same samples, the color was consistently more pronounced after 147 hours of submersion. Some leaching of the fuchsia color was observed arising from the scribes and both coatings showed signs of blistering. The control materials delaminated without any macroscopically detectable preemptive signs at 147 hours (*Figure 90*). The results confirm that macroscopic visible detection is often too late to retain substrate and/or coating integrity. The coatings containing microcapsules indicated the onset of corrosion 288% quicker than traditional signs of corrosion, e.g., blisters, rust and/or delamination could be seen.

Figure 89. Coating Containing Microcapsules. (From left to right) – 51 Hours of Submersion, 51 Hours of Submersion with Contrast Enhancement, 147 Hours of Submersion, and 147 Hours of Submersion with Contrast Enhancement.

Figure 90. Control Coating. (From left to right) – 51 Hours of Submersion, 51 Hours of Submersion with Contrast Enhancement, 147 hours of Submersion, and 147 Hours of Submersion with Contrast Enhancement.

Conclusions

Corrosion indicating pH-sensitive microparticles were successfully characterized and incorporated for function in thin films. The microparticles were successfully blended into a carefully selected epoxy themoset coating without falsely indicating corrosion based upon crosslinker-indicator chemical conflicts. Furthermore, coatings containing the corrosion indicating pH-sensitive microparticles visually indicated the onset of corrosion approximately 100 hours in advance of any signs of macroscopic, visually detectable corrosion indicated by blistering and/or delamination of the protective epoxy coating. Future research will focus on determining the quantified moment in time when corrosion is initiated. Since phenolphthalein provides a visible detection of corrosion in advance of traditional methods, it is difficult for a researcher to attend to the sample constantly for weeks. When corrosion is finally indicated, the nucleation event has passed and there is no data available to predict when corrosion begins. Fluorescent indicator molecules, similar in mode of action, but significantly more sensitive to phenolphthalein can be utilized uniformly in the bulk rather than encapsulated. [102] Fluorescent indicators can be used within a spectrometer to investigate, quantify and understand how emission intensity over an entire substrate

shifts during the earliest of corrosion processes. If sufficient data points are gathered, a line fit can be used to extrapolate back to when corrosion started. Quantification of corrosion initiation offers another tool to evaluate polymers, polymer characteristics, and directly interpret structure property relationships that can be safely utilized in situ during exposure to corrosive environments.

CHAPTER VI

pH STIMULI RESPONSIVE POLYMER

Detecting changes within a polymer at the polymer-metal interface before and after corrosive events is invaluable for polymer scientists and corrosion engineers. Most corrosion detection and characterization methods are typically destructive, in that the polymer must be removed from the substrate in order to measure the properties within the polymer and on the metal surface. The use of fluorescent probes as molecular sensors has been extensively investigated in organic coatings to monitor real-time molecular events with high sensitivity. [39,40,44,45,46,47,48,49] However, on the downside, smaller fluorescent molecular probes have a tendency to migrate and leach out of the polymer coating and this can compromise our experimental goal of locating and quantifying changes in emission intensity. This problem of fluorescent probe migration can be addressed by tethering a fluorescent probe to a coating resin. In this study, we have successfully tethered a pH stimuli responsive fluorescent probe to a resin, in an attempt to develop a non-destructive method of monitoring real-time changes in pH due to corrosion events under coated steel panels with respect to x-y dimensions. This chapter will discuss the development of a forensic method of detecting that quantifies corrosion events and seeks to improve the typical qualitative analysis of using UV light sources and a naked eye. [45,46] This method is based on the grafting of the pH sensitive, fluorescein isothiocyanate (FITC) onto a hydroxyl functional phenoxy polymer coating (summarized in Chapter II) and taking advantage of the changes in the photo-physical of the grafted polymer using fluorescence spectrometer plate reader to predict and detect early corrosion.

Characterization of Synthesis

Grafting and Conversion Efficiency

UV-VIS Spectroscopy was used measure the grafting efficiency of FITC to the polymer, as samples were prepared in dilute DMF solution with concentrations of 0.7800g/L (0.002M) and 7.8000g/L for FITC and PKHH-FITC respectively. All samples were spiked with dilute HCl to reduce any residual pH responses from DMF and analyzed with the assumption that there was no change in molar extinction coefficient in order to determine the concentration of reacted FITC. A normalized absorbance at 453nm was then calculated for the FITC and the polymer samples that determined the concentration of FITC in the polymer using Beer's Law as shown in *Figure 91* and Table 12.

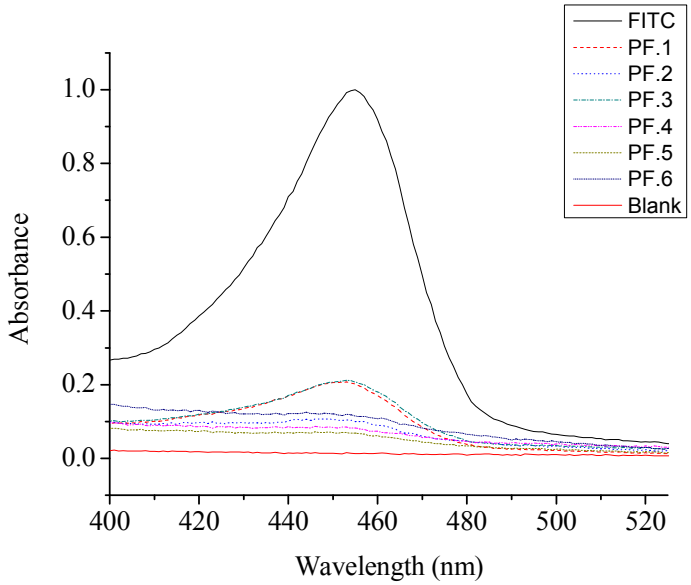

Figure 91. Absorbance Spectra at Low pH of the FITC and the Synthesized Graft Polymers, PKHH-FITC (PF) with Varying Concentrations of FITC.

Table 12

Summarized UV-Vis Data Showing Absorbance, Concentration, and FITC Content of Synthesized Polymers PKHH-FITC (PF)

Sample	Absorbance (453 nm)	Concentration (g/10mL)	FITC Content
FITC	1.000	0.0077	-
PF.1	0.207	0.0772	2.08%
PF.2	0.104	0.0777	1.04%
PF.3	0.212	0.0775	2.12%
PF.4	0.085	0.0797	0.83%
PF.5	0.070	0.0771	0.70%
PF.6	0.120	0.0775	1.20%

UV-Vis spectroscopy was also used to measure the pH conversion efficiency of FITC in the polymer. In a typical experiment, samples were converted by adding stock solution of a KOH saturated DMF solution with a pH >12 consisting of 0.7800g/L (0.002M) and 7.8000g/L of FITC and PKHH-FITC, respectively. The samples were analyzed with the assumption that there was no change in molar extinction coefficient in order to determine the concentration of reacted FITC. An average absorbance at 517nm was then calculated for the FITC and the polymer sample that determined the concentration of FITC in the polymer using Beer's Law is shown in *Figure 92* and Table 13.

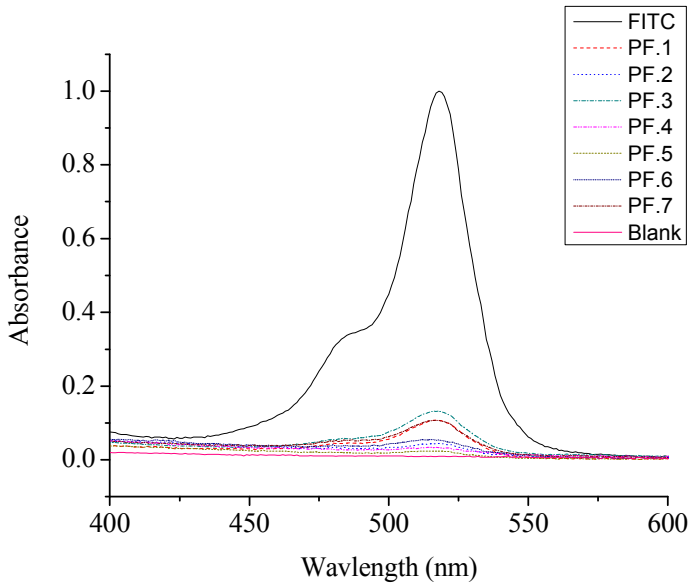

Figure 92. Absorbance Spectra at High pH of the Synthesized Graft Polymer Samples, PKHH-FITC (PF).

Table 13

UV-Vis Data Showing Absorbance, Concentration, FITC Content and % Conversion of FITC at a High pH of the Synthesized Polymers, PKHH-FITC (PF)

Sample	Abs. (517 nm)	Concentration (g/10mL)	FITC Content	Conversion of FITC
FITC	1.000	0.0077	-	-
PF.1	0.108	0.0772	1.08%	51.9%
PF.2	0.042	0.0777	0.42%	40.4%
PF.3	0.131	0.0775	1.31%	61.8%
PF.4	0.034	0.0797	0.33%	39.8%
PF.5	0.024	0.0771	0.24%	34.3%
PF.6	0.053	0.0775	0.52%	43.3%
PF.7	0.058	0.0779	0.59%	n/a

The FITC content in the grafted polymer dictates its sensitivity to pH changes. This varied between 0.24-1.31% and is enough to sufficiently detect corrosion since fluorescent probes are typically incorporated into coatings at 0.05-1.15% by weight.[45] It

should also be noted that the concentration of FITC in the polymer seemed elevated at lower pH compared to higher pH. This is possibly due to various factors: (1) the high temperature of 120 ˚C used in the synthesis deactivated some of the FITC molecules; (2) side reactions with phenolic and carboxylic acid moieties inhibited some of the FITC molecules from converting at high pH's; and/or (3) the molar extinction co-efficient of FITC may have been dramatically altered by tagging to the polymer PKHH. Future experiments may be warranted to investigate the discrepancy between high and low pH, even though this is will not be anticipated to significantly influence detection capability of the PKHH-FITC.

Fluorescence

All synthesized PKHH-FITC, functionalized phenoxy polymers fluoresced at an elevated pH after excitation at 517 nm. Samples showed fluorescence emission with the addition to the stock solutions of a KOH saturated DMF solution with a pH >12 consisting of 0.7800g/L (0.002M) and 7.8000g/L for FITC and PKHH-FITC, respectively. All synthesized polymers fluoresced with an emission intensity that is discernible against a control as seen in *Figure 93*.

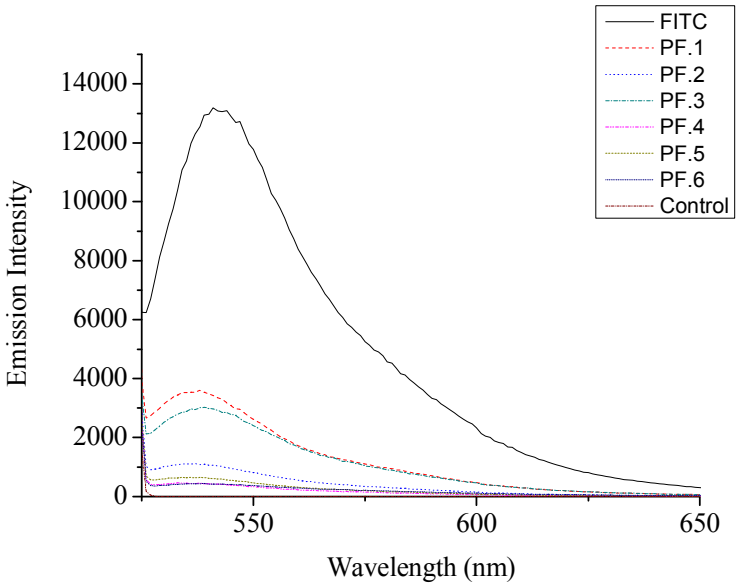

Figure 93. Fluorescence Emission Spectra at High pH of the PKHH-FITC Samples After Excitation at 517 nm.

The fluorescence emission intensities of all the synthesized PKHH-FITC increased with increasing FITC content and the order of emission strength was consistent with the data presented in Table 12. Low emission intensity such as the one exhibited by the PF2, PF4, PF5 and PF6 can also be advantageous in certain applications, including military, in which the need to conceal emission of light is desired without influencing the ability of the functionalized coating to detect corrosion. Thus using analytical tools like fluorescence spectroscopy provide an improved and more quantitative approach of detecting early microscopic changes at molecular level due to corrosion than visual inspection which will only detect corrosion after it has started as reported in literature. [45,46]

Differential Scanning Calorimetry, DSC

The glass transition temperatures (T_g) for the synthesized polymers were higher than the virgin phenoxy resin as presented in as seen in *Figure 94* below, thus resulting in a polymer that achieves slightly better packing. The T_g for the FITC functionalized

polymer was 98.80 ± 3.10°C while PKHH measured 88.58 ± 0.49°C. The 10°C increase can be attributed to a decrease in free volume and an increase in intermolecular forces provided by the FITC pendant groups which reduce the mobility of polymer chains or the removal of low molecular weight fractions during the purification process that utilized several precipitation cycles from chloroform into methanol.

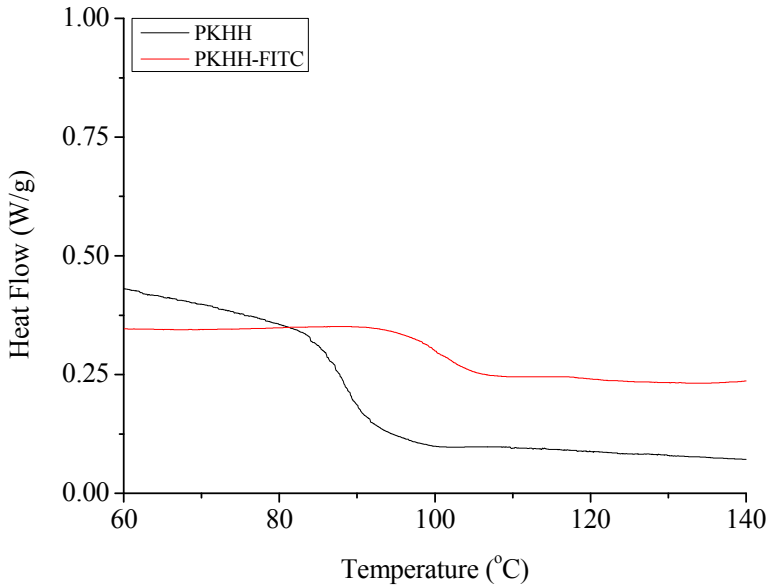

Figure 94. DSC of Neat PKHH and PKHH-FITC Polymer Showing Increase in T_g After Grafting.

Gel Permeation Chromatography, GPC

Gel permeation chromatography (GPC) was used to detect whether the fluorescence probe had grafted onto the high molecular weight polymer chain by using double detectors coupled in series to analyze the separated functionalized and non-functionalized units eluting from the column. *Figure 95* presents the refractive index (RI) response of the polymers that eluted through the column and shows that both the PKHH and PKHH-FITC gave similar RI response and the chromatograms were similar with respect to size shape and elution time. This indicates that the polymers, which had a concentration of 5 mg/mL, had similar number average molecular weights. Both the

ungrafted and grafted polymers eluted at 16.0 minutes, and their molecular weights were approximately 19,500 g/mol. Even though the supposedly heavier functionalized polymer was expected to elute faster, it was difficult to resolve and separate the chromatograms because of the low sensitivity of GPC used in this study coupled with the fact that the relatively low grafting caused insignificant changes in molecular weight that were below the detection limit of the GPC instrument.

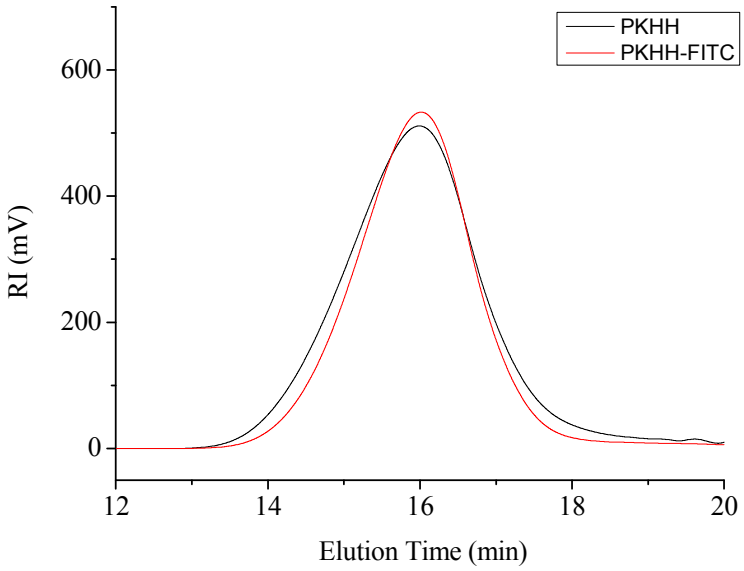

Figure 95. GPC Chromatogram Showing the Refractive Index (RI) Response of the PKHH and the Grafted PKHH-FITC.

Since fractional change in molecular weight of the PKHH was not detectable, grafting of FITC to the PKHH polymer was confirmed using an online UV detector coupled to the GPC. Because, FITC is sensitive to UV light and absorbs at a wavelength of 350 nm, and a functionalized polymer (PKHH-FITC) will be expected to show a stronger response compared to the virgin phenoxy resin as observed in *Figure 96*. The functionalized PKHH-FITC polymer produced a stronger UV response than the unmodified PKHH after injection at a concentration of 5 mg/ml. The stronger UV response is evidence that confirms the FITC was successfully attached to the PKHH.

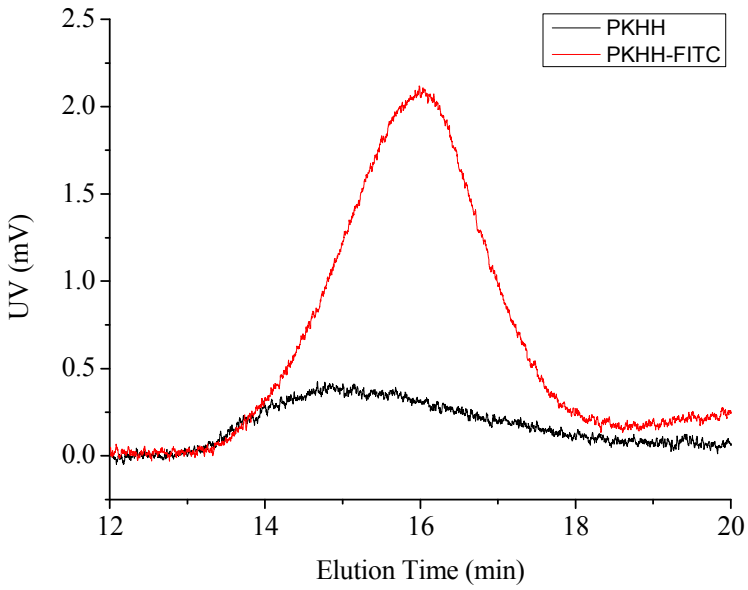

Figure 96. GPC Chromatogram Showing the UV Response of the PKHH and PKHH-FITC Injected at the Same Concentration of 5 mg/mL.

Proton Nuclear Magnetic Resonance, ^{1}H NMR

Since the FITC content was very low in the PKHH-FITC polymer ^{1}H NMR analysis before and after functionalization of PKHH did not show any significant spectral difference. However, to prove that a secondary hydroxyl is capable of reacting with FITC, a model system of isopropanol and FITC were allowed to react and characterized with proton NMR. It was assumed that the reactivity of isopropanol and FITC would be very similar to PKHH and FITC due to the fact that isopropanol is derived from the same structural unit found in the phenoxy resin. It was hypothesized that, after the reaction of isopropanol and FITC new peaks should appear on the ^{1}H-NMR spectra which can easily be differentiated from the reactants and should theoretically have peak integrals with a ratio of 9.0:1.0:6.0 for aromatic protons (6.3-9 ppm), tertiary carbon protons (5.2-6.3 ppm), and primary carbon protons (0.9-1.4 ppm), respectively. ^{1}H-NMR analysis of the reaction product from isopropanol and FITC showed new peaks that were consistent with the hypothesis and the experimental a peak

ratio of 9.0:1.0:6.6 demonstrating that the secondary alcohol such as the one isopropanol or PKHH can successfully react with FITC. In addition, two smaller peaks at 11.3 ppm and 11.4 ppm were observed in the ^{1}H-NMR spectra and these were assigned to thiourethane bonds formed from the reaction of the alcohol with the two isothiocyanate isomers. With proof that a secondary hydroxyl is reactive with FITC, it can be concluded that the secondary hydroxyl of a phenoxy polymer possesses the nucleophilicity to attack the isothiocyanate group on FITC and form the graft polymer PKHH-FITC.

Conclusions

GPC analysis using a UV detector confirmed that a high molecular weight thermoplastic phenoxy resin was grafted with a pendant pH stimuli-responsive FITC molecule. The FITC content in functionalized corrosion detecting polymers (PKHH-FICT) contained varied from 0.70-2.12 % which responds to high pH stimuli with an efficiency of 34.3-61.8%. At high pH, the resulting fluorescence produced emission intensities that differentiated from control specimens. Beside the photo-physical properties an increase in the glass transition temperature of 10 ˚C was observed after the graft polymer (PKHH-FICT). This increase in T_g was attributed to an increase in intermolecular forces and free volume due to the presence is the pendant FITC functional group. When all of the characterization of the polymer is considered, the ability for this system to be used in corrosion indication is easily correlated. In order to quantify the onset of corrosion, the polymer will be dissolved in an appropriate solvent, cast as a thin film onto a steel substrate, and monitored for increased basicity of the metal-polymer interface in real-time.

CHAPTER VII

DETECTION OF CORROSION

Several experiments were conducted that utilized the stimuli responsive nature of a PKHH-FITC polymer to indicate events directly correlated to steel corrosion. The experiments were coordinated for the validation that the pH fluorescent polymer could detect corrosion and measure events in a predictable manner. Specifically the polymer was used to track (1) corrosion rates in various halide solutions for comparison to current literature; (2) diffusion rates of ions as a correlation to corrosion initiation; (3) corrosion rates in varying concentrations of NaCl for comparison of literature; (4) corrosion mechanisms of multiple substrates to determine extent of versatility of PKHH-FITC polymer; and (5) corrosion events within natural weathering to determine practical application of the synthesized polymer.

The corrosion events and trends were monitored quantitatively through reflectance fluorescent measurements using a TECAN M1000® spectrometer allow for coated metal panels to be measured in real time. By mapping the panel's surface emission intensity values, information about where and when corrosion is occurring can be confidently gathered. When a coated steel panel was exposed to 0.5 M salt solution, corrosion initiation was quickly detected while scanning approximately every square millimeter of a 1536 plate definition (*Figure 97*). In *Figure 98* the digitized map represents the emission intensities of 248 out of the total 1536 points (in the middle of the panel) while the coating is exposed to the salt water solution.

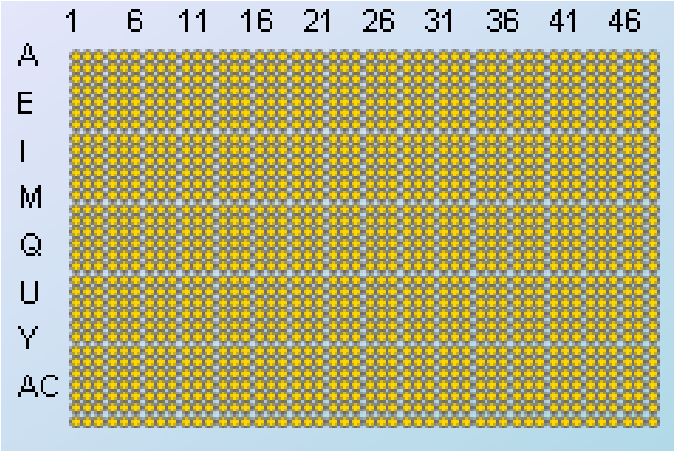

Figure 97. 1536 Points Plate Definition (a Single Point is Approximately 1 mm^2 area).

From this map, it can be calculated that the average fluorescence intensity was 24.7 with a relative standard deviation of 6.8%. The emission intensities across the coated surface at this point is considered to be homogeneous because the distribution of z-scores is Gaussian with a full width at half maximum (FWHM) value of 1.82 ± 0.13, as seen in *Figure 99*.

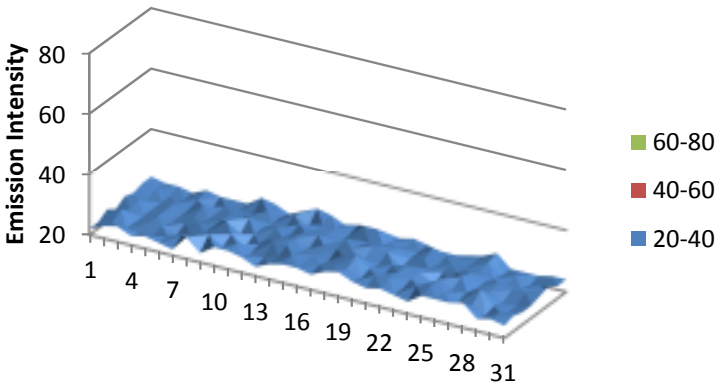

Figure 98. Fluorescence Emission Intensities of the Coated Steel Panel After Exposure for 4 Minutes in 0.5 M NaCl Solution.

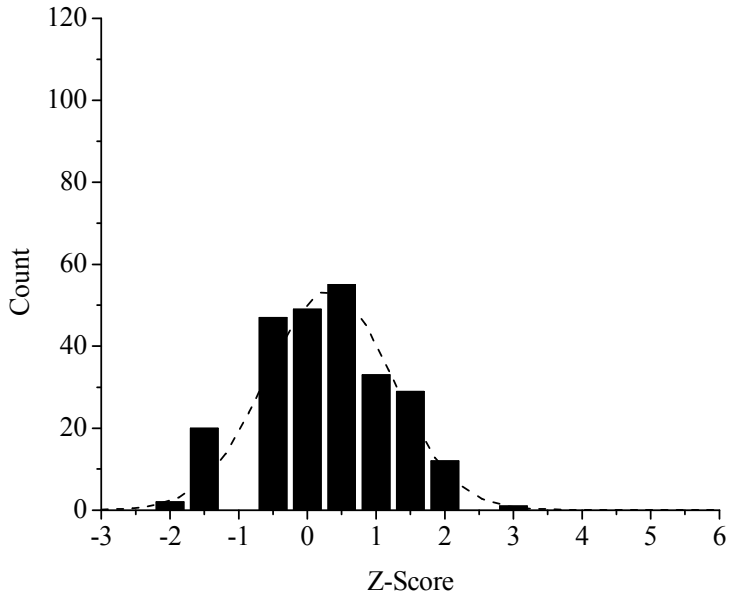

Figure 99. Statistical Distribution of Emission Intensities (After 4 Minutes Exposure).

Soon after exposure, discrete corrosion spots begin to appear which are represented by increased fluorescence intensity values as seen in *Figure 100*. Although the average fluorescence intensity only increased to 25.8 after 41 hours, the relative standard deviation rose to 17.8%. Since a large number of data points were acquired, the subtle changes at the metal-polymer interface might be overlooked when monitoring only the emission intensities. Therefore, monitoring the relative standard deviation will account for very minute changes that can be tracked with time. This was confirmed when the z-scores distribution was organized as represented in *Figure 101*. The data seems to lose the normal Gaussian distribution as the FWHM decreased to 0.83 ± 0.01 with a positive skew. The metal-polymer interface, at this point in time, can be labeled as 'heterogeneous' since areas of corrosion and corrosion-free regions exist simultaneously.

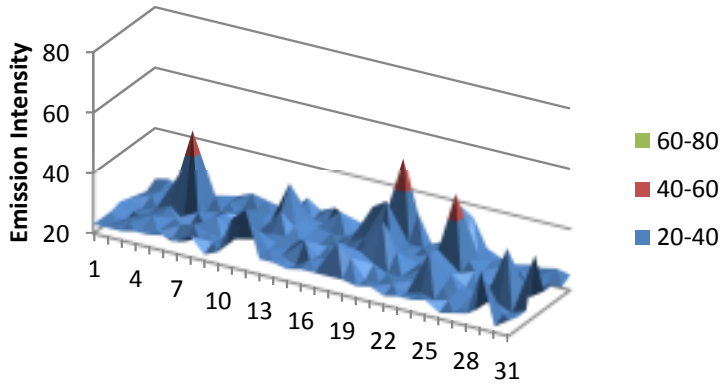

Figure 100. Fluorescence Emission Intensities of the Coated Steel Panel After 41 Hours of Exposure in 0.5 M NaCl Solution.

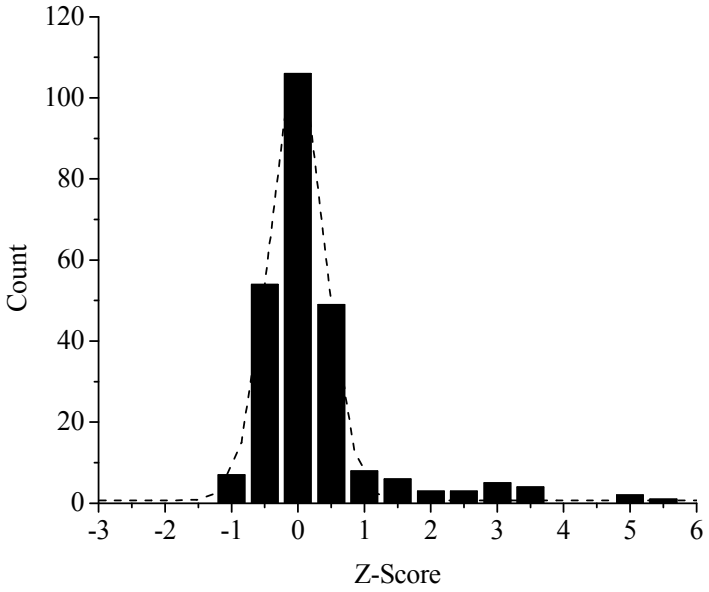

Figure 101. Statistical Distribution of Emission Intensities (After 41 Hours of Exposure).

Beyond the corrosion initiation after 206 hours of exposure, the progress of the corrosion reaction was very evident as seen in *Figure 102*. The reduction reaction of steel continually produced hydroxyl anions, which raised the local pH of the regions with larger changes in the fluorescence intensities.

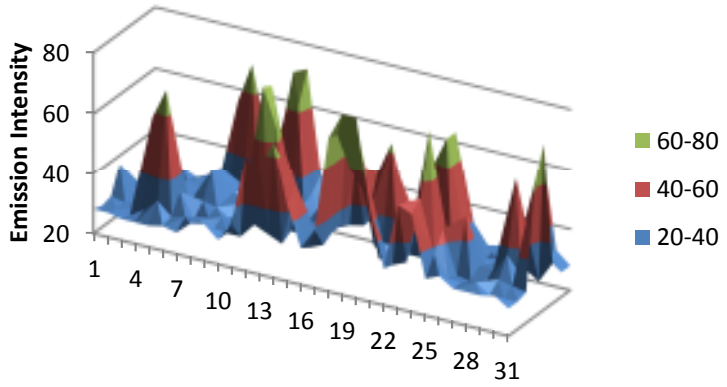

Figure 102. Fluorescence Emission Intensities of the Coated Steel Panel After Exposure for 206 Hours in 0.5 M NaCl Solution.

The continuous production of hydroxyl anions aided in monitoring the change in fluorescence emission intensity and relative standard deviation (or 'heterogeneity') over time, as trends were observed for four distinct zones as shown in *Figure 103*, *Figure 104*, and *Figure 105*. Zone I is the area where no corrosion has developed, followed by corrosion initiation in Zone II, 50% creep in Zone III, and 100% creep in Zone IV. Because of the large number of data points collected, the initiation of corrosion is difficult to identify while monitoring the average emission intensities. Therefore, monitoring the relative standard deviation as shown in *Figure 104* allows for more definitive quantification at the time when corrosion starts. Eventually corrosion would reach half of the area of the substrate, and at this point half of the panel has high fluorescence intensities while the other half has not relatively changed much. Thus the Zone III will show a maximum for the relative standard deviation because the distribution between values is the greatest. The rest of the panel would eventually corrode giving high intensities over the entire panel which drops the relative standard deviation as shown in Zone IV. The slope of the descending trend in Zone IV can be used to determine when corrosion has reached the entire surface, and its inverse can be

used as a unit for ‘corrosion severity’. The above mentioned method of quantification of the 'onset of corrosion' would allow for a valid ranking of corrosive environments that may occur well before the established ‘first stages’ of corrosion per ASTM 610-68. [72]

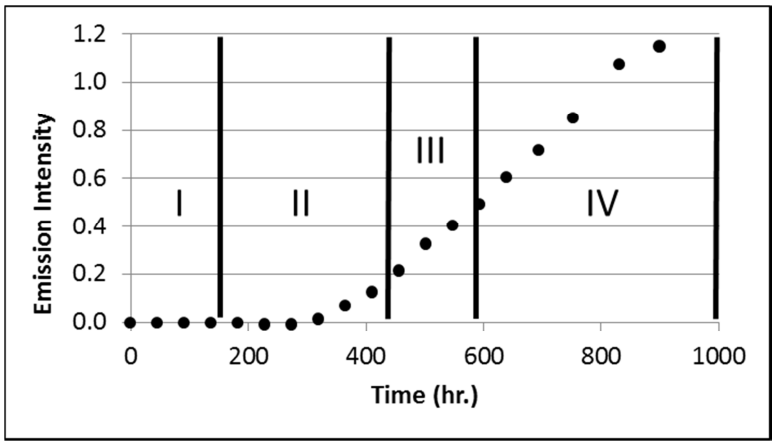

Figure 103. Representative Emission Intensity Plot.

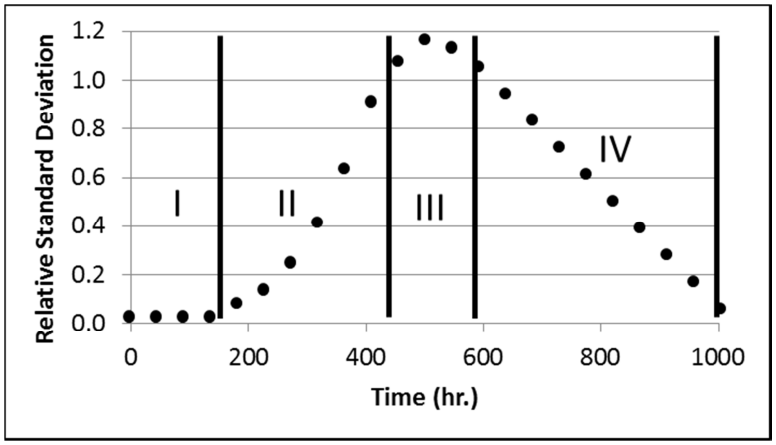

Figure 104. Representative Relative Standard Deviation Plot.

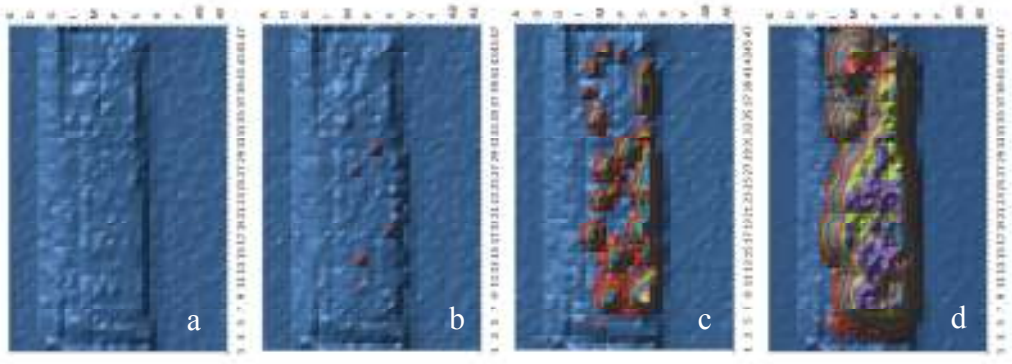

Figure 105. Emission Intensity Map Showing Zone I (a), Zone II (b), Zone III (c), and Zone IV (d) with 248 Data Points.

There was concern that the 1536 data point plate definition (*Figure 97*) for detecting corrosion was too low of a resolution since each data point is approximately 1mm apart from one another. There may be a possibility of development and spread of the reduction reaction occurring between these points causing erroneous results. Therefore another experiment was conducted that exhibited a plate definition of 26,600 (*Figure 106*).

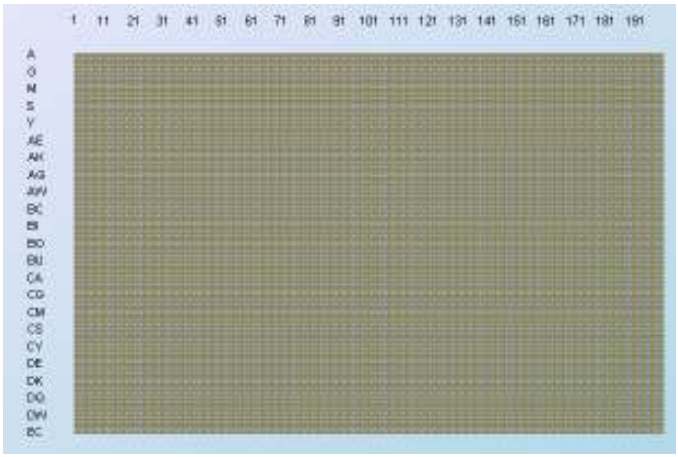

Figure 106. 26,600 Plate Definition.

Under these conditions, the resolution is greatly improved. If there is a corrosion event that is being missed, this plate definition should allow for a more detailed collection of data. However, the data gathered provided the same results as the lower

resolutions scan (*Figure 107*). Zones I, II, III, and IV all developed in the same time and manner as previously mentioned, but the digitalized images were more defined. Therefore, throughout this chapter, the plate definition used for collecting data is the lower resolution 1536, since it was justified to provide sufficient data for corrosion detection and it has a faster acquisition time by an order of magnitude.

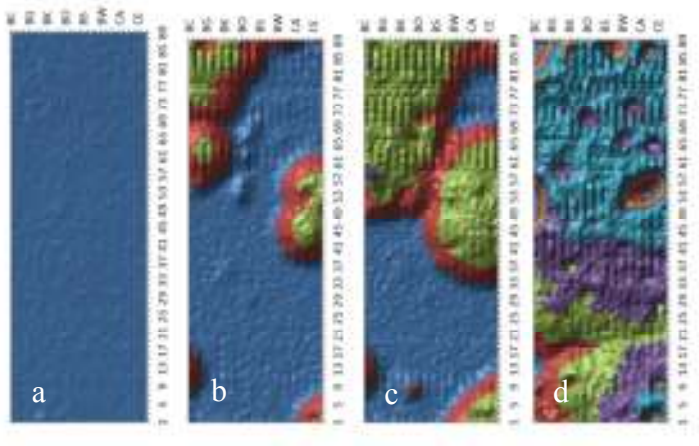

Figure 107. Emission Intensity Map Showing Zone I (a), Zone II (b), Zone III (c), and Zone IV (d) with 2403 Data Points.

Onset of Corrosion

Figure 108 depicts a polynomial line fit to the relative standard deviation of the 0.5 M NaCl exposure fluorescence intensities versus time, which is detailed in Table 14. The moment when the line leaves the x-axis would represent the time at which the corrosion is initiated on the metal and when high fluorescence intensity areas begin to appear that dramatically change the normal statistical distributions similar to what was shown in *Figure 99* and *Figure 101* previously. This method of fitting a line to the initial relative standard deviation will be used throughout this chapter as the method for quantification of corrosion initiation.

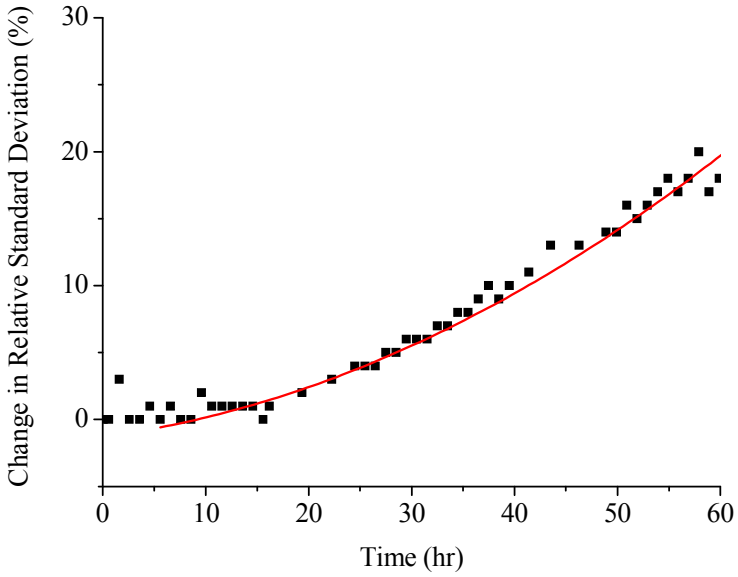

Figure 108. Changes in the Metal-Polymer Interface pH Heterogeneity for a 0.5 M NaCl Solution.

Halide Salt Composition Correlation to Corrosion

To determine the ability of a pH stimuli responsive polymer to detect corrosion, the polymer was exposed to environments known to start and facilitate corrosion at different speeds.[56,57] Each of the first four sodium halide salts in the group of the periodic table have been extensively studied for their ability to participate in iron dissolution from a substrate that will lead to the production of corrosion products.[56,57,61,62] Using the most common sodium halide, sodium chloride (NaCl), corrosion began at approximately 9.0 hours and rapidly rose in relative standard deviation compared to the other salts as shown in *Figure 108*. The corrosion initiation times and progress of the heterogeneity from Table 14 and *Figure 109*, respectively, ranks the corrosive nature of the salts as $Cl^- > Br^- > I^- > F^-$ as published by Tzaneva and coworkers.[56] Sodium chloride solution initiated corrosion the earliest and grew rapidly to the point where nearly half of the steel's surface had corroded after 150 hours.

Sodium chloride was able to achieve expedited corrosion since it is known to catalyze iron dissolution the fastest, which will release the electrons to produce the reduction reaction necessary for pH increase.[59] NaBr and NaI began corroding at a delayed rate compared to NaCl because they do not have the same capability of promoting the oxidation reaction as the chloride. The two grew in a similar manner, with NaBr displaying an earlier onset of corrosion than NaI which may be attributed to differences in ionic radii.[56,57] In Table 14, it was noted that the line-fit for the onset of corrosion for NaBr was an extrapolated linear fit rather than a polynomial, and the quadratic equation was not used. Sodium fluoride, as reported in literature, did not aggressively initiate corrosion to the degree that NaCl, NaBr, or NaI accomplished.[55] Corrosion did eventually initiate, however, it occurred nearly a week after exposure and only three data points consisting of the heterogeneity transition resulted in a correlation value of 1.000. The approximated time at which NaF initiated corrosion was recorded at 131.1 hours as seen in Table 14 and *Figure 109*. The dramatic lag of NaF behind NaCl, NaBr, and NaI results from the inability of NaF to participate in iron dissolution since a common intermediate of the process involves hypohalites.[56] The hypohalites for NaCl, NaBr, and NaI are stable at room temperature and will form during corrosion, however the hypohalite for NaF is not stable at room temperature and will not aid iron oxidation like other halide salts.

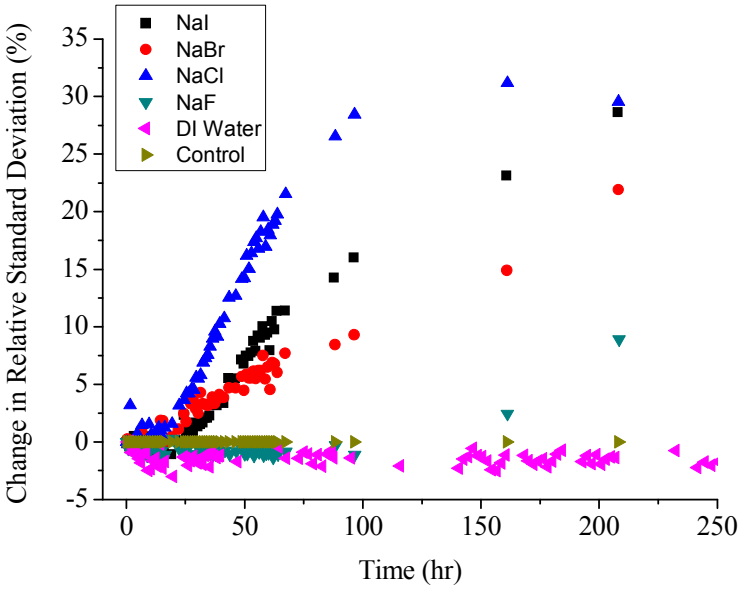

Figure 109. Change in the Metal-Polymer interface pH Heterogeneity for 0.5 M Sodium Halide Salt Solutions.

Table 14

Onset of Corrosion Line Fits

Salt	a	b_q	C	M	b_l	x (hr)	R^2
NaF	$7.0x10^{-6}$	-0.0013	0.0501	-	-	131.1	1.000
NaCl	$4.0x10^{-5}$	0.0011	-0.0131	-	-	9.0	0.992
NaBr	-	-	-	0.0029	-0.0486	16.8	0.825
NaI	$2.0x10^{-5}$	0.0011	-0.0318	-	-	20.9	0.967

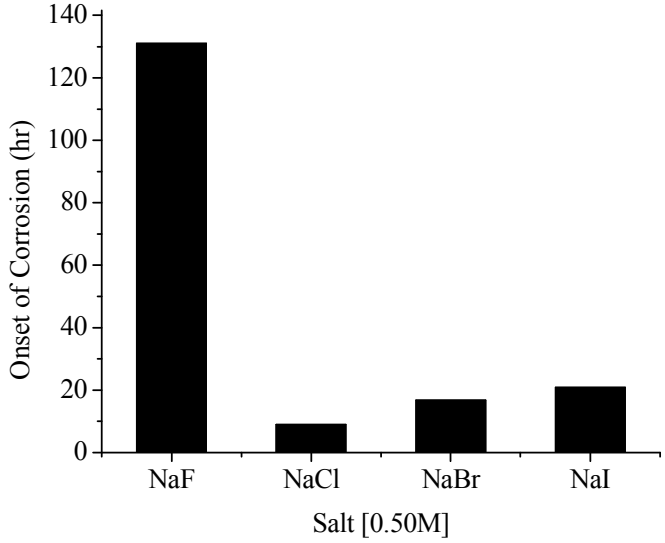

Figure 110. Onset of Corrosion for Sodium Halide Salt Solutions.

Conclusions

The aggressive trends in halide salts were confirmed as $Cl^- > Br^- > I^- > F^-$ using only a pH stimuli responsive polymer and fluorescence spectroscopy. Chloride must participate in the dissolution of iron at an accelerate rate compared to bromide and iodide with the changes in ionic radii. Although chloride, bromide, and iodide decrease in order of catalysis of iron dissolution by order of ionic radii, fluoride does not trend similarly. Therefore, fluoride must participate in a different mechanism before corrosion occurred at a dramatically slower rate. It could be assumed that fluoride does not participate in iron dissolution, but the conductivity of the aqueous solution promotes an environment that is more conducive for corrosion compared to a deionized solution. Therefore fluoride solutions are not inhibited, but rather they are also accelerated when compared to solutions devoid of ions and conductivity.

Meanwhile, the corrosion characterization technique of mapping the fluorescence intensities, location, and initiation of corrosion sites were proven able to correlate to

literature results. The developed fluorescence spectroscopic technique allowed each single steel panel/substrate to provide a large collection of data points, tracking the statistically relevant but subtle changes in pH at the metal-polymer interface and was determined to be a useful tool for non-destructive monitoring of corrosion underneath and within the protective organic coatings.

Ionic Diffusion Correlation to Corrosion

To confirm that ions are necessary at the metal-polymer interface to expedite corrosion, monitoring of the diffusion of those ions was developed using fluorescence spectroscopy. Since chloride and hydroxide ions have similar ionic radii and the polymer coated on the substrate is pH stimuli responsive, each was used to determine when ions reach the metal and if that event initiates corrosion. Four coated steel panels were prepared with the pH sensitive coating layer established as either the top coat, mid coat, or base coat as shown in *Figure 111*. When hydroxyl anions are allowed to diffuse through the first three coatings, each layer would fluoresce indicating penetration of ions along the z-axis. Once the ions have reached the surface, it is expected that the chloride sample shown on the far right would begin to show the early signs of corrosion. The time it takes for the ions to diffuse, saturate, and initiate corrosion were all quantified and compared to different diffusion speeds.

To change the speed of diffusion, dimethylformamide (DMF), was added to the 1M NaCl water solutions up to 50% by volume. At this level the refractive index of water does not change and all samples were easily assessed by the TECAN® since light was not traveling through the solution in any different manner. [103]

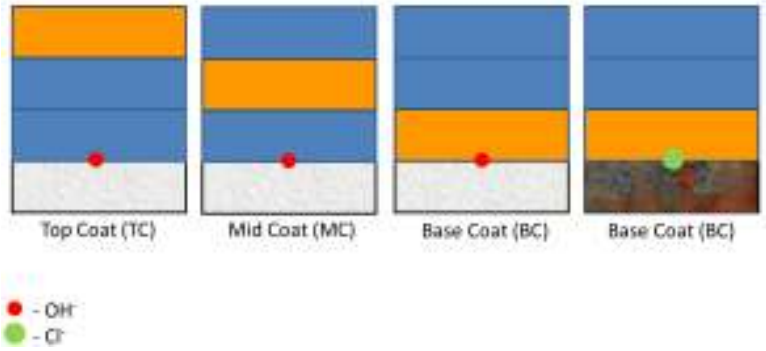

Figure 111. Schematic of Diffusion Corrosion Monitoring.

When the solution was put onto each of the four panels, and they were exposed simultaneously, the diffusion and initiation of corrosion were easily detected as shown in *Figure 112*. Within a day the top coat quickly saturates, while the entire coating is completely saturated with ions after one week. However corrosion is very evident after only a few hours. Therefore complete saturation of the base coat is not necessary to initiate corrosion, but the presence of a small amount of ionic moieties provides a sufficient environment for the onset of corrosion.

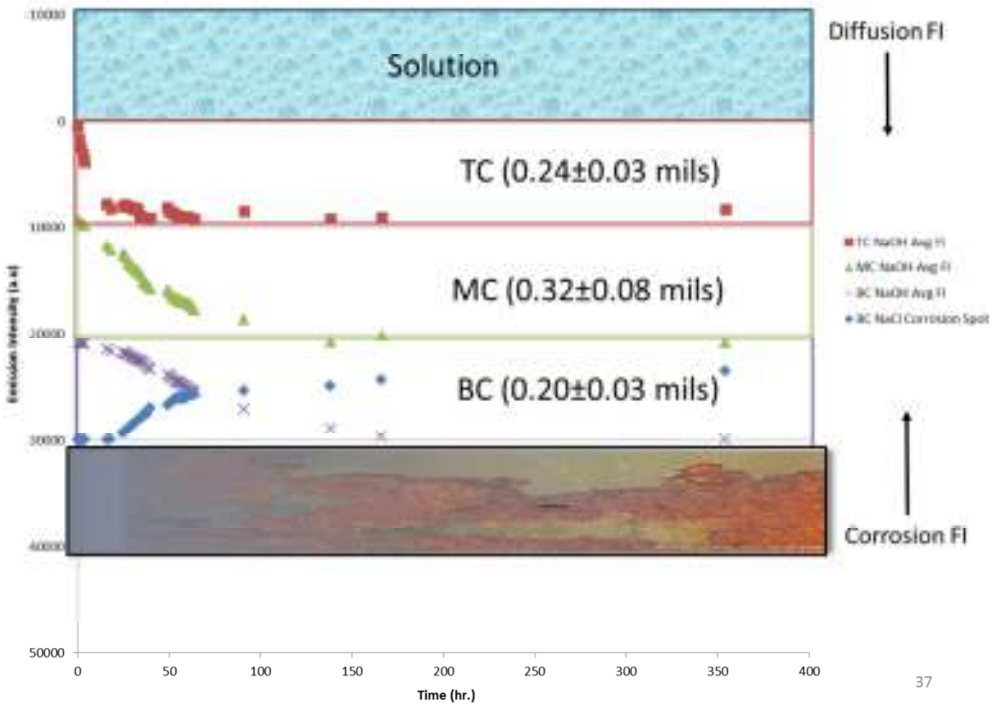

Figure 112. Diffusion and Corrosion Indication (90% Water, 10% DMF) Fluorescence Intensity (FI).

Although diffusion was seen dramatically increased with the addition of DMF (*Figure 113*), the ability to monitor the diffusion of hydroxyl anions in 100% water is problematic. Just as detecting magnesium ions in Chapter IV was difficult for an apolar medium, so is the detection of hydroxyl species within a bisphenol-A based polymer. Therefore, DMF was not only added to change the diffusion rates but also to allow for ions to separate from their contact pairs and be freely detected as they travel through the polymer.

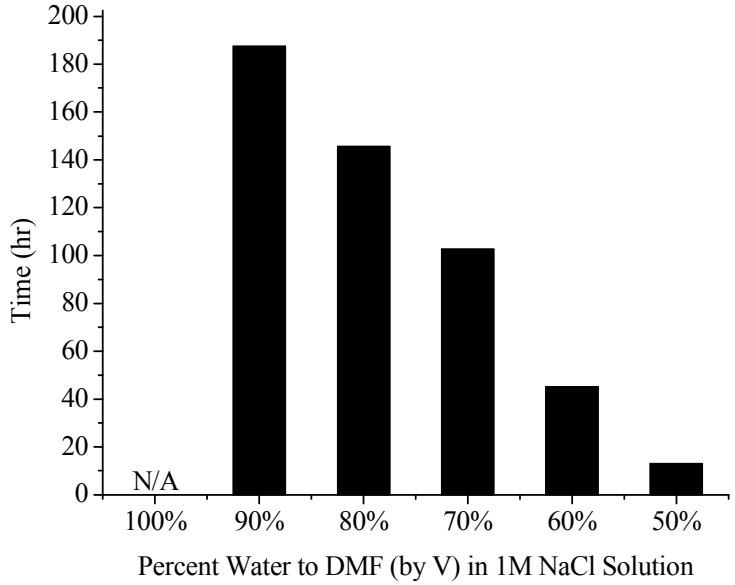

Figure 113. Saturation Point with Increased Amounts of DMF.

Although detecting ions within the polymer is difficult, detecting ions at the metal-polymer interface is a simpler procedure. As mentioned earlier, to fully quantify the first moment of corrosion, the relative standard deviation was monitored over time. When the values leave the x-axis, it is considered a change in the homogeneity at the metal-polymer interface from the corrosion related reduction reaction of steel. Therefore, when plotted and fitted with a line (*Figure 114*), each sample was given a quantified 'onset of corrosion' value as given in

Table **15** except for DI water, which did not initiate corrosion within the time scale of the experiment due to low solution conductivity.

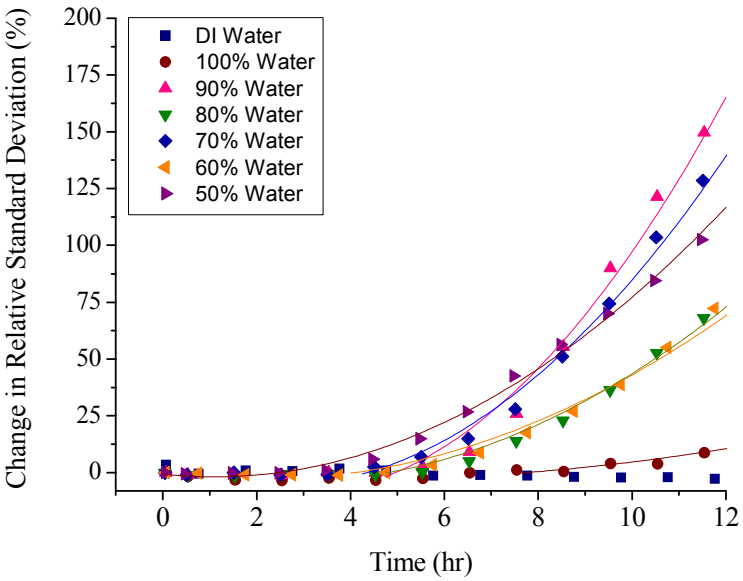

Figure 114. Change in Relative Standard Deviation (corrosion initiation).

Table 15

Polynomial Line Fits for Quantifying the Onset of Corrosion

% Water	a	b	c	x (hr)	R^2
100	0.0020	-0.0148	-0.0054	7.75	0.9874
90	0.0209	-0.1198	0.0799	4.96	0.9895
80	0.0087	-0.0450	0.0152	4.81	0.9963
70	0.0160	-0.0795	0.0429	4.35	0.9961
60	0.0048	-0.0141	0.0043	2.59	0.9997
50	0.0100	-0.0222	-0.0061	2.47	0.9953

As the amount of DMF increased, the diffusion rates increased causing the ions to appear at the metal's surface quicker. Once they reached the surface, corrosion is initiated at different times as shown in *Figure 115*. However, each of those initiation events did not occur in the same chemical environment at the metal-polymer interface. *Figure 116* shows the amount of ions within the basecoat at the point where corrosion began. Although the 90%, 80%, 70%, and 60% only needed less than 7% saturation to provide enough conductivity for corrosion to occur, the 50% water solution exceeded

35% saturation. At this point, the diminishing amount of water has to be considered. Since DMF is an aprotic solvent, it will not participate in the reduction reaction of iron degradation. Therefore, when the molar ratio of water to DMF goes below six (Table 16), there is not enough water present for the reactions and various solvation mechanisms. [104] This experiment shows how accelerated testing can provide quick corrosion results, but it must be monitored rigorously so that the mechanistic pathways of corrosion are not altered.

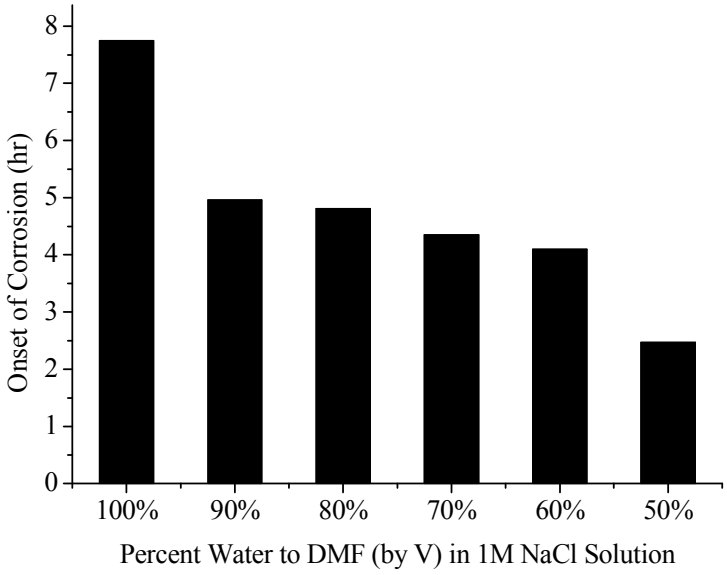

Figure 115. Time for Onset of Corrosion with Different DMF Loading Levels.

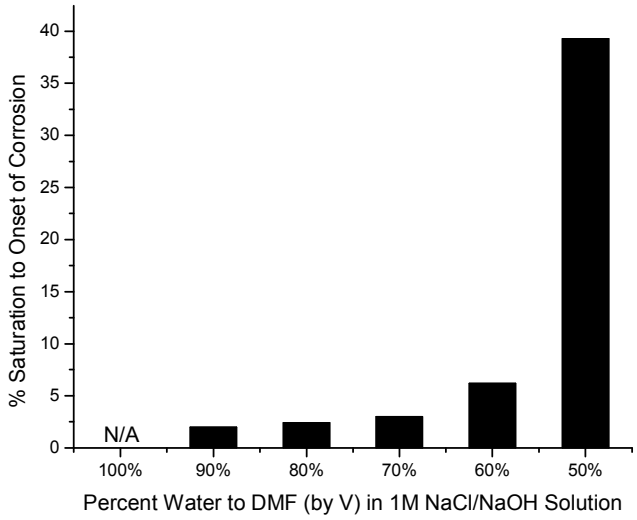

Figure 116. Percent Saturation of Base Coat Needed to Initiate Corrosion.

Table 16

Molar Ratios of Water to DMF

% Water by V	Molar Ratio (Water:DMF)
100	∞
90	38.67
80	17.19
70	10.03
60	6.44
50	4.30

DMF solution summary

It was determined that steel panels begin corrosion in less than 8 hours when exposed to a 1M sodium chloride solution on a sub-macroscopic level. This corrosion begins well before macroscopic or visible failure. Diffusion of hydroxyl ions cannot be thoroughly tracked through the mid coat of a three-layer thin film in 100% water. This is likely caused by the hydrophobicity of the PKHH resin causing the hydroxyl ion to

form a solvent separated pair with the sodium ion in order to decrease the solvation and residual water surrounding these ions. It was also demonstrated that the onset of corrosion occurs well before the base coat of the three-layer thin film is saturated. This means that only a fraction of the ions in the 1M sodium chloride solutions are required to initiate the onset of corrosion.

The rate of diffusion is directly related to the amount of DMF present in the solution the sample is exposed to. Thus, DMF causes saturation to occur more rapidly by facilitating the diffusion of ions through the coatings. Dimethylformamide also facilitates the dissociation of ions, as seen by the change in fluorescence intensity of the mid coat sodium hydroxide panel that was masked in the 1M sodium hydroxide in a water solution. The amount of DMF present is subsequently related to the rate of corrosion, since the ions can reach the substrate faster which causes corrosion to happen more rapidly. Meanwhile, even increasing the amount of DMF to 50% of the solution does not change the mobility of the fluorescence polymer. As seen in *Figure 117* the fluorescent polymer maintains its original position whether it was in the top coat, mid coat, or base coat. Therefore it can be confirmed that all of the preceding data was accurate and not the result of any diffusion of fluorescent molecules, which is possible in systems where the small molecules are not tethered to the polymer.

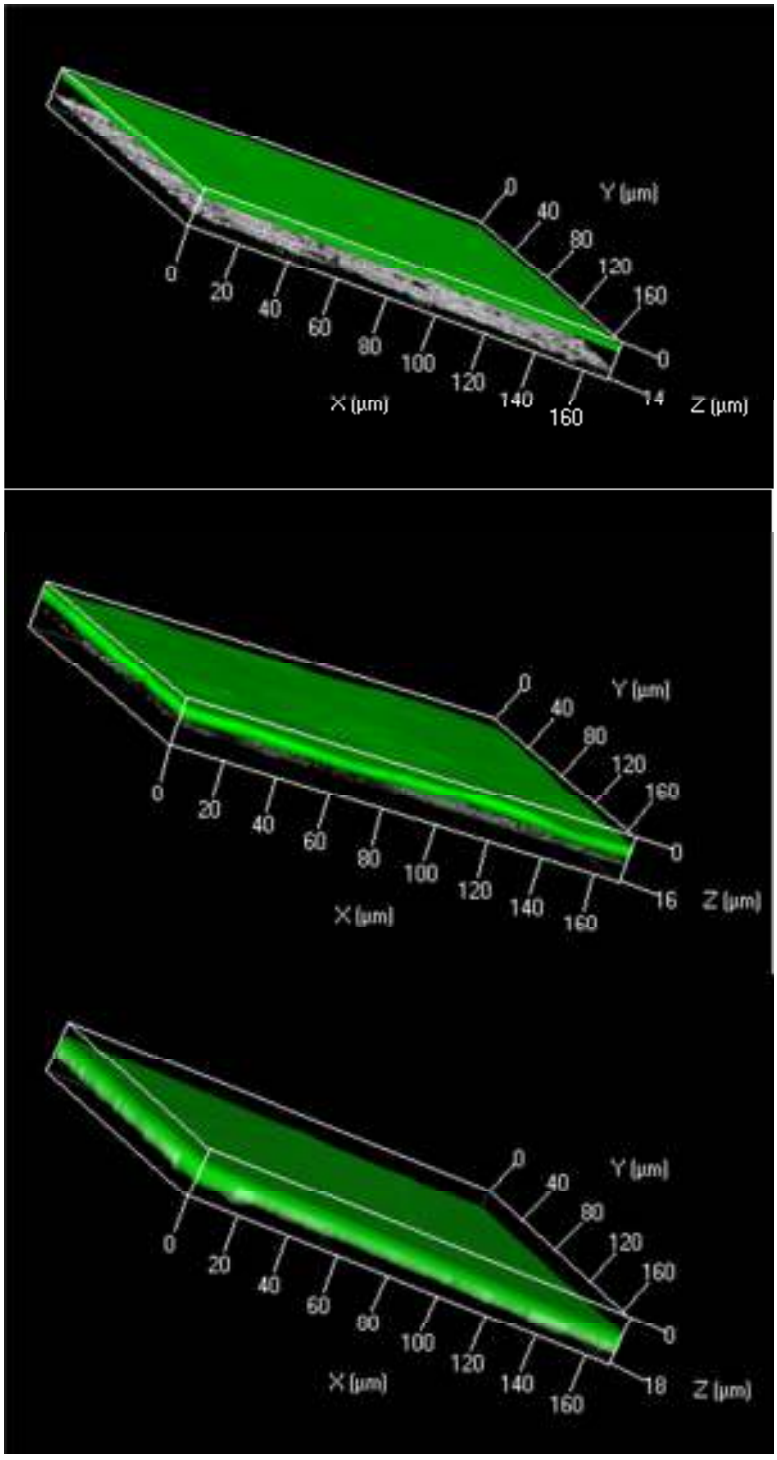

Figure 117. Confocal Z-Stack Images of TC (top), MC (middle), and BC (bottom) After Exposure to 50:50 Water:DMF 1M NaOH Solution.

Minimal amount of DMF needed for accelerated ionic testing

Although DMF has been shown to accelerate the rate of diffusion and corrosion reactions, it can also alter the corrosion mechanism above the water to DMF ratio of 6. DMF may also change chemically when introduced to water where it is known to degrade and may form amines. [105] If a plethora of amines are present in a diffusing or corrosion inducing solution, then the amine could act as a buffer, hydrogen bond disrupter, or inhibitor that can mask traditional corrosion pathways that need to be monitored. Therefore 1M NaOH solutions between 100% to 91% water (by volume) were prepared and titrated with various pH indicators. Phenolphthalein, methyl red, and bromophenol blue indicators were used that could illicit a different response from amine formation since they each tested pH ranges 8.0-10, 4.4-6.2, and 3.0-4.6 respectively. Therefore if amines were not developed from DMF in the alkaline aqueous solutions, each indicator would use the same amount of titrant to reach their specified endpoint.

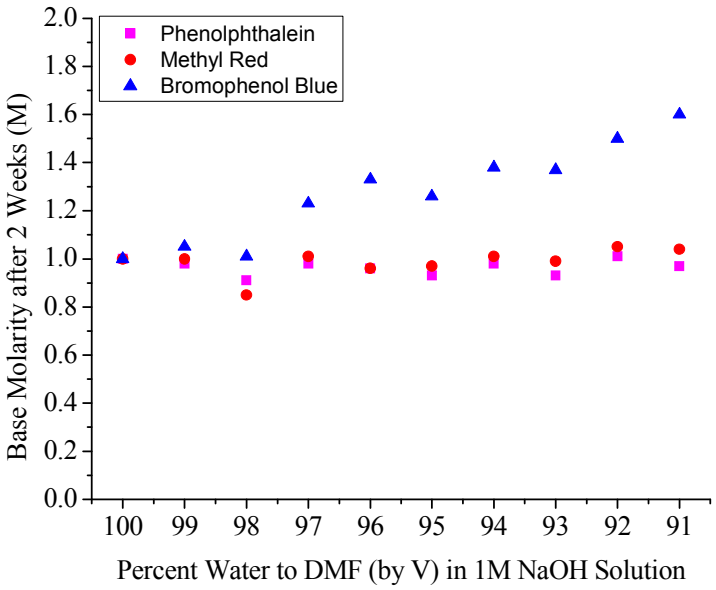

Figure 118. Titration Results of 1M NaOH Solutions Containing Various Amounts of Water to DMF with Three Separate Indicators.

However, as seen in *Figure 118*, the titration results for each indicator show that residual amines can be found. Phenolphthalein and methyl red did not distinguish a difference between any of the samples because their pH range is unable to detect weak bases that can form buffers. When bromophenol blue was used, it was able to detect a major difference in the amount of titrant used as the DMF content increased in water. This trend was also confirmed while using a universal indicator of thymol blue (*Figure 119*), which will turn from blue to green to yellow to orange to red in pHs from 10 to 8 to 6 to 4 to 2 respectively. This allows for the detection in changes of titrant use in a single experiment by finding the amount used for the yellow and red transitions. The yellow transition is similar to what phenolphthalein and methyl red demonstrated which showed no difference in its neutral point with the addition of DMF. However, the red transition mimicked the results found from bromophenol blue where buffered amines can be detected. Therefore as DMF increases, so does the contribution to the basicity from amines. Because the contribution was not shown for water to DMF ratios of 99 or 98, it can be assumed that these mixtures can be used in future diffusion versus corrosion experiments without altering corrosion mechanisms.

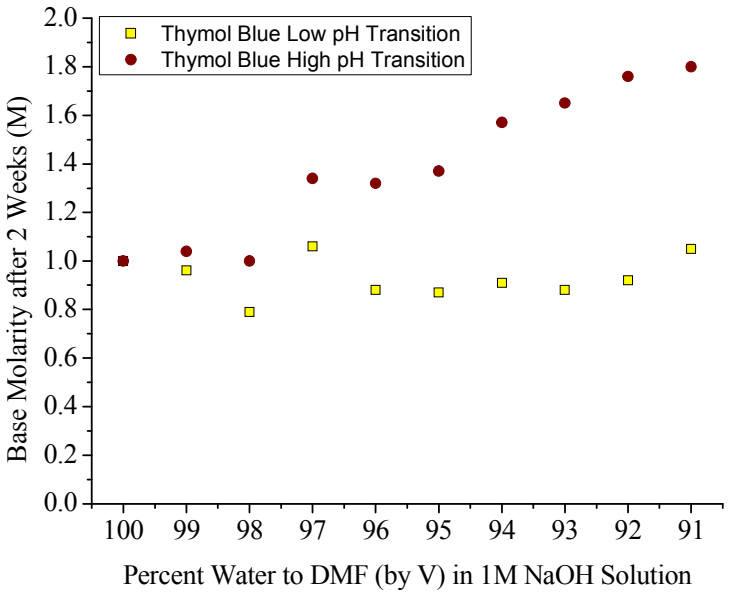

Figure 119. Titration Results of 1M NaOH Solutions Containing Various Amounts of Water to DMF with a Universal Indicator.

Although water to DMF ratios of 99 and 98 were not shown susceptible to DMF degradation, it had to be determined if their 1M NaOH solution could still induce response in a pH stimuli polymer. It is known that a purely aqueous 1M NaOH solution has insufficient amounts of hydroxyl anions for detection within an apolar polymer; therefore DMF was added to aid in the separation of ions so that corrosion diffusion rates could be determined. Since DMF has now been shown to degrade to form amines, it must be determined if DMF contributes to ion separation or increases base content to cause the indication. As shown in *Figure 120*, solutions containing 99 or 98% water indicated substantially more hydroxyl anions than the 100% water system without the aid of amine content. Therefore future experiments can utilize 1 or 2% DMF in a 1M NaOH aqueous solutions to allow for ionic separation within apolar polymers without the influence of compounds that could alter the data.

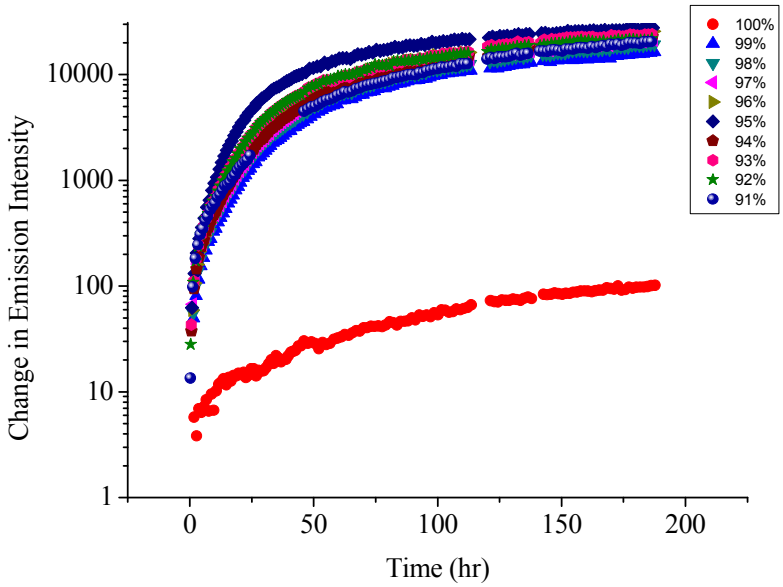

Figure 120. Change in Emission Intensity of pH Stimuli Responsive Polymer Exposed to 1M NaOH in Various Water to DMF Ratios.

Minimal amount of DMF diffusion studies with control substrate

When repeating the diffusion versus corrosion experiment with a new solution containing only 1% DMF, a new aspect was introduced to the experiment. While testing the corrosion behavior of steel, another control was added that used a substrate that did not corrode. By coating a polyester masking tape, commonly used to mask metal specimens for weathering, it can be determined whether the substrate has any role in the facilitation of diffusion. This will provide knowledge as to whether a metallic substrate provides any additional potential for a solution to approach a metallic interface through a polymer, or if diffusion is solely a polymer dependent process.

Figure 121 and *Figure 122* demonstrate the ability of NaOH to penetrate through three layers of a coating and quickly reach the substrate interface. Both substrates demonstrate their top coats saturating in less than a week followed by the base and mid coats after three weeks.

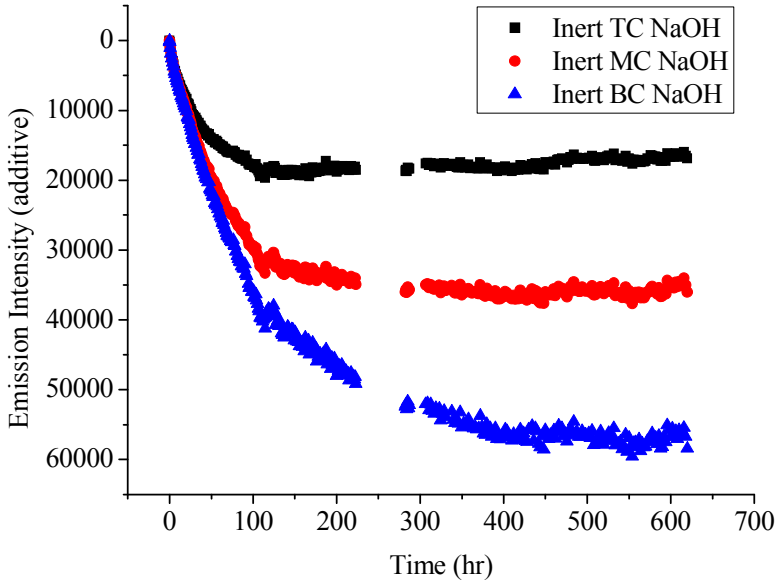

Figure 121. Diffusion of 1M NaOH Through Coating to Inert Substrate.

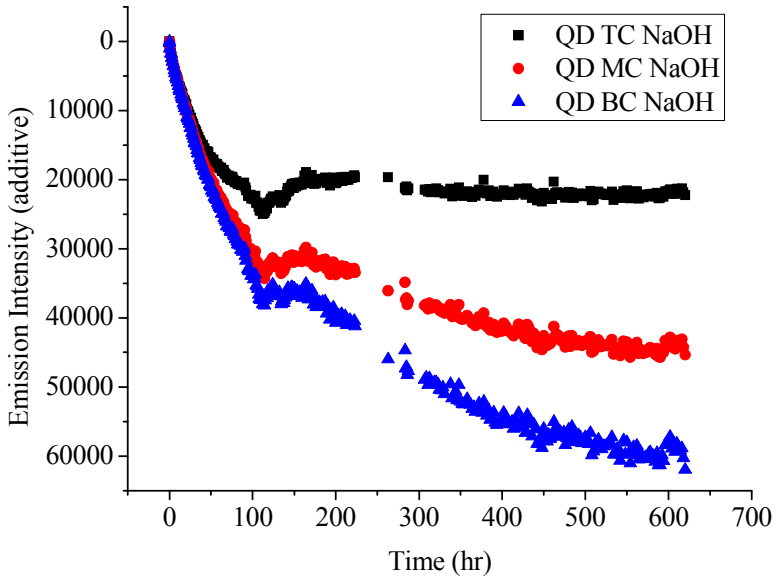

Figure 122. Diffusion of 1M NaOH Through Coating to Steel Substrate.

To differentiate between the two substrates, the initial slope of the diffusion was overlayed over another in *Figure 123*. The first 50 hours of diffusion for the two systems is identical. Within the first 50 hours the base coat contains enough ionic content to manifest products from the reduction reaction on over 25% of the steel

surface as seen in *Figure 124*. Therefore, diffusion of ions that directly relates to the initiation of corrosion is polymer related (dependent). The contributions from the substrate are not significant enough to drive diffusion any faster or slower since it is shielded from a large organic barrier.

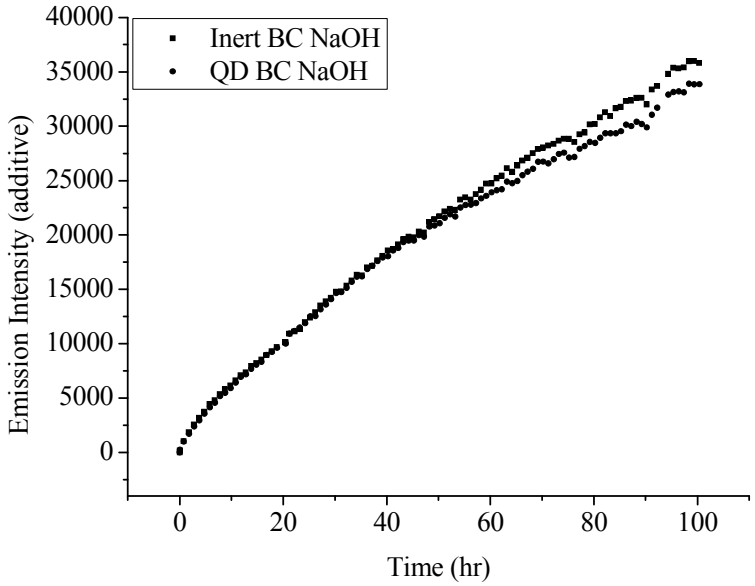

Figure 123. Initial Slope of Diffusion Through Coating to Both Substrates.

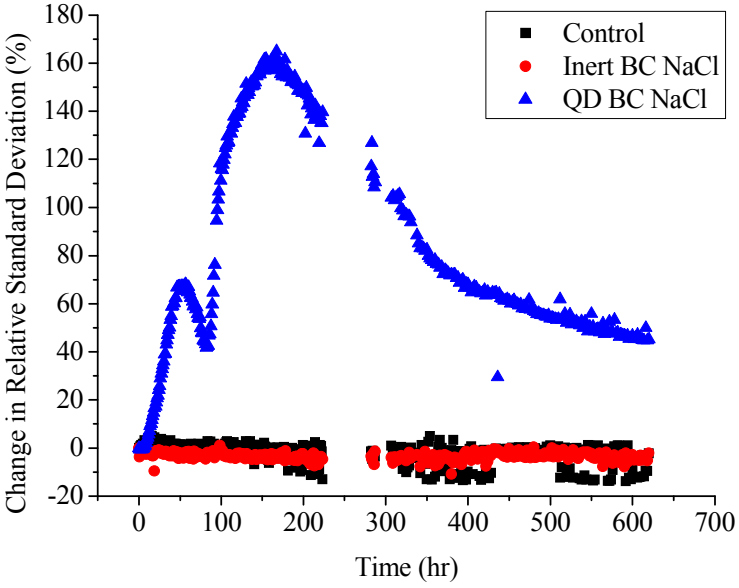

Figure 124. Change in Relative Standard Deviation in NaCl for Different Substrates.

The initiation of corrosion is easily tracked by monitoring the change in relative standard deviation for the steel substrate, whereas the inert substrate and dry control show no changes during the time scale of the experiment. This provides confidence in previous data, clarifying that contributions from NaCl would not give false positives during exposure. The initiation of corrosion, shown at 5.72 hours, also would fit into *Figure 115* where the 1% DMF corrosion initiation is between the 0% and 10% DMF start times of 7.75 and 4.96 hours respectively.

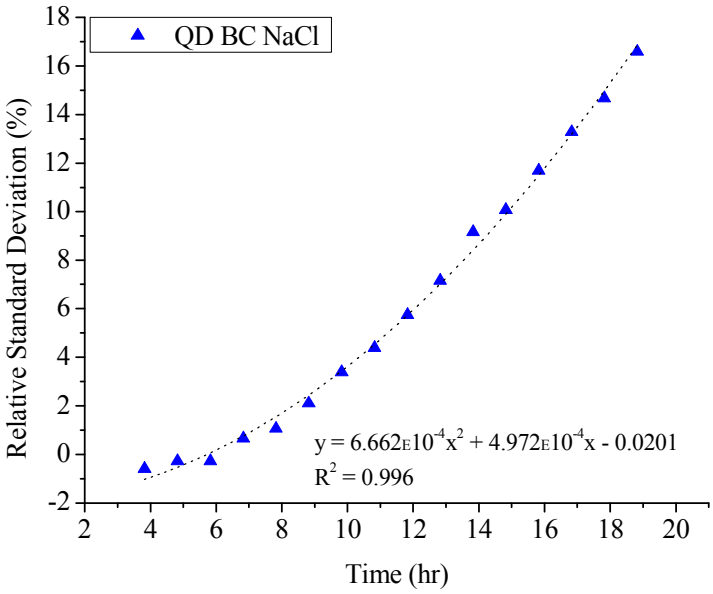

Figure 125. Initiation of Corrosion for QD BC in NaCl.

Correlation of Sodium Chloride Concentration to Corrosion

Since conductivity is an essential parameter for the initiation and severity of corrosion, the transfer rate of electrons to the reduction reaction can be changed by altering the sodium chloride concentration in water. Thus, when preparing deionized, 0.01M, 0.10M, 0.50M, 1.0M, 3.0M, and 5.0M sodium chloride aqueous solutions, the amount of ions present in water has a direct correlation to the initial conductivity of the solution as shown in *Figure 126*. Therefore it can be expected that rust formation will

begin and spread the quickest at high salt concentrations compared to deionized water where the altered pathway for electrons to travel causes the corrosion rate to slow.

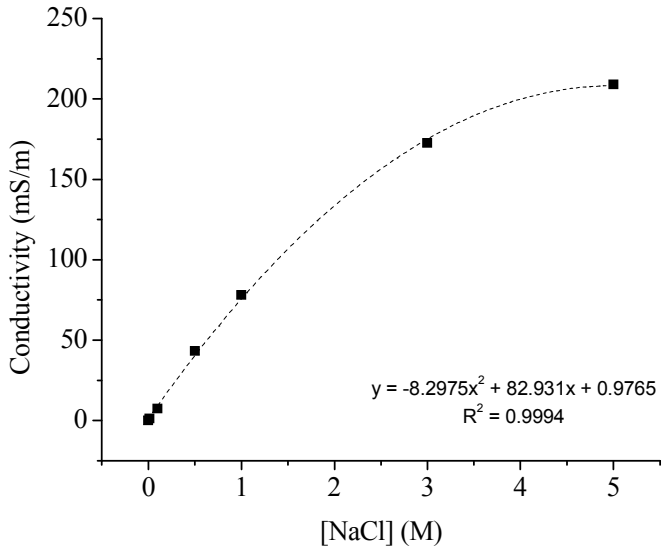

Figure 126. Conductivity of NaCl Solutions.

Figure 127 shows the change in relative standard deviation over the duration of the experiment trending as previously mentioned in which zones I, II, III, and IV are easily discernible. DI water and the control did not show corrosion within the time scale of the experiment. Concentrations 5.0 and 3.0M were the quickest to reach and complete all four zones while the other concentrations never fully reached zone IV within 1000 hours of exposure.

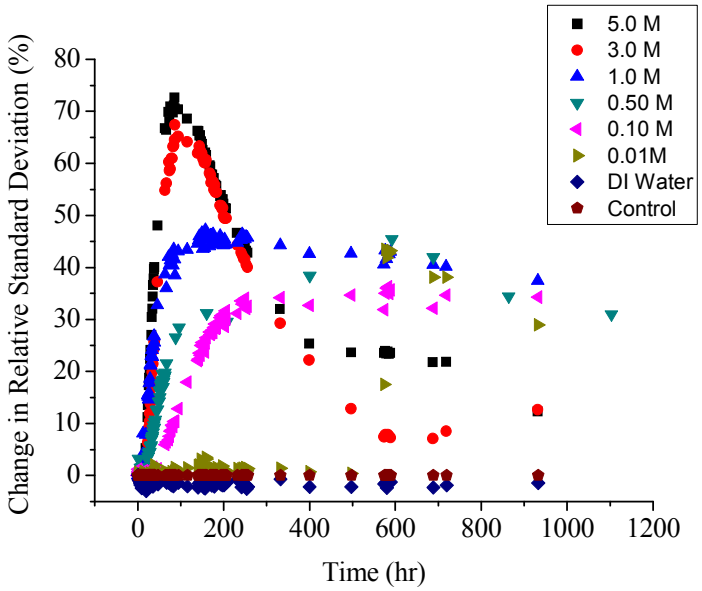

Figure 127. Change in Relative Standard Deviation of Varying [NaCl].

This is important because samples 5.0, 3.0, 1.0, and 0.50M initiated corrosion at similar times, noted in Table 17, however their corrosion mechanisms vary drastically outside of zone II.

Table 17

Onset of Varying [NaCl] Corrosion Line-Fits

[NaCl]	A	b_q	c	m	b_l	x (hr)	R^2
0.00	-	-	-	-	-	-	-
0.01	$8x10^{-5}$	-0.084	21.463	-	-	610.7	0.8111
0.10	-	-	-	0.0021	-0.0753	33.6	0.9943
0.50	$4x10^{-5}$	0.0011	-0.0131	-	-	9.0	0.9920
1.0	$5x10^{-5}$	0.0067	-0.0493	-	-	6.3	0.9759
3.0	$3x10^{-4}$	-0.0038	0.0045	-	-	11.3	0.9940
5.0	$4x10^{-4}$	-0.0034	0.0024	-	-	7.7	0.9959

Since 5.0 and 3.0M solutions quickly progress through zone III and complete zone IV, they can be considered to exhibit ‘fast corrosion initiation’ and ‘fast corrosion creep’. The 1.0 and 0.50M samples started corrosion promptly; however their creep in

zones III and IV was drastically delayed compared to 5.0 and 3.0M. Since their conductivities were so low, they were not able to facilitate in the creep mechanism as efficiently, therefore these samples were labeled 'fast corrosion initiation' and 'slow corrosion creep'. Samples 0.10 and 0.01M were even slower in the initiation and creep of corrosion and were labeled as 'slow corrosion initiation' and 'slow corrosion creep'.

From six concentrations, corrosion was easily quantified using initiation and creep parameters and corrosion behavior was characterized in a more effective manner than a typical ranking system. These quantifiable values can be plotted, *Figure 128*, for corrosion initiation and, *Figure 129*, for corrosion severity (or creep). The two charts demonstrate how the six samples can be divided into three specific groups that allow for a detailed and critical assessment of corrosivity in each environment. The 5.0 and 3.0M are highly corrosive since they are able to easily disrupt the formation of a protective oxide layer on iron through the constant attack from chloride anions.[68] Samples exposed to 1.0 and 0.50M solutions were able to initiate corrosion quickly but did not propagate extensively because the concentration of chloride ions is reaching the point where repassivation of the iron surface is competing with chloride, which makes it difficult for corrosion to be maintained at an accelerated pace.[66,68,69,70] Samples 0.10 and 0.01M are relatively slow for corrosion in all aspects because the repassivation reaction of iron is faster than the ability of chloride to destroy that surface.[66,68,69,70] Therefore, as seen previously in *Figure 116*, once the NaCl concentration has exceeded 7-10% of 1M (0.07-0.10M) the environment for rapid removal of steel's oxide layer and promotion of corrosion is evident.

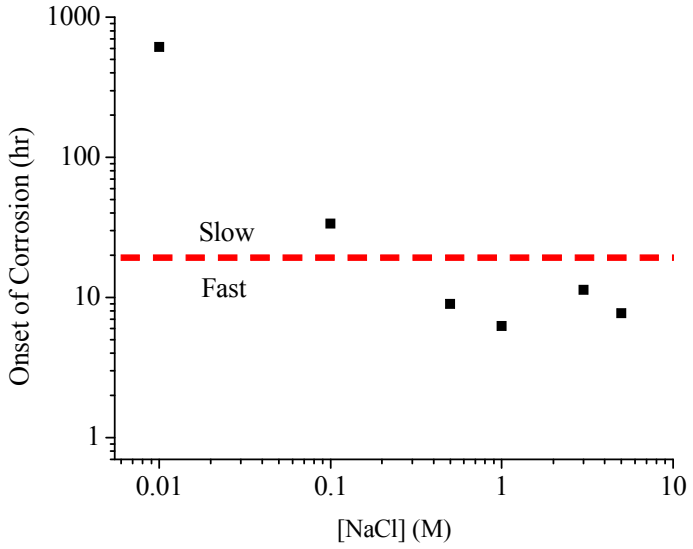

Figure 128. Onset of Corrosion of Varying [NaCl].

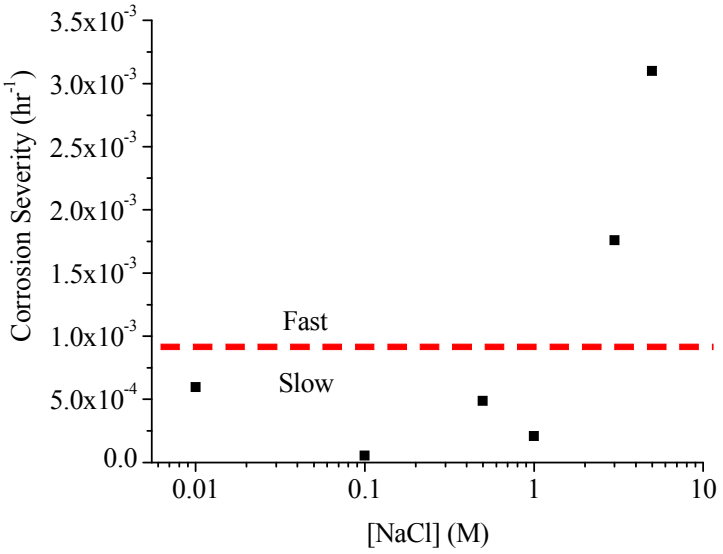

Figure 129. Corrosion Severity of Varying [NaCl].

Substrate Comparison

Although previous studies have shown the successes of a pH stimuli responsive polymer in detecting corrosion, there are limitations that will provide future work in this field of study. In particular, each of the previous studies have been conducted on ASTM

D 609 Type 3 steel which corrodes very easily and the FITC modified polymer was able to detect corrosion in real time when adhered to its interface. However a wide assortment of substrates are used throughout the world such as stainless steel (ASTM A 624), aluminum (3003 H14), and aerospace aluminum (Al-2024). Each of these substrates corrodes differently than bare steel, but they should show changes in pH that are related to corrosion. As seen in *Figure 130*, each substrate shows either a large or slight increase in emission intensity due to an increase in pH. Aluminum 3003 H14 showed a small change in emission intensity since aluminum is able to form protective oxide layers quickly. Stainless steel showed an increase in pH as well, however it was not maintained throughout the experiment since stainless steel is more prone to pitting corrosion which is difficult for the polymer to detect since the coating is only in intimate contact with the metal's surface. Therefore, once the corrosion progress underneath, the polymer will lose its detection ability. As our previous studies have shown, ASTM D 609 steel increases emission intensity during the corrosion process since the surface of the metal is very alkaline during corrosion. Also the corrosion stays on the surface since this metal seems to corrode via a more uniform corrosion mechanism. Meanwhile, aerospace aluminum shows a drastic increase in emission intensity within the first day of exposure but the emission plateaus soon thereafter. Substrate Al-2024 might be able to passivate quicker than 3003 H14 aluminum, which could explain why Al-2024 was stabilized early during exposure to salt water.

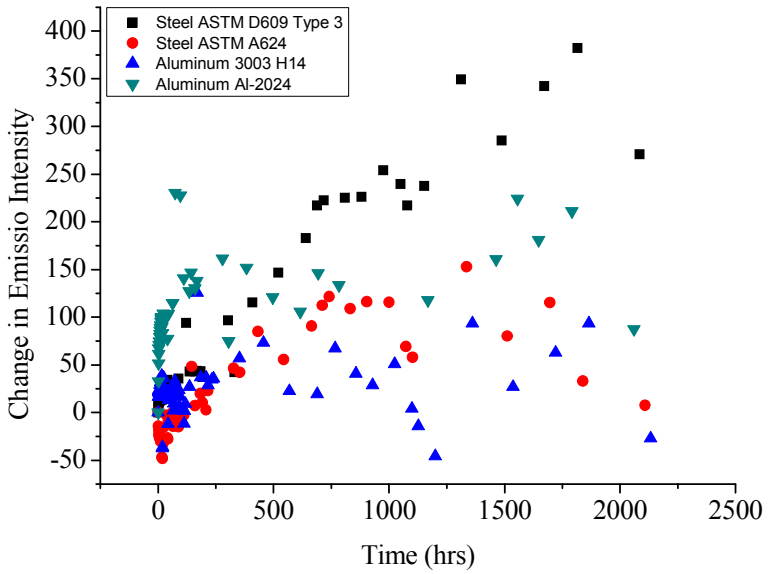

Figure 130. Emission Intensities from Multiple Metallic Substrates During Corrosion.

To clarify some of the corrosion mechanisms for each substrate, the relative standard deviation as shown in *Figure 131* can provide insight as to where and how corrosion progresses. When the two aluminum based substrates were exposed to salt water 3003 H14 fluctuated in emission intensity while Al-2024 increased quickly and plateaued. However they both showed no increase in relative standard deviation, thus indicating that whatever event caused the pH to change was occurring evenly over the entire substrate. A common event that occurs this fast on a metallic substrate is passivation, where a metal oxidizes quickly enough to protect itself. Therefore, even though Al-2024 showed an increase in emission intensity, it does not necessarily mean that corrosion was indicated for that substrate since the relative standard deviation remained the same. Optically, when Al-2024 corrodes (*Figure 132*), the corrosion initiation locations are not uniform and are distributed heterogeneously. Although the indicating (stimuli responsive) polymer is able to detect these events, it is difficult to decipher from the data when the corrosion began and ended for both of the aluminum

substrates. Likewise, it was difficult to obtain meaningful corrosion data from the stainless steel sample because of extensive pitting, depths that a glassy polymer is unable to reach. The relative standard deviation did show an early event that warranted a strong response, but once the corrosion began underneath the surface of the metal, the graph lowers and levels like the results for aluminum. This occurs because the pH environment on stainless steel after 400 hours is the same over the entire surface because corrosion has now moved in the z-axis downward. Luckily ASTM D 609 Type 3 steel was able to clearly reveal when corrosion started by both the emission intensities and relative standard deviation. As shown earlier in this chapter, this experiment went through Zones I and II and approached Zone III which is indicative of 50% of the panel initiating corrosion. No other substrate was able to provide this much quantifiable data, and new systems will have to be developed to detect aluminum and stainless steel substrate failures.

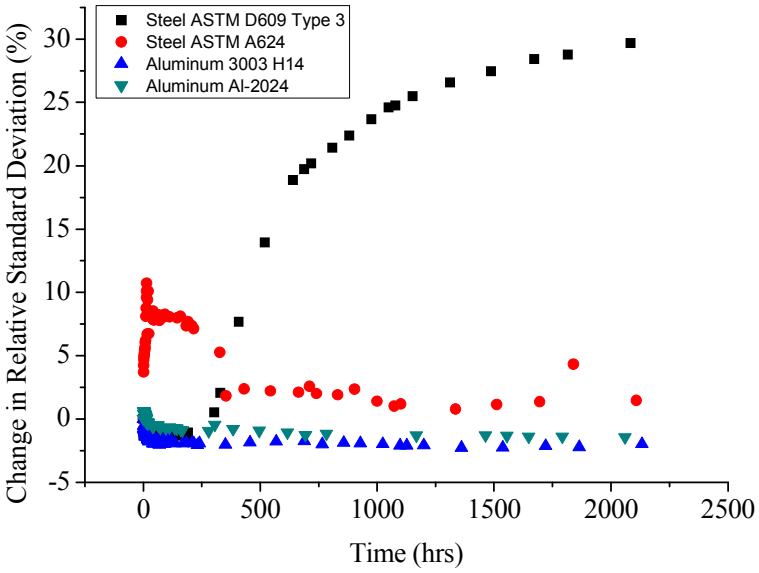

Figure 131. Relative Standard Deviation From Multiple Metallic Substrates During Corrosion.

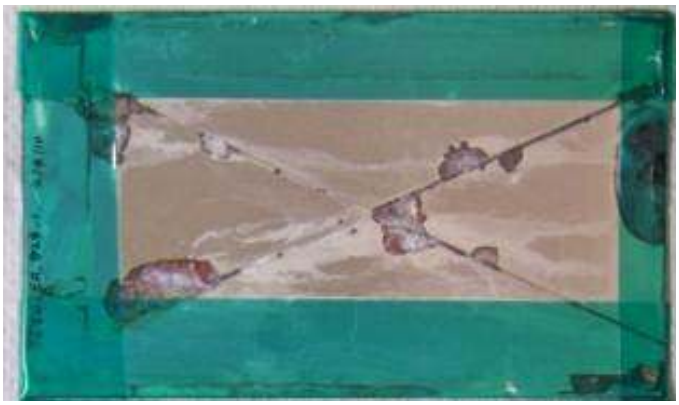

Figure 132. Corrosion of Coated Al-2024.

Natural Weathering

Fluorescence

When the pH stimuli responsive polymer was exposed to natural weathering in Hattiesburg, MS, the fluorescein based fluorescent molecule photobleached with and without the aid of an aliphatic acrylic top coat. As seen in *Figure 133*, both of the bare and top coated coatings reduced in emission intensity to values below the initially measured quantity. It can be noted that the acrylic system had an elevated emission intensity at the beginning of the experiment since a water based acrylic coating was used that had several stabilizers incorporated into the formulation that could be alkaline in nature. However those molecules are able to slowly evaporate from the film, thus not hindering the coating from detecting corrosion. The corrosion related increase in emission intensities resulted from the non-top coated system which started corroding after 5.2 days. The top coated system did not show any visual corrosion after 38 days which is approximately the same time period it takes to exhibit an increase in emission intensity (*Figure 133*).

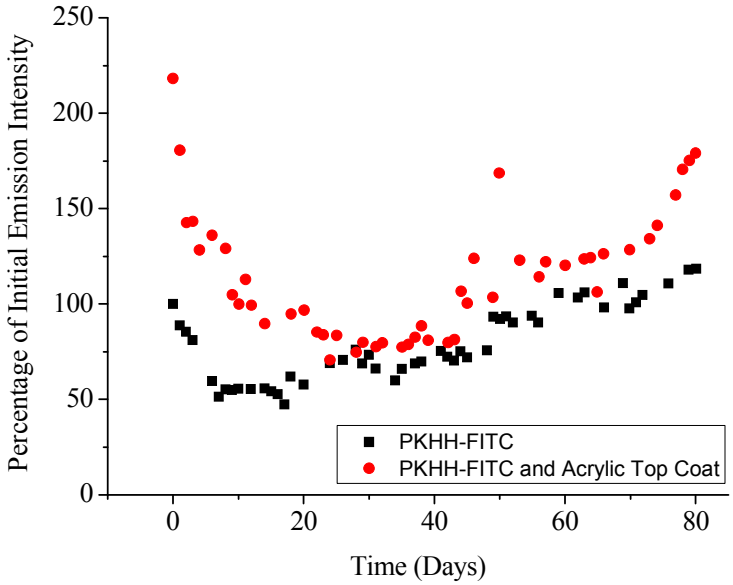

Figure 133. Emission Intensity Changes During Natural Weathering.

The corrosion initiation time was able to be quantified from the non-top coated coating since its relative standard deviation (*Figure 134*) maintained Zones I, II, III, and IV as described previously. Although it is not as pronounced as previous experiments, it is promising that natural weathering was able to produce curves similar to those found in a laboratory setting. Unfortunately, the top coated panels did not exhibit Zones I, II, III, or IV because of complications from the commercial coating formulation prematurely triggering some of the fluorescein molecules before exposure. Therefore, the baseline readings were not accurate to compare to each scan that occurred thereafter. However, the comparisons between the two coatings by using emission intensities still provided evidence of corrosion starting at the same time as that of visual inspection noticed initiation. Therefore it can be confidently stated that incorporating this particular top coat onto the PKHH-FITC polymer increases the corrosion resistance by a factor of 7.3. Being able to quantify the improvement a coating provides an important new monitoring tool that could replace previous ranking systems that are typically used when comparing one coating to another. Therefore this method, not only proves that the polymer is able

to detect corrosion in natural weathering, it is also able to provide hard evidence confirming the corrosion prevention capabilities of newer coatings versus old technologies.

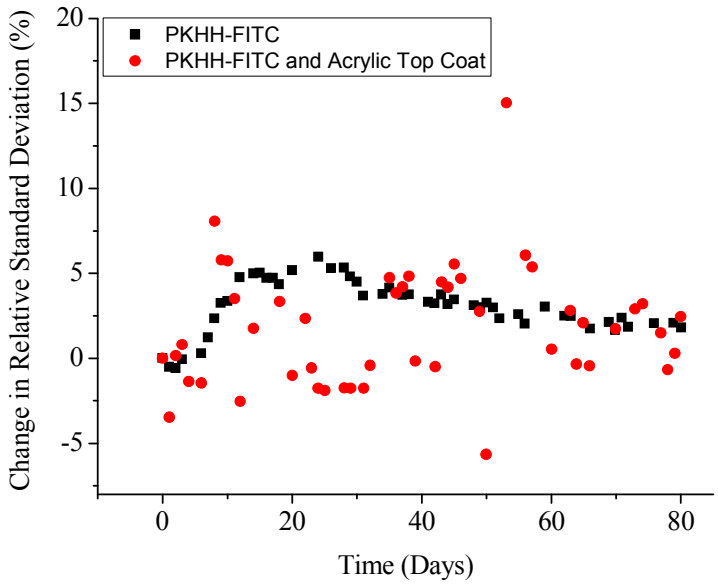

Figure 134. Change in Relative Standard Deviation During Natural Weathering.

Infrared Spectroscopy

Although application of a top coat greatly improved the corrosion resistance, corrosion still occurred and post-hoc analysis of infrared spectroscopy provided insight as to the reasons why both of the polymers eventually failed. After carefully removing the coatings from their respective substrate, they were analyzed using ATR-IR spectroscopy so that both the air and substrate interface could be analyzed. The air interface should include most of the products from UV degradation while the substrate interface will determine if those products were found throughout the matrix.[73] *Figure 135* shows the mid-IR spectra of the PKHH-FITC that is not top coated. The air interface shows extreme amounts of degradation product as the alkyl region (<3000cm^{-1}) is decreased and the carbonyl region (1800-1650cm^{-1}) increased, due to the alkyl

functionalities being sacrificed into more oxidized groups during degradation. However, the substrate interface shows a stronger alkyl and weaker carbonyl concentration which suggests that the degradation of the phenoxy polymer from UV radiation only occurs at the air interface. The substrate interface shows a large increase above 3000cm^{-1} and at 1530-1680cm^{-1} which are both representative of large amounts of water. Therefore, even though the substrate interface did not show large amounts of degradation from UV radiation, the ability of water to easily diffuse through the polymer and carry contaminants that induce corrosion was the mechanism for failure.

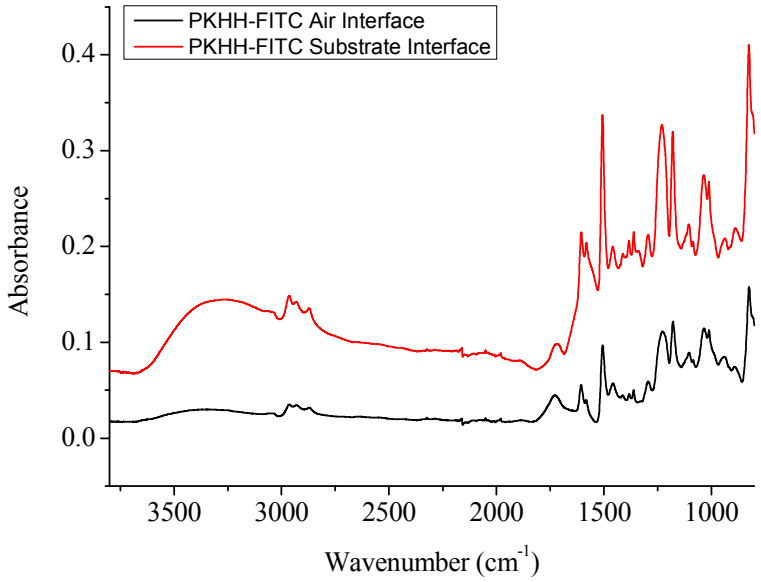

Figure 135. Infrared Spectroscopy of the Air and Substrate Interface After Exposure (Non-Top Coated).

When a top coat was added, water must have been withheld longer than the non-top coated system, however it must have eventually penetrated after the 38 days of exposure. *Figure 136* shows the mid-IR spectra of the PKHH-FITC polymer top coated with a commercial acrylic coating. The air-interface shows the absorbance of the acrylic polymer while the substrate interface shows the PKHH-FITC polymer. Once again the PKHH-FITC polymer shows a lack of degradation while showing increases above

3000cm^{-1} and at 1530-1680cm^{-1} from the inclusion of water into the coating system. Therefore, the aliphatic top coat resisted aqueous diffusion better than the phenoxy polymer, but corrosion was only delayed not prevented. By using fluorescent spectroscopy, top coat functioning was able to be quantified. Future experiments could test the effectiveness of pigment and more hydrophobic polymer in their ability to thwart water penetration prior to corrosion development.

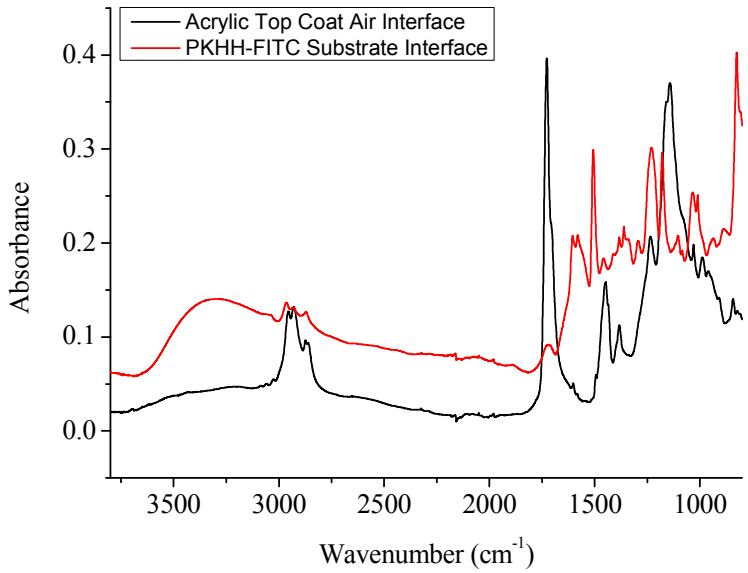

Figure 136. Infrared Spectroscopy of the Air and Substrate Interfaces After Exposure (Top Coated).

Conclusions

After successfully synthesizing a pH stimuli responsive polymer that fluoresces in alkaline environments, it was feasible to thoroughly monitor the bare steel substrates for their pre-rust reactions (behavior). Aided by the TECAN® M1000 plate reader, a new method of tracking corrosion was developed with an ability to quantify the aspects related to corrosion. This new characterization technique was able to replicate electrochemical experiments in literature in a real-time and in a non-destructive manner. Mentioned earlier, the novel pH stimuli responsive polymer was able to determine

(1) corrosion rates in various halide solutions for comparison to current literature; (2) diffusion rates of ions as a correlation to corrosion initiation; (3) corrosion rates in varying concentrations of NaCl for comparison of literature; (4) corrosion mechanisms of multiple substrates to determine extent of versatility of PKHH-FITC polymer; and (5) corrosion events within natural weathering to determine practical application of the synthesized polymer.

As ions are traveling (diffusing) through an apolar epoxy polymer matrix only 0.07-0.10M of chloride ions were necessary to initiate corrosion while the rate decreases as different halide anions interacted with steel. It was also determined that within an apolar polymer, ionic compounds like NaOH can only dissociate into their free ionic form at less than 1%. Therefore, utilizing an organic modifier to water without changing mechanistic pathways of corrosion proved to be advantageous to determine how ions are mobile through barrier coatings regardless of their association. Whether the ions are associated or dissociated, the rate that they reach a substrate (metal or an inert) is polymer dependent. Therefore any thoughts that a metallic substrate is participating as the driving force for ionic media to move through a polymer would be erroneous for this particular coating system. Therefore improvements upon enhancing permeability to ionic moieties must be done through polymer science advances in research. Overall, this technology could produce data in the real world conditions and at the early stages of corrosion that could give insight (detection) into the initiation of macroscopic coating system failure.

CHAPTER VIII

SUMMARY

In *Figure 7* the research tasks that accompanied this research document were listed, and they were completed to yield new understanding in polymer and corrosion science. For Task 1, it was essential to determine if chain scission was necessary to preface corrosion. Through the successful synthesis of model polymer that mimicked several different epoxy-amine thermoset formulations, it was proven that having more carbon-nitrogen bonds yielded a weaker polymer. However there was no correlation of carbon-nitrogen content to corrosion protection as they all behaved the same in accelerated weathering. Since changes within the polymer did not provide definitive pre-corrosion data, small molecules were used to indicate those events. While investigating Task 2, magnesium sensitive fluorescent molecules were tested to see if it can determine when a magnesium-rich primer needed replacement before corrosion. After determining the ideal environments for detection, use of an apolar epoxy polymer did not yield data for conclusive detection of corrosion activity. Therefore small molecules were incorporated into epoxy coatings for the purpose of detecting pH changes at the metal-polymer interface that occur before rust formation on steel. Not only did they detect corrosion in clear epoxies but also in a fully formulated coating with a compatible crosslinker that is not pH sensitive towards indicators like phenolphthalein. Although it was successful, the ability to quantify the onset of corrosion and gauge the severity of the environment was difficult. Therefore Task 4 was studied to develop a polymer that inherently fluoresces during corrosion events that could be quantified using a spectrometer. After successful synthesis and purification, the polymer was utilized in Tasks 5 and 6 to detect and quantify limits of corrosion initiated from different salts,

ionic environments, conductivities, and real-world testing. From these developments, corrosion was able to be detected by only using a polymer, metal, and visible light. The ability to detect corrosion without the aid of external sources and post-hoc destruction of samples can allow for more rapid sensing of corrosion activity in a realistic setting and allow for accelerated screening of new materials for faster commercialization.

Future Work

Although the utilization of the PKHH-FITC polymer was successful for the objective to determine the microscopic events that prefaced macroscopic corrosive failure, improvements could enhance this research. Three major research paths could be taken to better understand how to synthesize the fluorescent polymer, develop technologies for multiple substrates, and improve photobleaching resistance.

Even though the synthesis was successful in providing a material that could quantitatively measure corrosion on steel, it needs to be further studied how to improve the grafting efficiency so that lower amounts of FITC are used. This study would help understand the variables that inhibit this particular reaction and save money by using less material.

The study could also be directly related for the efficient development chemistries that are sensitive to multiple substrates. Fluorescein did well in providing pH data on bare steel; however it did not do well with aluminum and stainless steel. Therefore polymers that are able to detect the oxidation reaction of corrosion, and be sensitive to metallic ions should be developed to compliment that data of this document. This would provide validation of all of the information gathered from this research and could be better utilized for more diverse applications.

Lastly, the ability to get this technology to work in the real world could provide the greatest application of this polymer. By developing systems that are resistant to photobleaching, researchers could provide industrial and government agencies information that would save money, assets, and lives. Therefore, by delving into one or all three of these pathways, this research could continue to grow the understanding of how polymers protect and fail before corrosion occurs.

REFERENCES

1. Revie, W. R.; Uhlig, H. H. *Corrosion and Corrosion Control: An introduction to Corrosion Science and Engineering*, 4th; Wiley-Interscience: New Jersey, 2008.
2. Bhaskaran, R.; Palaniswamy, N.; Rengawamy, N. S.; Jayachandran, M. *ASM Hanbook; ASM International*, Materials Park, Ohio, 2005, 13B; pp. 621-628.
3. Shaw, B.; Kelly, a. R. What is Corrosion? *The Electrochemical Society Interface* 2006, *24*.
4. Fontana, M. G. *Corrosion Engineering*, 3rd; McGraw-Hill International Editions: Michigan, 1986.
5. Roberge, P. R. *Handbook of Corrosion Engineering*, McGraw Hill: New Jersey, 2000.
6. Forsgren, A. *Corrosion Control Through Organic Coatings,* Taylor & Francis, 2006.
7. Bierwagen, G. P. The Science of Durability of Organic Coatings: A Foreword. *Progress in Organic Coatings* 1987, *15*, 179.
8. Bierwagen, G.; Tallman, D.; Li, J.; He, L.; Jeffcoate, C. EIS Studies of Coated Metals in Accelerated Exposure. *Progress in Organic Coatings* 2003, *46*, 148.
9. Sorensen, P. A.; Kiil, S.; Dam-Johansen, K.; Weinell, C. E. Anticorrosive Coatings: a Review. *Journal of Coating Technology Research* 2009, *6* (2), 135.
10. Sinko, J. Challenges of Chromate Inhibitor Pigments Replacement in Organic Coatings. *Progress in Organic Coatings* 2001, *42*, 267.
11. Almeida, E.; Diamantino, T. C.; Figueiredo, M. O.; Sa, C. Oxidising Alternative Species to Chromium VI in Zinc Galvanized Steel Surface Treatment. Part 1 - A Morphological and Chemical Study. *Surface and Coating Technology* 1998, *106*, 8.

12. Weiss, K. D. Paint and Coatings: A Mature Industry in Transition. *Progress in Polymer Science* 1997, *22*, 203.
13. Chang, R. *Physical Chemistry*, University Science Books: Sausalito, CA, 2005.
14. Lide, D. *CRC Handbook of Chemistry and Physics,* Taylor & Francis: Boca Raton, 2007.
15. Almeida, E. Surface Treatments and Coatings for Metals. A General Overview. 1. Surface Treatments, Surface Preparation, and the Nature of Coatings. *Industrial & Engineering Chemistry Research* 2001, *40*, 3.
16. Thomas, N. L. The Barrier Properties of Paint Coatings. *Progress in Organic Coatings* 1991, *19*, 101.
17. McMurry, J. *Organic Chemistry*, 6th; Thomson Learning: California, 2004.
18. Hulden, M.; Hansen, C. M. Water Permeation in Coatings. Progress in Organic Coatings 1985, 13, 171.
19. Van der Wel, G. K.; Adan, O. C. G. Moisture in Organic Coatings - a Review. *Progress in Organic Coatings* 1999, *37*, 1.
20. Zhou, J.; Lucas, J. P. Hygrothermal Effects of Epoxy Resin. Part I: the Nature of Water in Epoxy. *Polymer* 1999, *40*, 5505-5512.
21. Zhou, J.; Lucas, J. P. Hygrothermal Effects of Epoxy Resin. Part II: Variations of Glass Transition Temperature. *Polymer* 1999, *40*, 5513-5522.
22. Funke, W. Toward a Unified View of the Mechanism Responsible for Paint Defects by Metallic Corrosion. *Ind. Eng. Chem. Prod. Res. Dev*. 1985, *24*, 343.
23. Sorensen, P. A.; al., e. Anticorrosive Coatings: a Review. *Journal of Coating Technology* 2009, 135.

24. Nguyen, T.; Hubbard, J. B.; Pmmersheim, J. M. Unified Model for Degradation of Organic Coatings on Steel in a Neutral Electrolyte. *Journal of Coatings Technology* 1996, *68* (855).

25. Dickie, R. A. Paint Adhesion, Corrosion Protection, and Interfacial Chemistry. *Progress in Organic Coatings* 1994, *25*, 3.

26. Sorensen, P. A.; Kiil, S.; Dam-Johansen, K.; Weinell, C. E. Influence of Substrate Topography on Cathodic Delamination of Anticorrosive Coatings. *Progress in Organic Coatings* 2009, *64*.

27. Clancy, T. C.; Frankland, S.; Hinkley, J. A.; Gate, T. S. Molecular Modeling for Calculation of Mechanical Properties of Epoxies with Moisture Ingress. *Polymer* 2009, *50*.

28. Xio, G. Z.; Shananhan, M. Irreversible Interactions Between Water and DGEBA/DDA Epoxy Resin During Hygrothermal Aging. *Journal of Applied Polymer Science* 1997, *67*.

29. Maton, L.; Taziaux, D.; Soumillion, J.-P.; Jiwan, J.-L. H. About the Use of an Amide Group as a Linker in Fluoroionophores: Competition Between Linker and Ionophore Acting as Chelating Groups. *Journal of Materials Chemistry* 2005, *15*, 2928-2937.

30. Suzuki, Y.; Komatsu, H.; Ikeda, T.; Saito, N.; Araki, S.; Citterio, D.; Hisamoto, H.; Kitamura, Y.; Kubota, T.; Nakagawa, J.; Oka, K.; Suzuki, K. Design and Synthesis of Mg2+ Selective Fluoroionophores Based on a Coumarin Derivative and Application for Mg2+ Measurement in a Living Cell. *Anal. Chem.* 2002, *74* (6), 1423-1428.

31. Otten, P. A.; London, R. E.; Levy, L. A. 4-Oxo-4H-quinolizine-3-carboxylic Acids as Mg2+ Selective, Fluorescent Indicators. *Bioconjugate Chem* 2001, *12*, 203-212.

32. Brunet, E.; Alonso, M. T.; Juanes, O.; Sedano, R.; Rodrigues-Ubis, J. C. Unusual Behavior of 7-Diethylamino-3-(3,4-ethylen-dioxybenzoyl)coumarin Towards Group IIA Cations: A Potential Photoactive Probe for Magnesium. *Tetrahedron Letters* 1997, *38* (25), 4459-4462.

33. Kim, M. H.; Jang, H. H.; Yi, S.; Chang, S.-K.; Han, M. S. Coumarin-Derivative-Based Off-On Catalytic Chemodosimeter for Cu2+ Ions. *Chem. Commun*. 2009, 4838-4840.

34. Capitan-Vallvey, L. F.; Fernandex-Ramos, M. D.; Lapresta-Fernandez, A.; Brunet, E.; Rodriguez-Ubis, J. C.; Juanes, O. Magnesium Optical One-Shot Sensor Based on a Coumarin Chromoionophore. *Talanta* 2006, *68*, 1663-1670.

35. Cha, J.-N.; Cheong, B.-S.; Cho, H.-G. Solvation of Magnesium Perchlorate in Deuterated Acetonitrile Studied by Means of Vibrational Spectrscopy. *J. Phys. Chem. A* 2001, *105*, 1789.

36. Renou, F.; Mostafavi, M.; Archirel, P.; Bonazzola, L.; Pernot, P. Solvated Electron Pairing with Earth Alkaline Metals in THF. 1. Formation and Structure of the Pair with Divalent Magnesium. *J. Phys. Chem. A* 2003, *107*, 1506.

37. Renou, F.; Mostafavi, M. Reactivity of the solvated electron toward divalent magnesium. *Chemical Physics Letters* 2001, *335*, 363.

38. Lee, K.-Y.; Chung, W.-S.; Jo, N.-J. Effect of Salt Species on Electrochemical Properties of Gel-Type Polymer Electrolyte Based on Chemically Crosslinking Rubber. *Electrochimica Acta* 2004, *50*, 295.

39. Peng, J.; Xiaoxiao, H.; Wang, K.; Tan, W.; Wang, Y.; Liu, Y. Noninvasive Monitoring of IntraCellular pH Change Induced by Drug Stimulation Using Silica Nanoparticle Sensors. *Analytical Biological Chemistry* 2007, *388*, 645-654.
40. Gao, F.; Tang, L.; Dai, L.; Wang, L. A Fluorescence Ratiometric Nano-pH Sensor Based on Dual-Fluorophore-Dope Silica Nanoparticles. *Spectrochimica Acta Part A* 2007, *67*, 517-521.
41. Sun, H.; Scharff-Poulsen, A. M.; Gu, H.; Almdal, K. Synthesis and Characterization of Ratiometric, pH Sensing Nanoparticles with Covalently Attached Fluorescent Dye. *Chemistry of Materials* 2006, *18* (15).
42. Frankel, G. S.; Zhang, J. Corrosion-Sensing Behavior of an Acrylic-Based Coating System. *Corrosion* 1999, *55* (10).
43. Augustyniak, A.; Tsavalas, J.; Ming, W. Smart Epoxy Coatings for Early Steel Corrosion Detection. *American Coatings Show*. 2010.
44. Augustyniak, A.; Tsavalas, J.; Ming, W. Early Detection of Steel Corrosion via "Turn-On" Fluorescence in Smart Epoxy Coatings. *Applied Materials & Interfaces* 2009, *1* (11), 2618-2623.
45. Liu, G.; Wheat, H. G. Coatings for Early Corrosion Detection. *ECS Transactions* 2010, *28*, 239-247.
46. Liu, G.; Wheat, H. G. Use of a Fluorescent Indicator in Monitoring Underlying Corrosion on Coated Aluminum 2024-T4. *Journal of the Electrochemical Society* 2009, *156* (4), C160-C166.
47. Bronk, K. S.; Michael, K. L.; Pantano, P.; Walt, D. R. Combined Imaging and Chemical Sensing Using a Single Optical Imaging Fiber. *Analytical Chemistry* 1995, *67*, 2750-2757.

48. Panova, A. A.; Pantano, P.; Walt, D. R. In Situ Fluorescence Imaging of Localized Corrosion with a pH-Sensitive Imaging Fiber. *Analytical Chemistry* 1997, *69*, 1635-1641.

49. Bryant, D. E.; Greenfield, D. The use of fluorescent probes for the detection of under-film corrosion. *Progress in Organic Coatings* 2006, *57*, 416-420.

50. Gotou, T.; Noda, M.; Tomiyama, T.; Sembokuya, H.; Kubouchi, M.; Tsuda, K. In Situ Health Monitoring of Corrosion Resistant Polymers Exposed to Alkaline Solutions Using pH Indicators. *Sensors and Actuators B* 2006, *119*, 27-32.

51. Burns, A.; Ow, H.; Wiesner, U. Fluorescent Core-Shell Silica Nanoparticles: Towards "Lab on a Particle" Architectures for Nanobiotechnology. *Chemical Society Reviews* 2006, *35*, 1028-1042.

52. Uthirakumar, P.; Hong, C.-H.; Suh, E.-K.; Lee, Y.-S. Yellow Light-Emitting Polymer Bearing Fluorescein Dye Units: Photophysical Property and Application as Luminescence Converter of a Hybrid LED. *Reactive & Functional Polymers* 2007, *67*, 341-347.

53. Uthirakumar, P.; Suh, E.-K.; Hong, C.-H.; Lee, Y.-S. Synthesis and Characterization of Polyesters Containing Fluorescein Dye Units. *Polymer* 2005, *46*, 4640-4646.

54. Allard, E.; Larpent, C. Core-Shell Type Dually Fluorescent Polymer Nanoparticles for Ratiometric pH-Sensing. *Journal of Polymer Science: Part A: Polymer Chemistry* 2008, *46*, 6206-6213.

55. Itagaki, M.; Tagaki, M.; Watanabe, K. Active Dissolution Mechanism of Iron Using EIS with Channel Flow Double Electrode. *Electrochimica Acta* 1996, *41*, 1201.

56. Tzaneva, B. R.; Fachikov, L. B.; Raicheff, R. G. Effect of Halide Anions and Temperature on Initiation of Pitting in Cr-Mn-N and Cr-Ni Steels. *Corrosion Engineering, Science and Technology* 2006, *41*.

57. Pagitsas, M.; Diamantopoulou, A.; Sazou, D. A Point Defect Model for the General and Pitting Corrosion on Iron/Oxide/Electrolyte Interface Deduced from Current Oscillations. *Chaos, Solutions and Fractals* 2003, *17*, 263.

58. Yazdanfar, K.; Zhang, X.; Keech, P. G.; Shoesmith, D. W.; Wren, J. C. Film Conversion and Breakdown Processes on Carbon Steel in the Presence of Halides. *Corrosion Science* 2010, *52*, 1297-1304.

59. MacFarlane, D. R.; Smedley, S. The Dissolution Mechanism of Iron in Chloride Solutions. *Electrochemistry Society* 1986, *133* (11), 2240.

60. Lochel, B.; Strenblow, H. H.; Sakashita, M. Breakdown of Passivity of Nickel by Fluoride. *Electrochemistry Society* 1984, *131* (3).

61. Bilgic, S.; Yilmaz, H. Effect of Alkaline Metal Halides on the Corrosion Inhibition of Steel in Sulfuric Acid Containing Benzoic Acid. *Materials Chemistry and Physics* 2003, *79*, 5.

62. Zhao, Y.; Li, X.; Liu, L.; Chen, F. Fluoride Removal by Fe(III)-Loaded Ligand Exchange Cotton Cellulose Adsorbent from Drinking Water. *Carbohydrate Polymers* 2008, *72*, 144-150.

63. Skoulikidis, T.; Ragoussis, A. Diffusion of Iron Ions Through Protective Coatings on Steel. *Science* 1992, *48* (8), 666-670.

64. Benosman, A. S.; Taibi, H.; Mouli, M.; Belbachir, M.; Senhadji, Y. Diffusion of Chloride Ions in Polymer-Mortar Composites. *Journal of Applied Polymer Science* 2008, *110*, 1600-1605.

65. Ramos, J. A.; Serrano, E.; Tercjak, A.; Salgueiro, W.; Goyanes, S.; Mondragon, I. PALS Study of Epoxy Matrices: Self-Assembly of Block Copolymers and its Capability for Nanostructuing Thermosetting Systems. *Physica Status Solidi* 2007, *4* (10), 3690-3699.

66. Leng, A.; Streckel, H.; Hofmann, K.; Stratmann, M. The Delamination of Polymeric Coatings from Steel Part 3: Effect of the Oxygen Partial Pressure on the Delamination Reaction and Current Distribution at the Metal/Polymer Interface. *Corrosion Science* 1999, *41*, 599-620.

67. Vasquez Moll, D. V.; Salvarezza, R. C.; Videla, H. A.; Arvia, A. J. The Pitting Corrosion of Nickel in Different Electrolyte Solutions Containing Chloride Ions. *Journal of the Electrochemistry Society* 1985, *132* (4), 754-760.

68. El Etre, A. Y.; Abdallah, M.; Soliman, M. G.; Mabrouk, E. M. Inhibition of Pitting Corrosion of C-Steel in NaCl Solution By Some Inorganic Compounds. *Communication of Faculty of Sciences, University of Ankara* 2000, *46*, 25-31.

69. Uhlig, H. H.; Morrill, M. C. Corrosion of 18-8 Stainless Steel in Sodium Chloride Solutions. *Industrial and Engineering Chemistry* 1941, *33* (7), 875-880.

70. Boichyshyn, L.; Kubishtal, Y.; Budn'ok, A.; Kovbuz, M. Influence of Iron Additives on the Corrosion Resistance of Al87Gd5Ni8 Amorphous Metal Alloy. *Materials Science* 2011, *46* (5), 599-606.

71. Wypych, G. *Handbook of Material Weathering*, 4th; ChemTec: Toronto, 2008.

72. Schweitzer, P. A. *Fundamentals of Corrosion: Mechanisms, Causes, and Preventative Methods*, CRC Press: Boca Raton, FL, 2010.

73. Shi, X.; Fernando, B. M. D.; Croll, S. G. Concurrent Physical Aging and Degradation of Crosslinked Coating Systems in Accelerated Weathering. *J. Coat. Technol. Res*. 2008, *5* (3), 299-309.

74. Shiga, T.; Narita, T.; Ikawa, T.; Okada, A. Stress Monitoring in Thin Polymer Coatings Using time Resolved Fluorescence. *Polymer Engineering and Science* 1998, *38* (4), 693-698.

75. Hu, H.; Larson, R. G. Preparation of Fluorescent Particles with Long Excitation and Emission Wavelengths Dispersible in Organic Solvents. *Langmuir* 2004, *20*, 7436-7443.

76. Elmas, B.; Tuncel, M.; Yalcin, G.; Senel, S.; Tunel, A. Synthesis of Uniform, Fluorescent Poly(glycidyl methacrylate) Based Particles and their Characterization by Confocal Laser Scanning Microscopy. *Colloids Surfaces A: Physiochem. Eng. Aspects* 2005, *269*, 125-134.

77. Talhavini, M.; Atvars, T. D. Z. Dye-Polymer Interactions Controlling the Kinetics of Fluorescein Photobleaching Reactions in Poly (Vinyl Alcohol). *Journal of Photochemistry and Photobiology A: Chemistry* 1998, *114*, 65-73.

78. Dibbern-Brunelli, D.; de Oliveira, M. G.; Atvars, T. D. Z. Temperature Dependence of the Photobleaching Process of Fluorescein in Poly(Vinyl Alcohol). *Journal of Photochemistry and Photobiology A: Chemistry* 1995, *85*, 285-289.

79. Klee, J. E.; Grutzner, R.-E.; Horhold, H.-H. Uncrosslinked Epoxy-Amine Addition Polymer, 44. *Macromol. Chem. Phys*. 1996, *197*, 2305-2323.

80. Klee, J. E.; Grutzner, R.-E.; Horhold, H.-H.; Flammersheim, H.-J. Uncrosslinked Epoxide-Amine Addition Polymers, 45. *Macromol. Chem. Phys*. 1998, *199*, 1603-1611.

81. De Belder, A. N.; Granath, K. Preparation and Properties of Fluorescein-Labelled Dextrans. *Carbohydrate Research* 1973, *30*, 375-378.

82. Holdcroft, S. J. J. *Polym. Sci., Part B: Polym. Phys*. 1991, *29*, 1585-1588.

83. Musto, P.; al., e. *Macromolecules* 2008, *41*, 5729-5743.

84. Lovering, E. G.; Laidler, K. J. A System of Molecular Thermochemistry for Organic Gases and Liquids II. Extension to Compounds Containing Sulfur and Oxygen. *Canadian Journal of Chemistry* 1960, *38*, 2367-2372.

85. Bedford, A. F.; Edmonson, P. B.; Mortimer, C. T. *J. Chem. Soc.* 1962, 2927.

86. Klee, J. E.; Flammersheim, H.-J. Uncrosslinked Epoxide Amine Addition Polymers, 46. *Macromol. Chem. Phys*. 2002, *203*, 100.

87. Min, B. G.; Stachurski, Z. H.; Hodgkin, J. H.; Heath, G. R. Quantitative Analysis of the Cure Reaction of DGEBA/DDS Epoxy Resins without and with Thermoplastic Polysulfone Modifier Using Near Infra-Red Spectroscopy. *Polymer* 1993, *34*, 3620.

88. Rigail-Cedeno, A.; Sung, C. S. P. Fluorescence and IR Characterization of Epoxy Cured with Aliphatic Amines. *Polymer* 2005, *46*, 9378-9384.

89. Dyankonov, T.; Mann, P. J.; Chen, Y.; Stevenson, W. T. K. Thermal Analysis of some Aromatic Cured Model Epoxy Resin Systems - II: Residues of Degradation. *Polymer Degradation and Stability* 1996, *54*, 67-83.

90. Terao, K.; Mays, J. W. On-line Measurement of Molecular Weight and Radius of Gyration of Polystyrene in a Good Solvent and in a Theta Solvent Measured with a Two-Angle Light Scattering Detector. *European Polymer Journal* 2004, *40*, 1623-1627.

91. Pathak, S. S.; Blanton, M. D.; Mendon, S. K.; Rawlins, J. W. Investigation on Dual Corrosion Performance of Magnesium-Rich Primer for Aluminum Alloys Under

Salt Spray Test (ASTM B 117) and Natural Exposure. *Corrosion Science* 2010, *52*, 1456-1463.

92. Pathak, S. S.; Blanton, M. D.; Mendon, S. K.; Rawlins, J. W. Carbonation of Mg Powder to Enhance the Corrosion Resistance of Mg-rich Primers. *Corrosion Science* 2010, *52*, 3782-3792.
93. Zhang, J.; Frankel, G. S. Corrosion-Sensing Behavior of an Acrylic-Based Coatings System. *Corrsion* 1999, *55* (10), 957-697.
94. Augustyniak, A.; Tsavalas, J.; Ming, W. Smart Epoxy Coatings for Early Steel Corrosion Detection. *American Coatings Conference*, Charlotte, NC, April 12-14, 2010.
95. Augustyniak, A.; Tsavalas, J.; Ming, W. Early Detection of Steel Corrosion via "Turn-On" Fluorescence in Smary Epoxy Coatigs. *Applied Materals & Interfaces* 2009, *1* (11), 2618-2623.
96. Gotou, T.; Noda, M.; Tomiyama, T.; Sembokuya, H.; Kubouchi, M.; Tsuda, K. In Situ Health Monitoring of Corrosion Resistant Polymers Exposed to Alkaline Solutions Using pH Indicators. *Sensors and Actuators B* 2006, *119*, 27-32.
97. Calle, L. M.; Li, W. Coatings and Methods for Corrosion Detection and/or Reduction. US Patent 7,790,225, Sep 7, 2010.
98. Li, W.; Calle, L. M. Controlled Release Microcapsules for Smart Coatings. *NACE Corrosion*, 2007.
99. Li, W.; Calle, L. M. A Smart Coating for the Early Detection and Inhibition of Corrosion. *Proceeding of the Smart Coatings* 2007, 191.

100. Kunimoto, K.-K.; Sugiura, H.; Kato, T.; Senda, H.; Kuwae, A.; Hanai, K. Molecular Structure and Vibrational Spectra of Phenolphthalein and its Dianion. *Spectrochimica Acta Part A* 2001, *57*, 265-271.

101. Sayed, L. E.; Bebawy, L. I.; Amer, M. M. Determination of Phenolphthalein in Pharmeceutical Preparations Using N-Bromosuccinimde. *Analyst* 1986, *111*, 379-381.

102. Boguta, A.; Wrobel, D. Fluorescein and Phenolphthalein - Correlation of Fluorescence and Photoelectric Properties. *Journal of Fluorescence* 2001, *11* (2), 129.

103. Idowu, O. S.; Fasanmade, A. A.; Olaniyi, A. A. Evaluation of Dimethylformamide (DMF) as an Organic Modifier in Hydrophobicity Index (Rm) Determination. *Tropical Journal of Pharmaceutical Research* 2002, *1* (2), 83-89.

104. Seeley, J. V.; Morris, R. A.; Viggiano, A. A. Gas Phase Reaction of Hydrate Halides with Chlorine. *J. Phys. Chem*. 1996, *100*, 15821-15826.

105. Julliard, J. Dimethylformamide: Purification, Tests for Purity and Physical Properties. *International Union of Pure and Applied Chemistry* 1977, *49*, 885-892.